FABRICATION AND CHARACTERIZATION OF Al_2O_3 / ZrO_2 MICRO/NANOSTRUCTURED COMPOSITE FROM POWDER-ALKOXIDE MIXTURE

Wathun Boonsorn

A Thesis Submitted in Partial Fulfillment of the Requirements for the

Degree of Doctor of Philosophy in Ceramic Engineering

Suranaree University of Technology

Academic Year 2014

การขึ้นรูปและการวิเคราะห์ลักษณะเฉพาะวัสดุเชิงประกอบโครงสร้างแบบไมโคร-นาโนจากของผสมผง-แอลคอกไซด์ อะลูมินา/เซอร์โครเนีย

นายวทัญญู บุญสอน

วิทยานิพนธ์นี้เป็นส่วนหนึ่งของการศึกษาตามหลักสูตรปริญญาวิศวกรรมศาสตรดุษฎีบัณฑิต
สาขาวิชาวิศวกรรมเซรามิก
มหาวิทยาลัยเทคโนโลยีสุรนารี
ปีการศึกษา 2557

FABRICATION AND CHARACTERIZATION OF Al$_2$O$_3$ / ZrO$_2$ MICRO/NANOSTRUCTURED COMPOSITE FROM POWDER-ALKOXIDE MIXTURE

Suranaree University of Technology has approved this thesis submitted in partial fulfillment of the requirements for the Degree of Doctor of Philosophy

Thesis Examining Committee

_____

(Assoc. Prof. Dr. SutinKuharuangrong)

Chairperson

_____

(Asst. Prof. Dr. SukasemWatcharamaisakul)

Member (Thesis Advisor)

_____

(Asst. Prof. Dr. Boris Golman)

Member

_____

(Assoc. Prof. Dr. CharussriLorprayoon)

Member

_____

(Assoc. Prof. Dr. SuthamSrilomsak)

Member

_____

(Dr. SomsakSiwadamrongpong)

Member

_____   _____

(Prof. Dr. SukitLimpijumnong)   (Assoc. Prof. Flt. Lt. Dr.KontornChamniprasart)

Vice Rector Academic Affairs   Dean of Institute of Engineering

and Innovation

วทัญญ์บุญสอน:การขึ้นรูปและการวิเคราะห์ลักษณะเฉพาะวัสดุเชิงประกอบโครงสร้าง
แบบไมโคร-นาโนจากของผสมผง-แอลคอกไซด์อะลูมินา/เซอร์โคเนีย (FABRICATION
AND CHARACTERIZATION OF
Al$_2$O$_3$/ZrO$_2$ MICRO/NANOSTRUCTUREDCOMPOSITE FROM POWDER-
ALKOXIDE MIXTURE)อาจารย์ที่ปรึกษา:
ผู้ช่วยศาสตราจารย์ ดร.สุขเกษม วัชรมัยสกุล,127 หน้า.

การศึกษาวัสดุเชิงประกอบอะลูมินา/เซอร์โคเนีย โครงสร้างแบบไมโคร-นาโนจากของ
ผสมผงแอลคอกไซด์โดยเตรียมจากสารละลายเซอร์โคเนียมโพรพอกไซด์ที่มีความเข้มข้นแตกต่าง
กัน ได้แก่ 25%, 33.3%, 50%, 66.7%, 75% และ 100% โดยน้ำหนักและเผาผนึกที่อุณหภูมิ
แตกต่างกัน งานวิจัยนี้ได้ทำการศึกษาความสัมพันธ์ระหว่างความเข้มข้นของสารละลาย
เซอร์โคเนียมโพรพอกไซด์ที่ให้ปริมาณของวัสดุเสริมแรงเซอร์โคเนีย 10% โดยน้ำหนักที่ส่งผล
ต่อการกระจายตัวของวัสดุเสริมแรงเซอร์โคเนียขนาดอนุภาคระดับนาโนเมตรในเนื้อวัสดุ
หลักอะลูมินาขนาดไมโครเมตรและศึกษาตัวแปรต่างๆที่มีผลต่อสมบัติเชิงกลของวัสดุ
เชิงประกอบ

จากการศึกษาพบว่าวัสดุเชิงประกอบที่ได้จากการเผาผนึกประกอบด้วยวัฏภาคของ อัลฟา-
อะลูมินาและเตตระโกนอลและ โมโนคลินิคเซอร์โคเนีย โดยปริมาณความเข้มข้นของสารละลาย
เซอร์โคเนียมโพรพอกไซด์ที่เพิ่มขึ้นจะส่งผลให้ปริมาณวัฏภาคของเตตระโกนอลเซอร์โคเนีย
ลดลง ซึ่งจะทำให้ความเหนียวของวัสดุเชิงประกอบลดลงด้วยเช่นกัน ส่วนการเผาผนึกชิ้นงาน
ที่อุณหภูมิ 1700°C เป็นเวลา 4 ชั่วโมงทำให้ได้วัสดุเชิงประกอบมีความหนาแน่นสูงสุดที่ 91.70%
ของความหนาแน่นสัมพัทธ์และจากการทดสอบสมบัติเชิงกลพบว่าชิ้นงานที่ได้จากของผสมที่มี
ความเข้มข้นของสารละลายเซอร์โคเนียที่ 100% โดยน้ำหนักและเผาผนึกที่อุณหภูมิ 1700°C เป็น
เวลา 4ชั่วโมง จะมีค่าความทนทานต่อแรงดัดโค้ง และความแข็งสูงสุดเท่ากับ 1437 MPa และ
13.96 GPa ตามลำดับ ในขณะที่ค่าความเหนียวสูงสุดของวัสดุเชิงประกอบที่ 14.22 MPa.m$^{1/2}$
ได้จากของผสมที่มีความเข้มข้นของสารละลายเซอร์โคเนียโพรพอกไซด์ที่ 25% โดยน้ำหนัก
ซึ่งเมื่อศึกษาโครงสร้างจุลภาคของวัสดุเชิงประกอบพบว่าการกระจายตัวของอนุภาคเซอร์โคเนีย
ที่มีความสม่ำเสมอได้จากของผสมที่มีความเข้มข้นของสารละลายเซอร์โคเนียที่ 50 และ 75%
โดยน้ำหนัก ซึ่งมีการกระจายตัวอยู่ทั้งภายในเกรนและบริเวณขอบเกรนของวัสดุหลักอะลูมินา

จากการศึกษาสามารถสรุปได้ว่าปริมาณความเข้มข้นของสารละลายเซอร์โคเนียมโพรพอก
ไซด์จะมีผลต่อการกระจายตัวของอนุภาคเซอร์โคเนียในอะลูมินาเนื้อหลักและมีผลต่อสมบัติเชิงกล
ของวัสดุเชิงประกอบโดยเฉพาะอย่างยิ่งความเหนียว

สาขาวิชา<u>วิศวกรรมเซรามิก</u>   ลายมือชื่อนักศึกษา_____

ปีการศึกษา2557   ลายมือชื่ออาจารย์ที่ปรึกษา_____

                                           ลายมือชื่ออาจารย์ที่ปรึกษาร่วม_____

WATHUN BOONSORN :FABRICATION AND CHARACTERIZATION OF Al$_2$O$_3$/ZrO$_2$MICRO/NANOSTRUCTUREDCOMPOSITE FROM POWDER-ALKOXIDE MIXTURE. THESIS ADVISOR: ASST. PROF. SUKASEM WATCHARAMAISAKUL, Ph.D.,127PP.

ALUMINA-ZIRCONIA/POWDER-ALKOXIDE/NANOCOMPOSITE/IMAGE ANALYSIS

The Al$_2$O$_3$/ZrO$_2$ micro/nano composites have been prepared from powder alkoxide mixture with various Zrpropoxide concentrations. The effect of the concentration of Zrpropoxide solution on the distribution of ZrO$_2$nano-grains in Al$_2$O$_3$ matrix was investigated on the correlation with the mechanical properties such as the flexural strength, hardness and fracture toughness of composites.

It was found that the phase compositions of sintered samples exhibited with α-Al$_2$O$_3$phase and tetragonal and monoclinic ZrO$_2$ phases. The concentration of Zrpropoxide solution was influenced to ZrO$_2$ phase composition. The tetragonal ZrO$_2$ phase decreased with the increasing of Zrpropoxideconcentration while monoclinic increased. The highest relative density of 92.12 ±0.66% was obtained with samples sinteredat 1700°C. The flexural strength and hardness of composites were increased with the increasing of Zrpropoxide concentration and sintering temperature. The highest flexural strength and hardness of 1437 MPa and 13.96 GPa respectively, were found for the sample prepared with concentrated Zrpropoxide solution and sintered at 1700°C. However, the highest toughness of 14.22 MPa.m$^{1/2}$ was obtained with 25wt% Zrpropoxide solutionat high sintering temperature. The microstructures of sintered composites showed particles of ZrO$_2$ distributed in Al$_2$O$_3$ grains and grain boundaries

with wide size distribution. The high uniformity distribution of ZrO_2 particles was obtained withZrpropoxide concentration of 50 and 75wt%.

Consequently, the mechanical properties of composite materials could be explained by the phase composition and the uniformity distribution of reinforcing ZrO_2 phase in Al_2O_3 matrix.
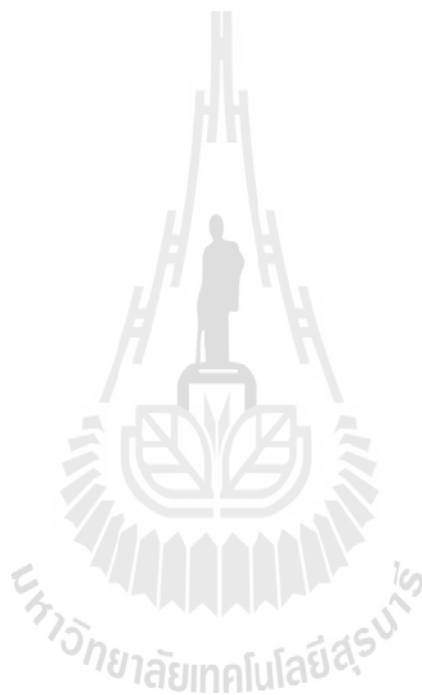
School of Ceramic Engineering   Student's Signature_____

Academic Year 2014   Advisor's Signature_____

                                             Co-Advisor's Signature_____

ACKNOWLEDGEMENTS

TABLE OF CONTENTS

Page

TABLE OF CONTENTS (Continued)

TABLE OF CONTENTS (Continued)

TABLE OF CONTENTS (Continued)

TABLE OF CONTENTS (Continued)

Page

LIST OF TABLES

LIST OF FIGURES

LIST OF FIGURES(Continued)

LIST OF FIGURES(Continued)

Figure   **Page**

LIST OF FIGURES(Continued)

CHAPTER I

INTRODUCTION

Recently, ceramic materials have been used successfully in orthopedic and dental applications such as hip-knee prosthesis,dental implants,etc.Ceramic materials demonstrate improved wear resistance and excellent biocompatibility compared to the ordinary metal and polyethylene materials. Over the past decades, the orthopedic implants devices have been rapidly developed. The new generations of metal-on-metal and ceramic-on-ceramic hip and knee implants bring new hopes for patients. The promise of implants in erasing some of the thorniest issues of old and middleaged people has led to an outpouring of demand for these new procedures. From 2000 to 2009, the number of yearly joint replacement surgeries in the U.S. has nearly doubled, from 575,000 in 2000 to 1.1 million in 2009 (600bn, www, 2010). The total expenditures for orthopedic procedures increased more than twofold in the same time period, as shown in Figure 1.1. The main reason of growing costsisa substantialincrease in the number of complicated procedures performed on patients. However, all-ceramic materials are brittle and sensitive to stress. Thus, there is a need to improve the mechanical properties of ceramics materials for orthopedic applications.
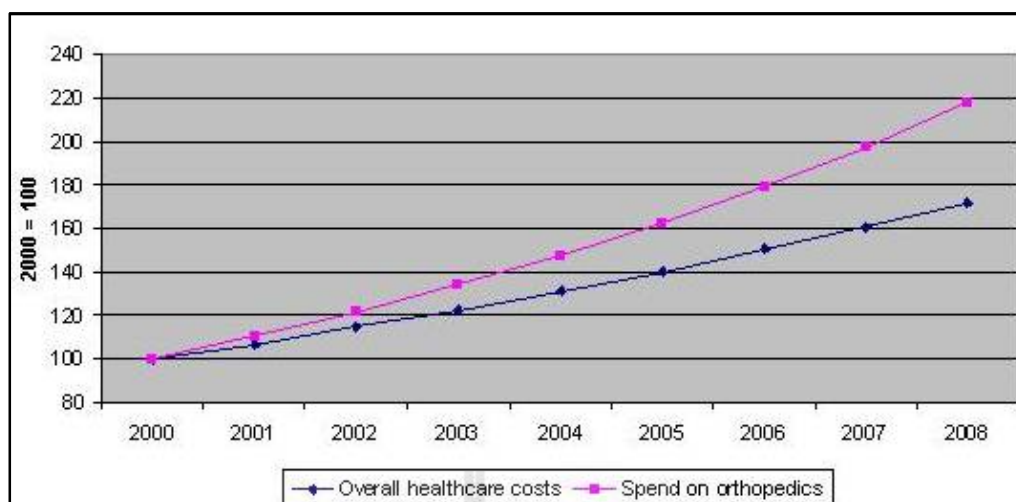
Figure 1.1 Total expenditures on orthopedics vs. overall healthcare costs,

indexed (600bn,www, 2010)

Alumina (Al_2O_3) was used as a material for orthopedic bearing over the past decade. This ceramic is the cheapest and its hardness is 9 on Moh's scale which ranks the hardness of diamond at 10 as the hardest existing materials (McColm, 1990). Alumina ceramic is the most often considered as 'bioinert' material since no direct bone-material interface is created. For implants application, alumina is widely used in manufacturing of hip-joints ordental restorations and wear partsbecause of low wear rates of bearing components and negligible amount of ion release.Unfortunately, since alumina is also brittle and susceptible to slow crack growth (SCG), the fracture rate of implants is quite high (De Aza et al., 2002). The old generation of alumina ceramic implants was produced using conventional procedure that increases the green density (Bocanegra-Bernal et al., 2009). Nowadays, alumina properties are improved for long-term by several methodssuch as refinement of manufacturing processes and addition of additive.

Zirconia (ZrO_2) is a ceramic material that exhibits the best mechanical properties of oxide ceramics as the consequence of phase transformation toughening, which increases its crack propagation resistance (Chevalier and Gremillard, 2011). The transformations of zirconia phase demonstrate extremely high strength and fracture toughness achieved by exploiting the martensitic phase transformation of thermodynamically metastable tetragonal phase (Stevevs, 1986).Zirconia is one ofmaterialswhich are usually added to alumina for improving its properties as structural ceramic (Piconi et al., 1999), because of substantially higher fracture toughness and strength. Zirconia has the largest value of fracture toughness of any monolithic ceramic. The mechanisms governing thetoughnessof zirconia are the phase-stabilizationand phase transformation of the tetragonal zirconia phase to retain the high-temperature phase at room temperature, which gives zirconia its desirable properties as an engineering ceramic.

An application of composite materials is the way to improve lifetime and reliability of orthopedic implants by enhancing theirfracture toughness and mechanical strength.   Many researcheshavealready studiedcomposite materials and have successfully proven that alumina, zirconia and other ceramics possess the ability to withstand the environment of the human body (Schehl et al., 2002).Alumina and zirconia composites havefound practical application as biomaterials due to their proven biocompatibility and superior mechanical properties as compared to alumina (Piconi et al., 2014).They are considered as biologically inert materials due to the formation of a soft tissue interlayer that shields the bone from the implant. Zirconia is also used mixed with materials other than alumina to improve their properties.

Recently, alumina-zirconia composites were developed as alternative bearing materials for orthopedic implant. Two kinds of composites can be prepared by using alumina and zirconia: a phase-stabilized zirconia matrix reinforced with alumina particles, commonly known asalumina toughened zirconia (ATZ), or an alumina matrix reinforced with zirconia particles referred to as zirconia toughened alumina (ZTA). With both materials, the higher toughness was obtained in comparison with the single phase ceramics. However, ZTA composite toughness is higherthan that of ATZ one. Interactions of the crack front with the second phase (crack blunting, crack deviation) and pre-existing micro cracks, formed during the tetragonal – monoclinic transformation of zirconia, were considered as the main reasons of the enhancement of the fracture toughness. In addition, the transformation toughening associated with the tetragonal – monoclinic phase transformation around particles in front of crack, as well as other mechanisms, such as crack deflection, crack bridging and the presence of micro cracks, may also contribute to the toughness enhancement.

Table 1 Coefficients of thermal expansion of alumina and zirconia (Morrell, 1985)

Ceramics	$\alpha/(10^{-6}\ K^{-1})$						
	100K	200K	293K	500K	800K	1100K	1500K
Alumina Al_2O_3	0.6	3.3	5.5	7.8	8.5	9.4	10.2
Zirconia (ZrO_2 stabilized)	-	-	8-9	9-10	11-13	13-15	13-15

The phenomenon of transformation toughening obtained by the difference of coefficients of thermal expansion between alumina and zirconiais illustrated in Table 1. Thethermalmismatchwasthoughtto create stressfieldaroundZrO₂particles. The transformations of tetragonal to the monoclinic zirconia phase providevolume

expansion, 3-5%, and shear strain ≈ 7%(Stevens andEvans, 1984). The high toughness of zirconia ceramics is attributed to the stress induced phase transformation of metastable tetragonal grains towards the monoclinic symmetry aheadofapropagatingcrack,leadingtoanincrease of the work of fracture(Garvie et al., 1975).

Al_2O_3/ZrO_2 composite is one of the mostwidely used composites system for orthopedics application. Many researchers have tried to improve the lifetime and mechanical properties of materials. Several attempts have been made to develop various composite systems such as micro/micro, nano/nano, micro/nano system and theirfabricationmethods including infiltration, colloidal route, etc. Both tetragonal and monoclinic phases in alumina matrix with 10wt% total zirconia contents provided higher strength and toughness than individual tetragonal and monoclinic zirconia phase (Tuan et al., 2002). The uniformgrain size distributions of alumina/zirconia withhomogeneous microstructure of fine zirconia particles were obtained by powder alkoxide mixture method (Calderon-Moreno and Schehl, 2004). The microstructure of the alumina–zirconia composites manufactured by the colloidal technique was very fine with sub micrometer alumina grains and, mainly intergranular, nano-sized zirconia particles with a narrow grain size distribution (De Aza etal., 2002). The Vickers hardness ofpowder processed samples decreased indefinitely with increasing ZrO_2, but the hardness of samples produced by colloidal method increased to highest value at 10wt% of ZrO_2. Additions of glacial acetic acid were needed to form stable suspensions (Rafferty et al., 2009). The digital image analysis was used for microstructural characterization. Digital image processing-assisted quantitative analysis of micrographs was carried out and provided plenty of data that are fairly

important.The method could apply to other systems(Horovistiz and Muccillo, 2011).The image analysisof sintered microstructure confirmed the existence of correlationsbetween the areal fraction, grain size distribution, uniformity of spatial distribution expressed by the void size distribution of each componentand mechanical properties of samples such as Vicker's hardness and transverse rupture strength under various sintering temperatures(Kangwantrakoolet al., 2003).

As mentioned previously, the development of advanced ceramic materials on the basis of widely recognized intrinsic relationships between their properties and microstructure should, thus, rely on robust and reliable techniques of microstructural analysis. When ceramic materials are fabricated, their properties will be determined by the morphology of the microstructure, which depends on the process used.

Therefore, the present research focuses on the relationship betweenthe uniformity of distributions of zirconia nanoparticles in Al_2O_3micro-grainsprepared at various conditionsand the mechanical properties of sintered composite.

1.1   Research Objectives

The general objective of this research is to improve the mechanical properties of alumina by addition of zirconia nanoparticles as a reinforcing material using the colloidal method.

Following are the specific objectives of the study:

1. To investigate the effects of alkoxide composition and sintering temperature on mechanical properties of alumina/zirconia micro-nano composites such as hardness, toughness and flexural strength.

2. To clarify the relationship between the uniformity of zirconia dispersion and the mechanical properties of sintered composites.

1.2   Scope and limitation of thesis.

1. Investigate the effect of composition of zirconia alkoxide solution on the dispersion of zirconia nanoparticles in the sintered composite material

2. Clarify the relationships between the mechanical properties, such as hardness, toughness and flexural strength, the sintering temperature, and the microstructure of alumina/zirconia micro/nano composite materials.

1.3   Expected results

The main advantages of the research are summarized below:

1. The highdensity alumina/zirconia micro-nano composite with optimum mechanical properties will be obtained by using the colloidal method. This composite could possibly be used as the structural material for orthopedic implants.

2. The proper powder preparation method and the sintering parameters will be identified for fabrication of micro-nano composites with superior mechanical properties.

3. The quantitative approach to the microstructure characterization will be farther advanced in order to define the correlation betweenmicrostructural characteristics and mechanical properties.

CHAPTER II

LITERATURE REVIEW

2.1 Materials

2.1.1 Alumina (Al_2O_3)

Alumina is the most widely used oxide ceramic material becauseit exhibits an excellent combination of high compression strength, high abrasion resistance, high chemical resistance, high thermal shock resistance and high degree of refractoriness.It also retains its hardness at higher temperature than other ceramics(Suchaneket al., 2010).Thus, alumina has found widespread applications in industry and medicine ranging from electronic substrates, grinding media, cutting tools, abrasion resistant tiles, to bioceramics(hip-joints).The physical properties of alumina are summarizedin Table 2.1.

Alumina (Al_2O_3) is the compound of aluminium and oxygen. Al_2O_3 usually occurs in nature, mostly as the mineral corundum and other form such as the precious gemstones, ruby and sapphire. Alumina exists in several metastable crystalline structures: η-, γ-, δ-, θ-, β-, κ-, χ, and α-alumina. Hexagonal α-alumina with lattice parameters of a = 4.758 Å and c = 12.991 Å is the most thermodynamically stable phase of alumina (Shackelford and Doremus, 2008).

Table 2.1 Alumina physical properties (Cheremisinoff, 1990)

Physical properties	$\alpha - Al_2O_3$
Density, g/cm^3	3.96
Melting temperature, °C	2054
Elastic modulus, GPa	520
Coefficient of thermal expansion (25-1000°C),10^{-6}/°C	8.5
Indentation hardness,GPa	20

Alumina as a biomaterial,has been used for more than 40 years, because of its good bio-inertcharacteristics, high corrosion resistance, hardness, excellent biocompatibility, and stability in the human body. The first generation of aluminaproduced for industrial applications was ofpoor microstructure with low density, lowpurity and large grain sizes due to long sintering times. Thus, it was unsuitable for biomedical applications(ASTM F603-1983; ISO 6474, 1994). Then alumina has been developedin a positive wayto producebioceramic materialswith satisfactory medical application properties. Therefore, aluminaof high purity with goodbiostabilityand biocompatibility characteristicsis suitable for ceramic bone substitution materials as bone spacers, bone replacements, and components of orthopedics joint prostheses.However, alumina also has disadvantages of low purity and low toughness that influenceonquality of alumina materialfororthopedics application. Many factors, like grain size, density and purity,influencethe mechanical properties of alumina such as the wear rate that decreases with decreasing grain size (Mukhopadhyaya and Yiu-Winga, 1993).

2.1.2 Zirconia (ZrO$_2$)

Natural zirconium dioxide (ZrO$_2$,zirconia) is generally obtained from baddeleyite (ZrSiO$_2$) with a monoclinic crystalline structure.Zirconia has three crystallographic forms, namely: monoclinic, tetragonal and cubic phases, as shown in

Figure 2.1.Normally pure zirconia has a monocliniccrystal structure at room temperature. The tetragonal phase is formed starting from 1170°C up to 2730°C and the cubic phase at higher temperature.The transformation of pure zirconia from the tetragonal phase to monoclinic one occurs during cooling at about 950°C. To use the full potential of zirconia, the properties of the zirconia should bemodified extensively by the addition of a stabilizing oxide. Sufficient amount of additive could help in transformation a partially stabilized zirconia (PSZ) to a fully stabilized that is in a cubic form. Various oxides such as magnesium oxide (MgO), calcium oxide (CaO), and yttrium oxide (Y_2O_3) are usually addedfor stabilize zirconia to be in the cubic phase. Therefore, zirconia is usefulin a stable phase and whichphase of ZrO_2 should be stabilizeddepends on application. Upon heating, zirconia undergoes disruptive phase changes by addition of small percentages of additives. However, the tetragonal phase is ametastable one. When stressesed,the tetragonal phase at a crack tip is converted to the monoclinic with the volume expansion of 4.6 vol.%.This expansiongenerates both dilatational and shear stresses, and these stresses could prohibit the crack propagation and enhance the fracture toughness properties of zirconia.This mechanism is known as a phase transformation toughening which significantly extends the reliability andlifetime of products made with stabilized zirconia (Stevens, 1986).
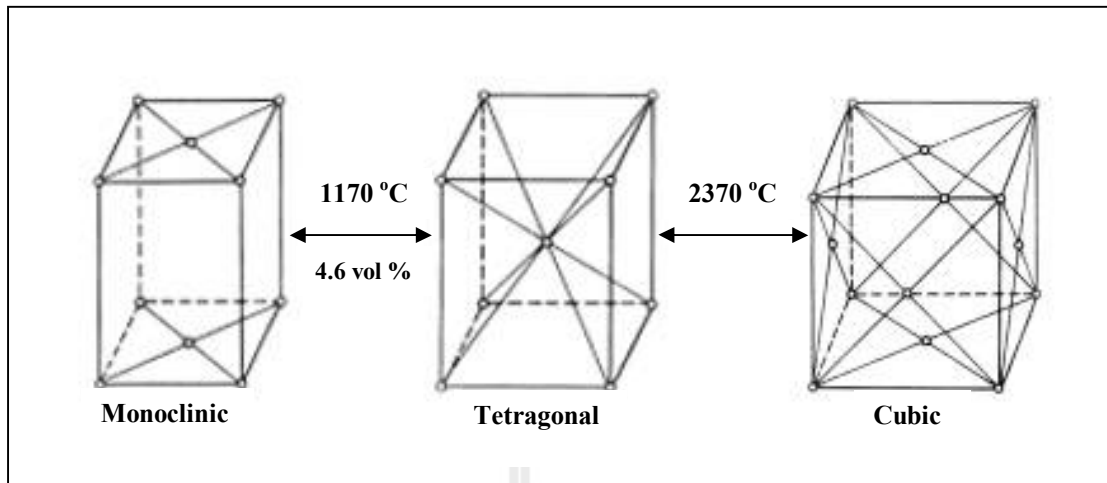
Figure2.1 Crystallographic forms of zirconia

2.1.2.1 Stabilization of zirconia

Magnesium oxide (MgO), calcium oxide (CaO), and yttrium oxide (Y_2O_3) oxides are used as the additive for zirconia stabilizationto form:

1. Partially stabilized zirconia

2. Tetragonal zirconia polycrystals

3. Partially stabilized zirconia in a non zirconia matrix

Zirconia microstructure and compositeabbreviations are explained below:

TZP   Tetragonal zirconia polycrystals

PSZ   Partially stabilized zirconia

FSZ   Fully stabilized zirconia

TTC   Transformation toughened ceramics

ZTA   Zirconia toughened alumina

TTZ   Transformation toughened zirconia
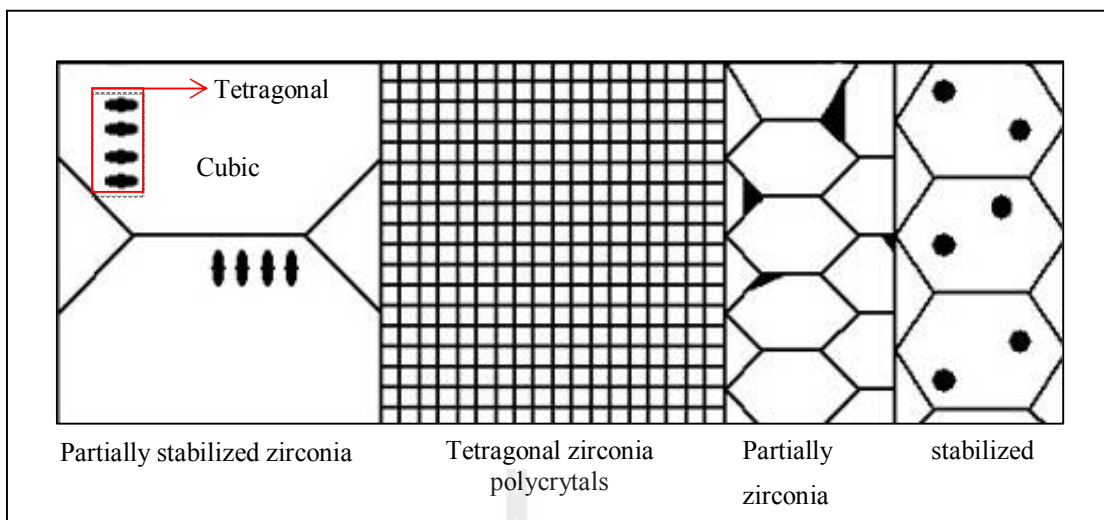
Figure 2.2 Transformation toughened zirconia schematic microstructures

(Birkby, 1994)

2.1.2.2 Partially stabilized zirconia

Partially stabilized zirconia with tetragonal phaseis formed by adding the stabilizing additivessuch as MgO, CaO, and Y_2O_3 etc. Ideally, the stabilizing additive should be uniformly distributed on an atomic scale. The phases of zirconia are illustrated on the phase diagram shown in Figure 2.3 for ZrO_2-MgO system. The ZrO_2 with 6-8 mol% MgO content at 2000°C to 2450°C shows the solid solution state with cubic phase. However, when the materials are quenched, ZrO_2 phase will change into the tetragonal phase. This process is fundamental for the partially stabilized zirconia (PSZ).
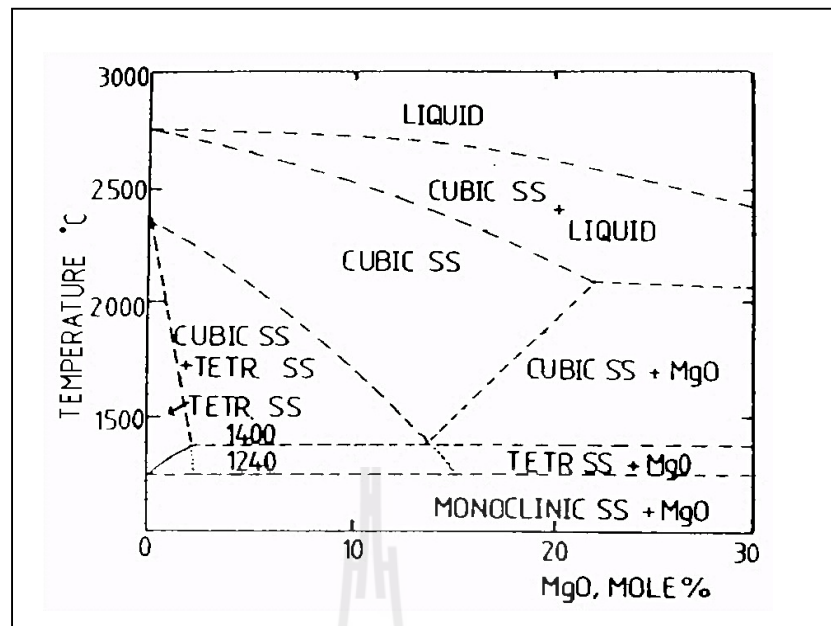
Figure 2.3 The ZrO_2 – MgO phase diagram (Grain, 1967)

2.1.2.3 Tetragonal zirconia polycrystals

The tetragonal zirconia phase is stabilized using Y_2O_3 additive as a stabilizer. Considering phase diagram of ZrO_2-Y_2O_3 system shown in Figure 2.4,almost all of zirconia is in the tetragonal-phase fieldin the composition range of 0-5 mol% of Y_2O_3 at 1300°C to 1650°C heating temperature. The composition containing greater than 5mol% amount of yttriastabilizes 'non transformable'zirconia when cooling to the room temperature.In addition, it has been found that the critical grain size also depends on the amount of stabilizer added and the degree of mechanical constraint. Such factors are interdependent, as illustrated by the relationship of the critical grain size with stabilizer content on 'as sintered' surface, as shown in Figure 2.5(Stevens, 1986).
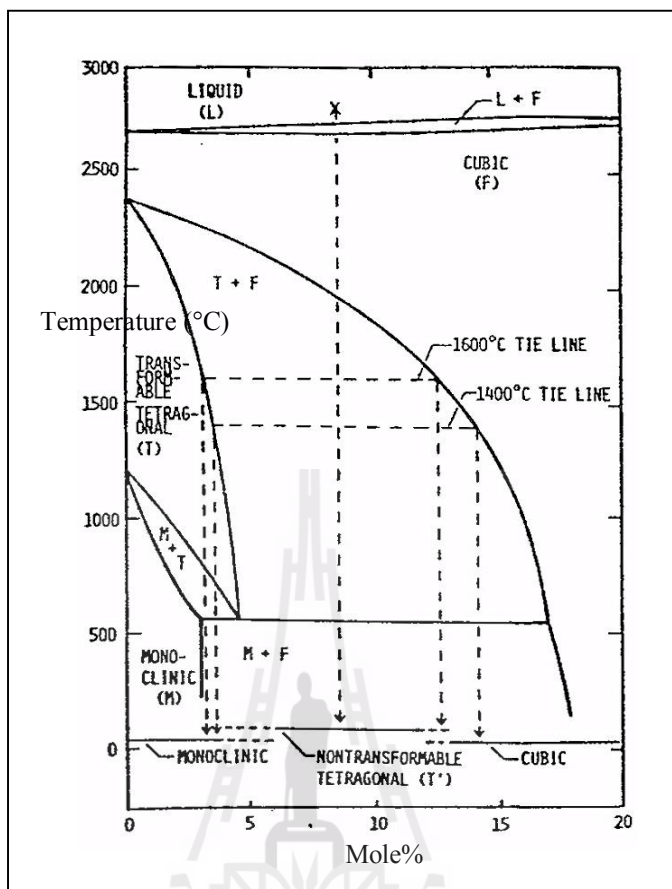
Figure 2.4 The ZrO_2 – Y_2O_3 phase diagram (Stevens, 1986)
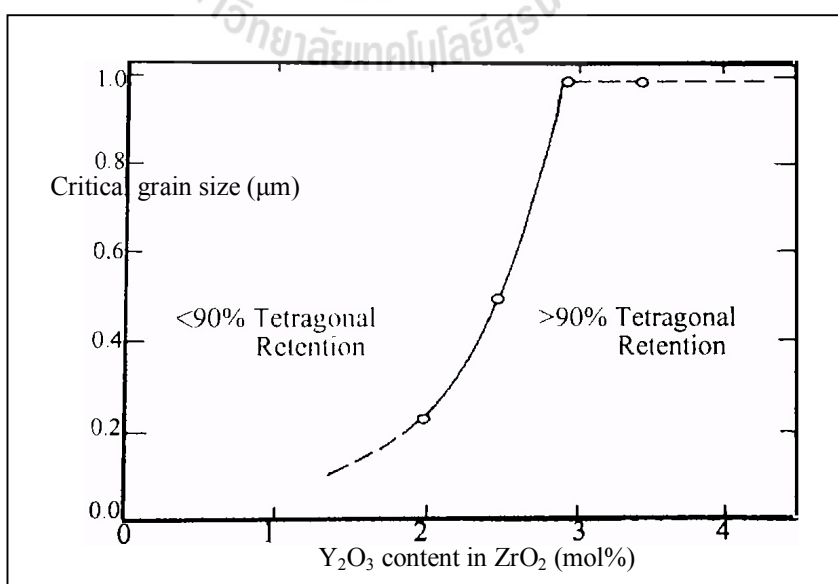
Figure 2.5 Dependence of the critical grain size on the yttria content (Stevens, 1986)

2.1.2.4 Partially stabilized zirconia in non zirconia matrix

The use of fine zirconia particles less than one micrometer distributed in the other matrix leads to the formation of so-called partially stabilized zirconia in non-zirconia matrix such as zirconia toughened alumina (ZTA) or zirconia toughenedmullite (ZTM).

2.1.3   Composite materials

Composite materials are materials made from two or more constituent materials with significantly different physical or chemical properties.The composite material is the one way to produce new materials with characteristics different from the individual components. The individual components are separated and distinct within the finished structure. The new materials are preferred for many reasons.For instance,the composite materials are used in engineering applications where a single component material could not provide the specific properties. There are two main categories of constituent materials: matrix and reinforcement. The matrix material forms a continuous phase that surrounds and supports the reinforcement materials by maintaining their relative positions. The reinforcements impart their special mechanical and physical properties to enhance the matrix properties.Normally, the reinforcements should be harder, stronger, and stiffer than the matrix. They may be spherical, platelets, or any other regular or irregular geometry. Thus, the application of composite materials opens a new way for materials development to reach target forimproving the lifetime of orthopedic implant materials.

Tuan et al. (2002) reported that,the strength of the Al_2O_3 / (tetragonal ZrO_2 + monoclinic ZrO_2) composites reached values as high as 940 MPa, which is roughly three times that of Al_2O_3 alone. The addition of both t-phase and m-phase

zirconia, also could enhance the toughness of alumina.The toughening effect was attributed mainly by the zirconia tetragonal to monoclinic phase transformation.

Weimin et al. (2008) studied the effects of the contents of ZrO_2 3 mol% Y_2O_3 and ZrO_2 2 mol% Y_2O_3 on the densification of composite samples prepared by the wet chemical method. The results showed that when the contents of $ZrO_2$3 mol%and ZrO_2 with 2 mol% Y_2O_3 were 15 and 20 vol. %, the relative densities of the Al_2O_3/ZrO_2 (Y_2O_3) composites were 99.6% and 99.1%, and the average grain sizes of ZrO_2 (Y_2O_3) were 1.3 and 1.5 μm, respectively.

Bocanegra-Bernal et al.(2009) studied the densification of submicron alumina powders by pressureless sintering and sintered-HIP process. The relative density of over 98% was obtained with sample preformed at 150 MPa by using uniaxial pressing and sintered at 1350°C by sintered-HIP process. The grains of submicron size were obtained withpressurelesssinteringand sintered-HIP process. The low remaining porosity seems to be responsiblefor the high hardness and fracture toughnessof the sample prepared bysintered-HIP process.

2.2   Toughening phase transformation of zirconia

The addition of zirconia results in anincreaseof both strength and fracture toughness of ceramics due tothe tetragonal to monoclinic phase transformation of metastable tetragonal particles induced by the presence of the stress field ahead of crack. The expansion volume of 3-5% during phase transformation provides the stress field around zirconia particles that is useful to inhibit crack propagation in materials, and the shear strain. Thestress fields developed in the martensitic reaction were recognized as opposing the opening of the crack and therefore acting to increase the

resistance of ceramics to crack propagation by stress induced phase transformation of zirconia.The micro-cracking can be induced by incorporatingZrO_2 particles in ceramic matrix such as Al_2O_3 or mullite.It is generally recognized that apart from crack deflection which can occur in two phases ceramics, the tetragonal to monoclinic phase transformations can develop significantly improved mechanical properties via this mechanism(Stevens, 1986).In addition to the transformation toughening associated with the tetragonal – monoclinic phase transformation around particles in front of crack, other mechanisms, such as crack deflection, crack bridging and the presence of microcracks, may also contribute to the toughness enhancement.

2.2.1   Stress induced phase transformation toughening

During cooling of ZrO_2 from over 1200°C to room temperature the tetragonal phase will be transformed to the monoclinic one. However, when ZrO_2 is finely dispersedor constraining pressure is exerted on it by matrixthen the zirconia particles can be retained in metastable tetragonal form. The zirconia particles can be introduced as a second phase during the initial fabrication. The toughening mechanism is considered as a stress induced phase transformation of the metastable tetragonal phase to monoclinic form when crack is propagatingunder stress, large tensile stresses are created around the crack and especially at the crack tip, as shown in Figure 2.6. The zirconia particles are increasing the volume expansion > 3% and shear strain ~ 1-7%, with the resultant compressive strain being generated in the matrix. These phenomena occur around the crack(Stevens, 1986).
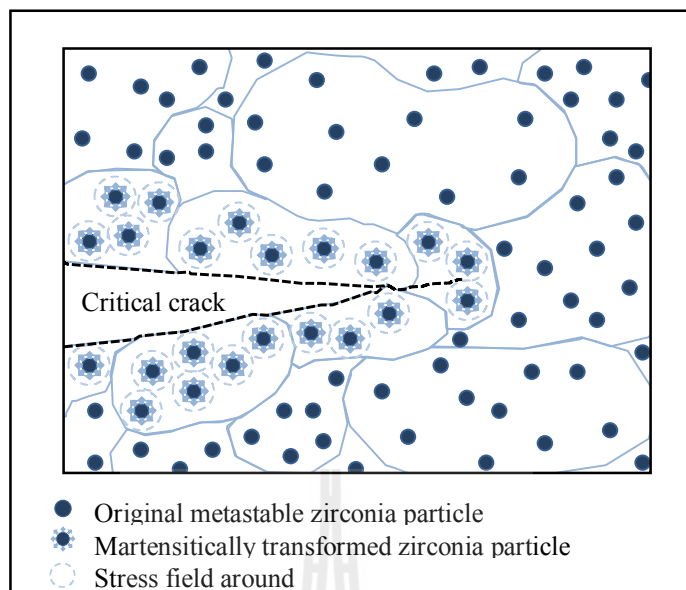
Figure 2.6 Stress induced phase transformation of metastable ZrO_2 particle in the

elastic stress field of crack

2.3   Preparation of Al_2O_3/ZrO_2 micro/nano composite

The mechanical properties of composite materials depend on several factors such as reinforcement type, content, homogeneity and microstructure. Previous results have been reported that allfactors mentioned above affect to the effectiveness of mechanical properties of materials. Thus,many attempts have been made to develop thenew powder processing techniques with Al_2O_3-ZrO_2 systemthat could produce better microstructurefor improving the mechanical properties of Al_2O_3-ZrO_2 composite system.

2.3.1   Conventional Powder Processing

The uniformity of thedistribution of reinforcing phases in the sintered composite significantly effects on the mechanical properties of materials. Moreover, the uniform distribution of the reinforcing particles in the powder mixture used for

sintering will largely governthe phase distribution in the sintered composite. However, it is really difficult to achieve the uniform mixing of small particles of a few micrometers or less than micrometer in diameter by conventional powder processing. Ideally, in a binary mixing process the various species should intimately be mixed so that any small sample taken from the mixture would contain the optimized proportion of the composition. This is considerably hard to achieve, particularly with cohesive powder or if the compositions to be mixed aredifferent in size. When the particles are cohesive, they naturally to agglomerates and particle mixing involves breaking up agglomerates.For the constituents differ in size or density there is an increasing tendency for segregation.

2.3.2 Colloidal Processing

The new powder processing techniquessuch as sol-gel, CVD and powder alkoxide mixture could be utilized to attain the high uniformity dispersion of small zirconia particles with narrow size distribution to increase the fracture toughness of alumina.Schehl et al. (2002) reportedthatthe colloidal processing route has many advantages compared to conventional processing routes. The nano-composites with a very small amount of secondary phases can be synthesized and the formation of these phases can be predicted by referring to the information presented in phase equilibrium diagrams of the powder-alkoxide mixture. New composites can easily be designed when consider the phase evolution as a function of temperature and the thermal expansion coefficient of the different phases. The powder processing route could also produce homogeneous microstructures with a narrow particle size distribution of secondary phases and high final densities.
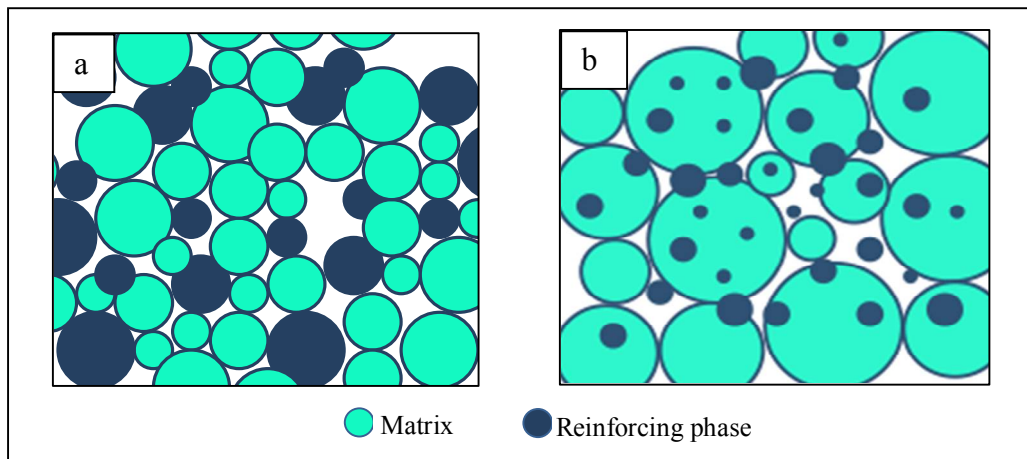
Figure 2.7 Illustration of mixture model of composite system with particles different in size, (a) Conventional Powder Processing and (b) Colloidal Processing (powder alkoxide mixture)
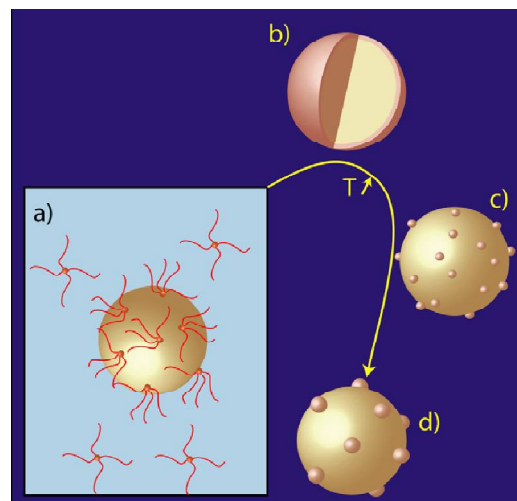
Figure2.8 Illustration of alumina–zirconia composite via modified colloidal route: (a) zirconium precursor and alumina powder are dispersed in liquid medium; (b) after drying, alumina powder is coated by a zirconium precursor layer; (c and d) during thermal treatments, the layer decomposes and zirconia nanoparticles nucleate and grow on the surface of the alumina grains (Rafferty et al., 2009)

Schehl et al. (2002) investigated the preparation Al_2O_3/ZrO_2 micro/nano composite via colloidal processing. This system has many advantages compared with classical processing route. Nano-composites with a very small amount of secondary phases, very homogeneous microstructure with a narrow particle size distribution of secondary phases and high final density could be obtained by using powder alkoxide mixture method. The reinforcing phases are in nanoscaleuniform size and distributed at alumina grain boundaries, thus increasing the effectiveness of the reinforcement mechanism that operates in these nanocomposites.

De Aza et al.(2002) investigated a new generation of alumina–zirconia nano-composites having a high resistance to crack propagation, and as a consequence may offer the option to improve lifetime and reliability of ceramic joint prosthesis. A major research effort was concentrated on a new colloidal processing. The microstructure of sintered composite was very fine with submicrometer alumina grains and, mainly intergranular, nano-size zirconia particles with narrow grain size distribution. The sample density was upto 98% of theoretical density with10vol% of zirconia contentsand the value of composite hardness was similar to that of alumina. The microstructure obtained by the colloidal technique was very fine with submicrometer alumina grains and, mainly intergranular, nano-sized zirconia particles.

Ye et al. (2008) prepared the yttria-stabilized ZrO_2/Al_2O_3 (abridged as YSZ/Al_2O_3) nano-composite ceramics by co-precipitation method. The relative density of the YSZ/Al_2O_3nano-ceramics was over 95% and hardness as high as 19.8 GPa were obtained by the pressureless sintering.

Rafferty et al. (2009) manufactured the alumina–zirconia composites by two routes: powder processing and colloidal processing. Additions of glacial acetic acid were needed to form stable suspensions. The composite prepared via the colloidal method exhibited much higher mechanical properties than the powder processed equivalent.

Calderon-Moreno et al. (2004) studied the microstructure evolution during superplastic creep of alumina-zirconia prepared viapowder-alkoxide mixture.The microstructure of alumina-zirconia washomogeneous with a narrow grain size distribution. Almostall of zirconia particles were located at the triple junction of alumina grains. The composite microstructure is advantageous for achieving superplastic deformation without significant creep damage. The zirconia addition using powder-alkoxide mixture method can significantly increase the ductility of alumina-base composite by controlling grain size and distribution of both phases.

2.4   Characterization

2.4.1   Image analysis

The development of advanced ceramic materials on the basis of widely recognized intrinsic relationships between their properties and microstructure should, thus, rely on robust and reliable techniques of microstructural analysis. When ceramic materials are fabricated, their properties will be determined by the microstructure,

which depends on the process used. To characterizethe composite microstructure of samples at various sintering temperatures, the corresponding binary images are analyzed on the grain and void size distributions, and the areal fraction of each component by using the image analysis software.An image analysis is a powerful tool that quickly gives objective results on the particle size, dispersion, orientation, shape, numbers of objects, etc.The spatial distribution of grains or phase aremeasured by generating large number of circles of specified diameter at random positions in the image and checking whether they overlap or touch objects on binary image with white background, as shown in Figure2.9.
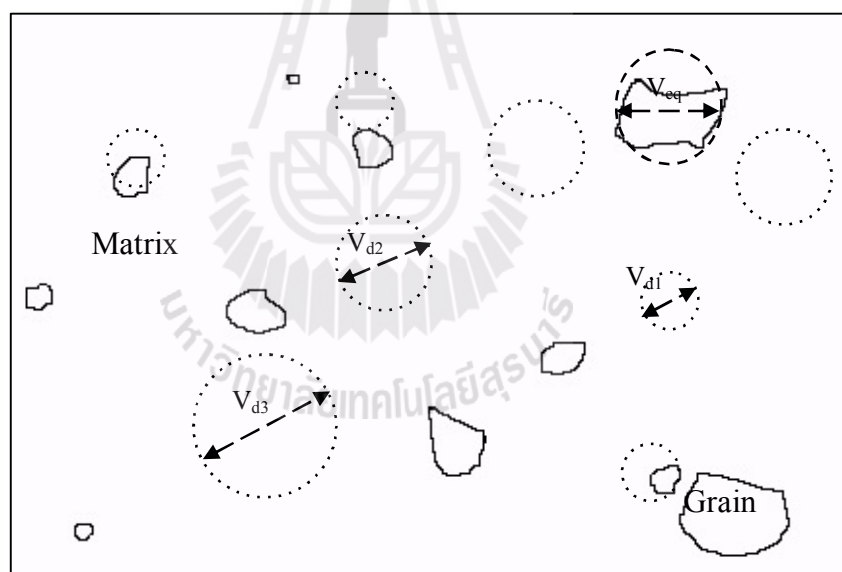
Figure 2.9 Illustration of measurement of grain and void size distributions

The distribution of grain sizes was measured, after detection of boundaries of all grains on the binary image of *i*-component of each grain area, for more than 80 grains in terms of the Heywood, projected area equivalent, diameter, $D_{eq,i,j}$ as follows:

$$D_{\text{eq},i,j} = \sqrt{\frac{4 \cdot A_{i,j}}{\pi}} \qquad\qquad (2.1)$$

where $A_{i,j}$ is the area of the j-object of i-component.

The percentage of i-component in the sintered sample was computed as an areal fraction, A_i :

$$A_i = \frac{\sum_{j=1}^{N} A_{i,j}}{A_t} \qquad\qquad (2.2)$$

where N is the total number of objects of i-component and A_t is the total analyzing area of the binary image.

The spatial distribution of grains or phase is an important microstructure characteristic of sintered composites, which coulddefine the mechanical properties. Here, an existence probability function of circular voidsof size, V_d, fitted in the interspaces among grains is used to express the uniformity of grain distribution. The void size distributions measured in such a way were fitted with a theoretical distribution curve proposed by Alonso *et al.* (1995). The theoretical equation was derived as the distribution of the probability of finding of a spherical void of a given size in the random packing of equal-sized spheres. It allows for the infinite number of void spheres of any size. In the case of the sintered composite sample, the packing of irregular-shaped grains differs from that of the ideal spherical

particles. Therefore, an adjustable parameter,v_m, was used in the theoretical distribution equation instead of v_{HCP} for more close fitting of experimental curves (Oidaet al., 1999). The existence probability function, $P(\chi_2)$, of finding of the circular void of diameter equal or greater than χ_2 obtained by sectioning the void sphere of diameter χ_3 was evaluated as:

$$P(\chi_2) = \frac{3v(1-v)}{1-(v/v_m)} \int_{\chi_2}^{\infty} (1+\chi_3)^2 \times \sqrt{1-\left(\frac{\chi_2}{\chi_3}\right)^2} \exp\left\{-\frac{v}{1-(v/v_m)} \times [(1+\chi_3)^3 - 1]\right\} d\chi_3 \quad (2.3)$$

where$v$ is the packing density and (1-v) is the probability of finding a void space of any size; in other words, when a certain point is selected at random within the cross-section of a sintered sample, the point has the probability, (1-v),belonging to the void space between grains. χ_2 and χ_3 are the diameters of the circular and the spherical voids normalized with the associated average grain size, respectively.

Horovistizand Muccillo(2011) developed a digital image processing and analysis method to evaluate the microstructural features of chemically synthesized gadolinia-doped ceria powders containing small amounts of co-dopants. The effects of particles/clusters sizes, porosity and grain size distribution were examined in detail and compared to those parameters of the standard composition without co-dopants.The digital image processing-assisted quantitative analysisof micrographs was carried out in thisstudies.The method provides plenty of data that are fairly important for the purpose of thestudyand can be extended to other systems.

Kangwantrakoolet.al. (2003)characterized quantitatively the microstructure of WC-Co/TiC-Al$_2$O$_3$ sintered composites by means of the image analysis. The areal fraction, the grain size distribution and the uniformity of spatial

distribution expressed by the void size distribution of each component have been correlated with the mechanical properties of samples such as Vicker's hardness and transverse rupture strength under various sintering temperatures. Void size distributions of total components were relatively uniform due to the high degree of mixing of powder achieved in ahigh impact machine. Further, more uniform dispersions of WC and Al_2O_3 grains were obtained at low sintering temperature, while TiC-WC phase was dispersed uniformly at high temperature. Thus, the areal fraction and spatial uniformity of WC and Al_2O_3 components were most influential to the higher strength of composite, while the higher hardness wasgoverned by those of β-phase.

Thus, the sintered microstructures could be characterized quantitatively by measuring void and grain size distributions with the aids of image analysis. These data could be correlated with mechanical properties of sintered materials to provide important information on composite particles preparation method and sintering conditions.

CHAPTER III

EXPERIMENTAL

3.1   Experimental equipment

Equipment and devices used in this research are listed in Table 3.1.

Table 3.1 Equipment and devices used in this research

Equipment	Manufacturer	Model
High Temperature Furnace (1800°C)	Carbolite	HTF 18/10
Cold Isostatic Press (CIP)	Avure Technologies	L CIP 22260
Uniaxial Press	Carver	2702
Microhardness Tester	Galileo	Microscan/Isoscan Ac Plus
Universal Testing Machine	Instron	5565
Scaning Electron Microscope (SEM)	JEOL	JSM-6010
Energy Dispersion X-ray Spectrometer (EDS)	JEOL	JSM-7800 & AURIGA
X-ray Diffractometer (XRD)	Bruker	D2 Advance
Grinding & Polisher Machine	Buehler	Ecomet5
High speed Diamond Saw	Buehler	Isomet 1000
Ball Mill	Cernusco	Conlrols
pH meter	Mettler Toledo	Seven Compact

3.2 Raw materials

Raw materials used in this research are listed in Table 3.2.

Table 3.2 Raw materials used in this research

Raw materials	Chemical formula	Manufacturer	Grade/Type
Alumina powder	Al_2O_3	ACC product	A-5M 5 micron
Zirconium IV propoxide, (70 wt% solution in 1-propanol)	$Zr(OCH_2CH_2CH_3)_4$	Sigma-Aldrich	-
Acetic acid	$C_2H_4O_2$	VWR BDH Prolabo	100% purity
Polyvinyl Alcohols (PVA)	Molecular Weight 77,000-82,000	Ajax Finechem	Analytical grade

3.2.1 Alumina powder (Aluminium oxide)

Alumina powder (Al_2O_3) A-5M of average particlesize of 5 micronswas utilizedto form a matrixof the sinteredcomposite. According to information supplied by the manufacturer, the purity of alumina powder is 99.7% by weight and themain impuritiesare sodium 0.26%, silica 0.02% and ferric oxide 0.01%.

3.2.2 Zirconium IV propoxide solution

The zirconium propoxidesolution is the solution of zirconium propoxide(70wt%) in 1- propanol. The density of solution is 1.004 g/cm^3. Thus, 100 mlor 100 gof solution contains70 g of zirconium propoxide. The molecular weight of zirconium propoxide, $Zr(OCH_2CH_2CH_3)_4$ or $ZrO_4C_{12}H_{28}$, is 327.58 g/mole.

During heating, zirconium propoxide decomposesreleasing carbon dioxide and water according to the reaction:

$$Zr(OCH_2CH_2CH_3)_4 + 18O_2 \longrightarrow ZrO_2 + 12CO_2 + 14H_2O. \qquad (3.1)$$
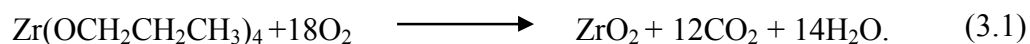
On the right hand side of equation, only ZrO_2 remains as a solid. Thus, one mole of zirconium oxide is formed from one mole of zirconium propoxide. In terms of the molecular weight, this can be expressed as:

$$327.58 \text{ g} \longrightarrow 123.22 \text{ g} \qquad (3.2)$$

As zirconium propoxide is used as 70 wt% solution, 100 ml of the solution contains $70 \times (123.22/327.58)$ g = 26.33 g of zirconia (Rafferty et al., 2009).

Therefore, 100 g of composite material consisting of 90 g of alumina and 10 g of ZrO_2 will require: $10 \times (100/26.33)$ = 37.98 ml of Zirconium (IV) propoxide solution.

3.3 Experimental procedure

3.3.1 Preparation of composite powder

The Al_2O_3/ZrO_2 Micro/Nano composite powderwasprepared via chemical route by the powder alkoxidemethod.The composition of composite material was fixed at 90wt% (91.59 mole%) of alumina powder and 10wt% (8.41 mole%) of ZrO_2. Tuan et al.(2002)reported thatthe optimum contentof meta-stable ZrO_2 phasein aluminaproviding good mechanical properties to composite materialsis 10wt%. To study the distribution of nanozirconia particles in alumina matrix,Zrpropoxidewas mixed with absolute ethanolin different proportions, as summarized in Table 3.3. The absolute ethanol was used dilute Zrpropoxide because of smallermolecule than propanol that easier to remove.A flow chart of the preparation procedure of composite

powder is shown in Figure 3.1.The compositions of composite materials are shown in Table 3.4.α-alumina powder(90 g) was mixed withabsolute ethanol (270 g)at a weight ratio of 3:1 using ball milling with alumina ballsto obtain colloidal alumina. Acetic acid (25 g approx)was used to improve stability of colloidal aluminadispersion by adjusting the pH at 7.1.The isoelectric point of alumina particles suspended in ethanolwas stable at pH 7.1(Wang et al., 1997).pH of colloidal alumina was measured by a commercial pH meter. The zirconium solution was prepared by dilutingofzirconium IV propoxidesolutionwith ethanol.The fixed amountof Zrpropoxideof37.98 g was mixedwith a specified amount of ethanol (Table 3.4)using a magnetic stirrer.The stabilized colloidal aluminawas addeddropwisefrom a pipette into Zrpropoxidesolution under stirring to prepare the slurry. The slurry was first dried on a heater equipped withmagnetic stirrer at 70°C. Then, theresidual ethanol was removed by heatingpowder in an oven at 120°C for 24 hours. Dried synthesized powder wasde-agglomerated using analumina mortar and sieved with screen No. 325 mesh to less than 45 μm. Finely, powder wascalcined at 850°C for 2 hoursin air.The calcination temperature profile is shown in Figure 3.2. After calcination the composite powder was agglomerated and need to be broken down to tens micrometers. Thus, powder was again de-agglomerated using the alumina mortarand sieved to less than 45 μm to obtain fine composite powder.

Table 3.3 Zrpropoxidein ethanol solution compositions

Sample code	Zrpropoxide: Ethanol weight ratios		Zrpropoxide: ethanol weight concentration
	Zrpropoxide	Ethanol	
100	1	-	100
75	3	1	75
66.7	2	1	66.7
50	1	1	50
33.3	1	2	33.3
25	1	3	25

Table 3.4 Thevolume and weight composition of composite material

Sample code	Zrpropoxide ethanolsolution (ZrO_2 10 g)			Alumina suspension (Al_2O_3 90 g)	
	Zrpropoxide solution	Ethanol		Al_2O_3 (g)	Ethanol (g)
	(ml/g)	(ml)	(g)		
100	37.98	0	0	90	270
75	37.98	16.05	12.66	90	270
66.7	37.98	24.07	18.99	90	270
50	37.98	48.14	37.98	90	270
33.3	37.98	96.27	75.96	90	270
25	37.98	144.41	113.94	90	270

| Alumina Powder (90 g) | Ethanol 99.9% (270 g) | | Zirconium IV Propoxide (fixed amount at 37.98 ml/g) | Ethanol 99.9% Ratio 1, 2, 3 |

```
Alumina Powder          Ethanol 99.9%              Zirconium IV Propoxide        Ethanol 99.9%
   (90 g)                 (270 g)                  (fixed amount at 37.98 ml/g)   Ratio 1, 2, 3
       └──────┬──────────────┘                              └──────────┬──────────────┘
              ▼                                                        ▼
   Ball milling with alumina balls                              Sol
              │                                          (Zrpropoxide solution)
              ▼                                                        │
       Alumina suspension                                             │
              │                                                       │
              ▼                                                       ▼
   Adjust pH to 7.1          Dropwise addition              Mixing with
   by acetic acid (25 g) ──▶ from a pipette        ──▶     magnetic stirrer
                                                                      │
                                                                      ▼
                                                                   Slurry
                                                                      │
                                                                      ▼
   Dried Powder  ◀──  Removing of residual  ◀──  Drying at 70°C on
                      ethanol by oven              hot plate with stirrer
        │             at 120°C, 24 h in air
        ▼
   De-agglomeration
   with mortar
        │
        ▼
   Powder
   Characterization
        │
        ▼
   Calcination
   at 850°C, 2 h in air
        │
        ▼
   Attrition mill with de
   ionization water using
   alumina balls for 1h
        │
        ▼
   Drying at 120°C, 24 h
   in air
        │
        ▼
   Sieving          ──▶   Al2O3/ZrO2        ──▶   Characterization
   45μm aperture           Composite powder        Phase analysis by XRD
```

Figure 3.1 Al_2O_3/ZrO_2 Micro/Nano composite powder preparation process
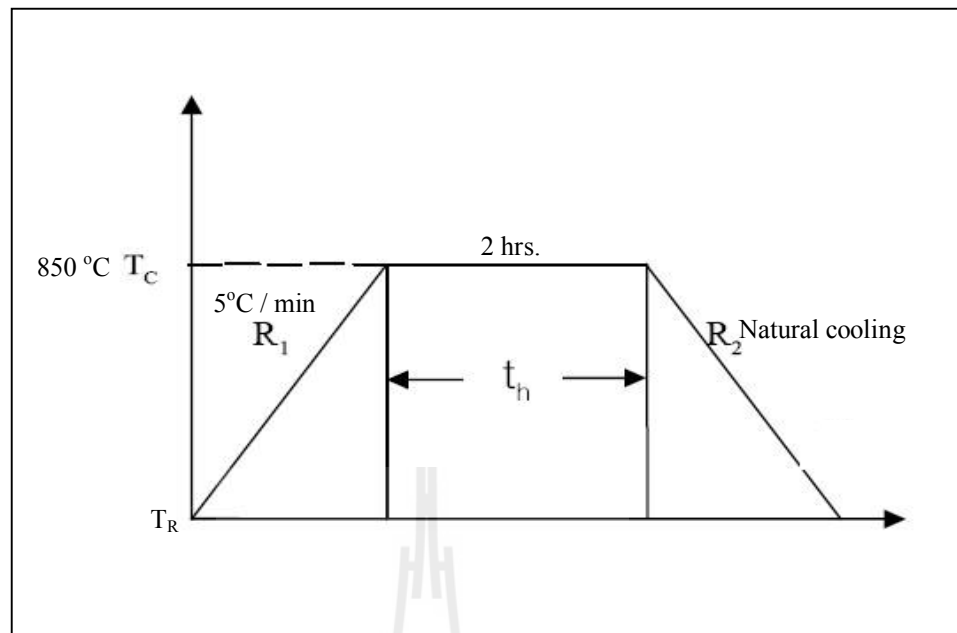
Figure 3.2 Diagram of calcination process of composite powder

3.3.2 Sintered composite preparation and characterization

The flowchart of sintered composite preparation and characterization processesis shown in Figure 3.3. Al_2O_3/ZrO_2micro/nanocomposite powderwas mixed with0.5 wt.%polyvinyl alcohol (PVA) binder withmolecular weight ranging from 77,000 to 82,000g/mol. 10wt% PVA solution was prepared bydissolving PVA in deionized water.Then, binder was sprayed into composite powder andthecomposite powder was screened through a 60 mesh in order to obtain composite granules. 15 g of composite granuleswere preformedin 3.5 × 3.5 cm iron mold at 100 MPa by using anuniaxial press and subsequently consolidated by cold isostatic pressing (CIP) at 350 MPa to improve the green strength of samples. The CIPed composite samples were sintered at three different sintering temperatures,1600°C, 1650°C and 1700°C for 4 hoursunder pressureless sinteringusing an electric furnace to investigate the effect of sintering temperature on the microstructure and mechanical properties of sintered

composite. The diagram of sintering process is shown in Figure 3.4.
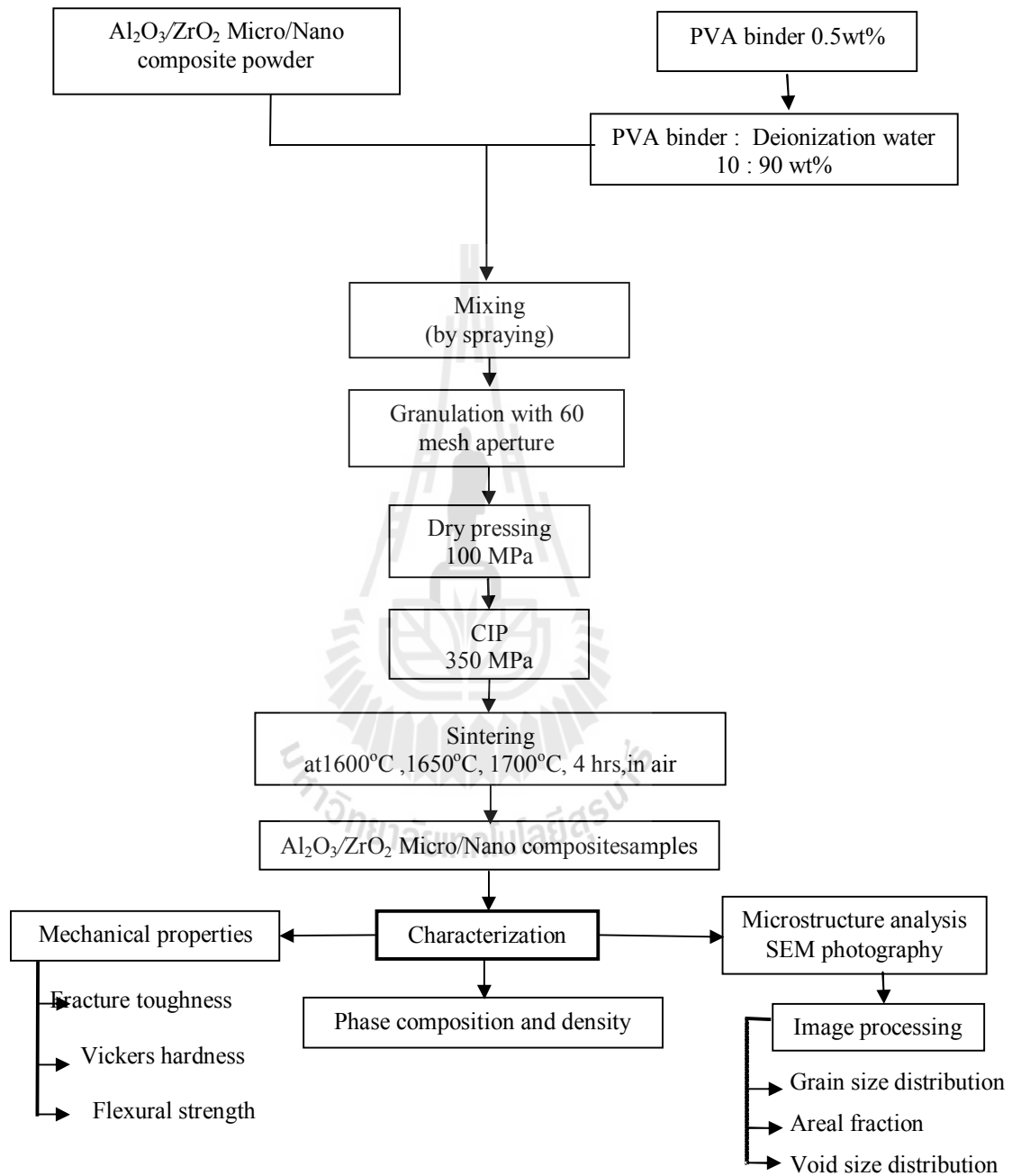
Figure 3.3 Al_2O_3/ZrO_2 Micro/Nano composite preparation and characterization
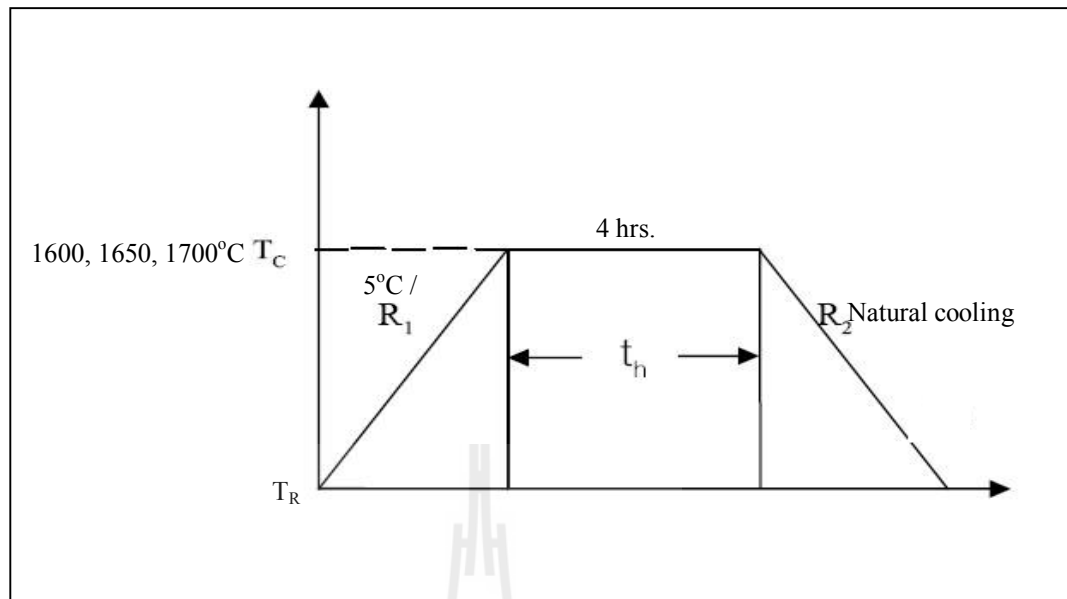
Figure 3.4 Diagram of sintering process of composite

3.4 Characterization

3.4.1 Phase characterization

Crystalline phases and thepercentage of crystallinity of synthesized composite powder and sintered composite sample were examined by powder X-ray diffraction (XRD) using Bruker Model D2Advance for composite powder and Bruker model D8Advance forsintered compositeunder the following conditions:

Radiation	=	$Cu\text{-}K_\alpha$
Generator voltage	=	40 kV
Generator current	=	40 mA
Start angle 2θ	=	20°
End angle 2θ	=	80°
Step time	=	0.5 s
Step size	=	0.02°

The quantitative of each elements of composite was analyzed by using TOPAS program.

3.4.2 Density measurement

The density of sintered samples was measured following ASTM C373-88 standard (1994). The Archimedes' methodwas utilized for measuring the density of sintered composites using deionized water.The dry weight of 5 specimens of sintered composite was measured after heating specimens in an oven at 150°C and cooling down in desiccator (WD).Then specimens were boiled for 5 hrs and soak for an additional 24 hrs. After thatdeterminethe mass of each specimen while suspended in deionizedwater (Wss) and thesaturated mass (W_s)were determined

The density of sintered samples was calculated by:

$$\text{Volumeof sample } (V) = W_S-W_{SS}$$

$$\text{Bulk density} = W_D/V$$

where W_{SS} is the apparent weight of the sample in fluid,

W_S is the weight of the saturated fluid,

W_D is the dry sample weight.

The bulkdensity of sintered composite was compared to theoreticaldensity of 90% alumina and 10% zirconia calculated following rule of mixtureas:

Theoretical density of 90% Al_2O_3 and 10% ZrO_2

$$\left(\frac{\%_i}{100}\right)(\rho_i) + \left(\frac{\%_{ii}}{100}\right)(\rho_{ii}) = \rho_{total} \tag{3.3}$$

where $\%_i$ is percentage of i component

   $\%_{ii}$ is percentage of ii component

   ρ_i is density of i component

   ρ_{ii} is density of ii component

$$\text{Relative density} \quad = \frac{\text{bulk density}}{\text{theoretical density}} \times 100\% \tag{3.4}$$

3.4.3   Mechanical properties

3.4.3.1 Flexural strength

The flexural strength of sintered composite was measured using the three-point bending method following ASTM C1161-94 with Universal Testing Machine (UTM). The composite materials were cut with diamond blades rotated at 150 RPM under 150 g of load. Specimenswere chamfered with sandpapers from No. 400 to 1500 and testedunder the following conditions:

Sample size (mm)   ~   5 x 5 x 30

Span length (mm)   =   20

Crosshead speed (mm/sec)   =   0.2

Number of specimens   =   5

Room temperature
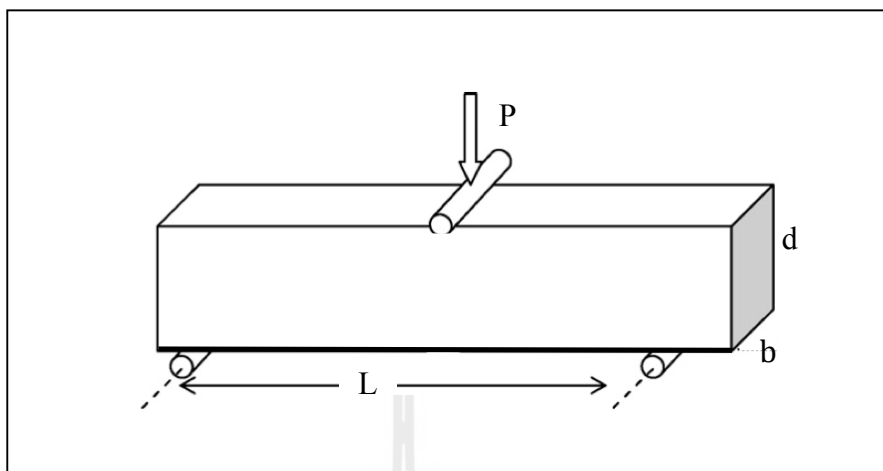
Figure 3.5 Illustration of three-point bending method

The flexural strength of sintered specimen wascalculated by:

$$MOR = \frac{3PL}{2bd^2} \quad \text{MPa} \tag{3.5}$$

where MOR =   Flexural strength of specimen (MPa)

P   =   Critical load (N)

L   =   Supporting span length (mm)

b   =   Specimen width (mm)

d   =   Specimen height (mm)

The mean of flexural strength can be expressed as:

$$\overline{X} = \frac{\sum X}{N} \tag{3.6}$$

where $\overline{X}$ = Mean of flexural strength

$\sum X$ = Summation of flexural strength values

N = Number of specimens

The standard deviation of flexural strength was evaluated as:

$$S.D. = \sqrt{\frac{\sum_{i=1}^{N}(X_i - \overline{X})^2}{N}} \qquad (3.7)$$

where S.D. = Standard deviation of flexural strength

x_i = Flexural strength of specimen

$\overline{X}$ = Mean of flexural strength

N = Number of specimens

3.4.3.2 Vickers hardness

The hardness of sintered composite was determined by using Vickershardness indentation method with GALILEO micro-hardness tester. The surface of specimen was polished with sandpapersfrom No. 180 to 1500in various directions as shown in Figure 3.6.Then, thesurface of material was finished using 0.3micron alumina polishing slurry. Finally, the specimen was cleaned upwith ethanol before testingunder the following conditions:

Load (kg) = 5 (49.033 N)

Soaking time (s) = 15

Number of indentations = 25

Magnification for measure indentation = 400×

Indenter   =   136°
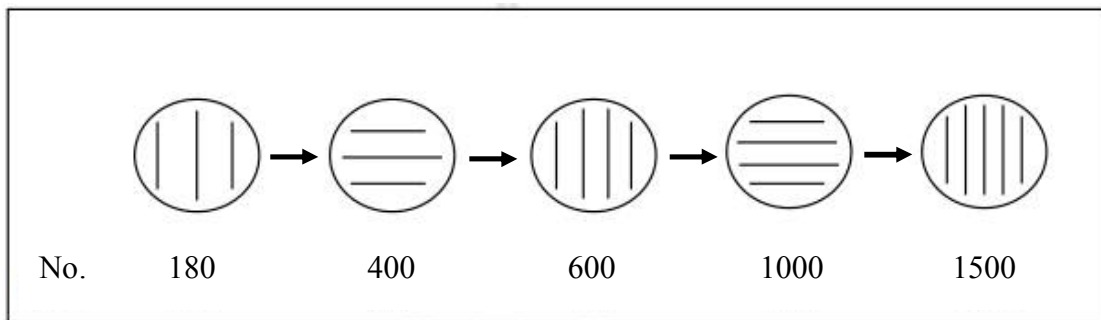
Figure 3.6 Sandpaper machining procedure
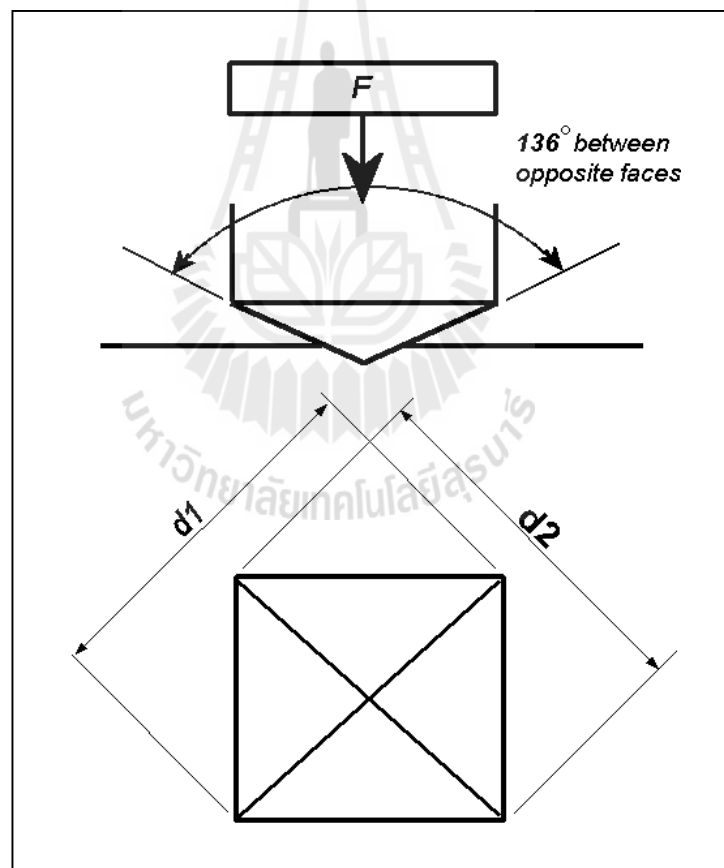
Figure 3.7 Illustration of Vickers hardness method

The Vickers hardness of specimen can be expressed as:

$$\text{Vickers hardness (N/mm}^2) \ = \frac{0.1891 \cdot F}{d^2},$$ (3.8)

where d = Arithmetic mean of the two diagonals, d1 and d2 (mm)

F = Load (N)

3.4.3.3 Fracture toughness

The fracture toughness of sintered composite was measured by utilizing the single edge notch beam (SENB) method with INSTRON universal testing machine (UTM). The specimen was cut with0.3 mm in thicknessdiamond bladerotated at 150 RPM underload 150 g following sample size and chamfered with sandpapers No. 400 to 1500. The sampleswere center-notched to half of their thickness using 0.3 mm thick diamond blades as show in Figure 3.8. Finally, the specimen was cleaned up by ethanol. Theconditions for measuring follow:

Sample size (mm) ~ 3 x 5 x 20

Supporting span length (mm), (S) = 15

Notch depths (mm), (c) ~ 1.5

Crosshead speed (mm/sec) = 0.1

Number of specimens = 5

Room temperature
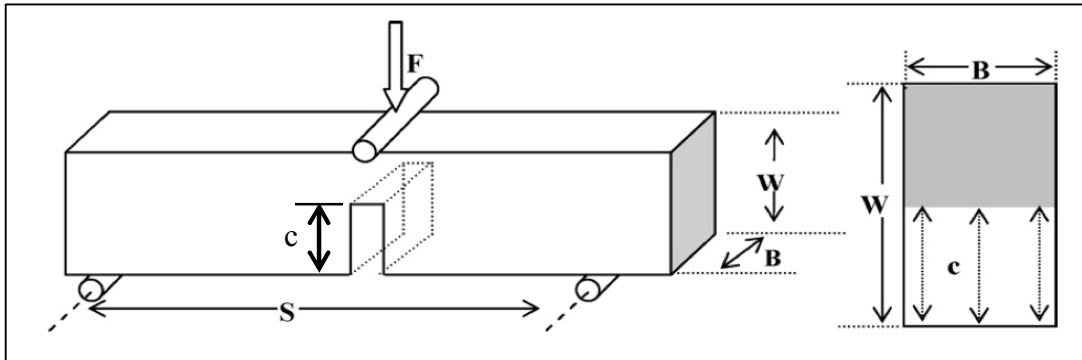
Figure 3.8 Illustration of single edge notch beam (SENB) method

(Wang et al., 2007)

The fracture toughness of sintered specimen was evaluated by:

$$K_{IC} = \frac{F_c}{B} \frac{S}{W^{3/2}} \, f\left(\frac{c}{W}\right)$$

$$f\left(\frac{c}{W}\right) = 2.9\left(\frac{c}{W}\right)^{1/2} - 4.6\left(\frac{c}{W}\right)^{3/2} + 21.8\left(\frac{c}{W}\right)^{5/2}$$

$$-37.6\left(\frac{c}{W}\right)^{7/2} + 38.7\left(\frac{c}{W}\right)^{9/2},$$

(3.9)

where F_c =   Critical load (N)

   B   =   Specimen width (mm)

   S   =   Supporting span length (mm)

   $f\left(\frac{c}{W}\right)$ =   Stress intensity shape factors

   c   =   Saw depth (mm)

   w   =   Specimen height

3.4.4 Microstructure characterization

The cross-section surface of sintered composite was polished with sandpapers (No. 180-1500)as shown in Figure 3.6.Then, the surface of material was

finished with 0.3micron alumina polishing slurry and thermallyetched at 100°C below the sintering temperature for 1 hour to obtain clearly grain boundaries of each components. This procedure was used toprepare cross-section surface of sintered composite sample for analyses the elements of composite and microstructure. The distribution of individual elements ofzirconia and aluminain the sintered samples was detected by an energy dispersive x-ray spectrometry (EDS)(JEOL JSM-7800 & AURIGA). Themicrostructures were observed by means of a scanning electron microscopy (SEM), (JEOL JSM6010LV). The specimenSEM micrographs weretaken at magnification X2000. Each SEM image covers a real sampling area of 64 x 48μm^2.

3.4.4.1 Image Preparation

A flowchart of the SEM image preparation and analysis procedureis shown in Figure 3.9. The digitized SEM imagestaken from sintered samples were importeddirectlyto a computer, as illustrated in Figure 3.10 (a). In the case of composite materials, the discrimination of components caused a major problem in image analysis, since the component gray levels were very close to each other. Therefore, the enhancing software was usedtoadjust thecontrast of image to getreach sharpenedges of each component images, as shown in Figure 3.10 (b).It enabled us to separate accurately the individual phasesofZrO_2 and Al_2O_3. Then, the threshold level of the enhanced image was manually adjusted by using anintensity histogram. This step isextremely important, because it correspondsto the maximum loss of information (Coster and Chermant, 2001). After that, the image having a total range of up to 256 different shades of gray wasconverted into the binary (black and white) one, where white pixelsrepresent Al_2O_3 grains and ZrO_2grains are recognized by theirblack color. To analyze ZrO_2particles in Al_2O_3 matrix, image was adjusted by

using software (ImageJ) to removeAl$_2$O$_3$grain boundaries and pores.Then remaining ZrO$_2$particleslocated in Al$_2$O$_3$ matrix wererendered as shown in Figure 3.10 (c). Finally, only ZrO$_2$particlesembedded in Al$_2$O$_3$grainswere selected by utilizing function in ImageJ program(Figure3.10(d)).
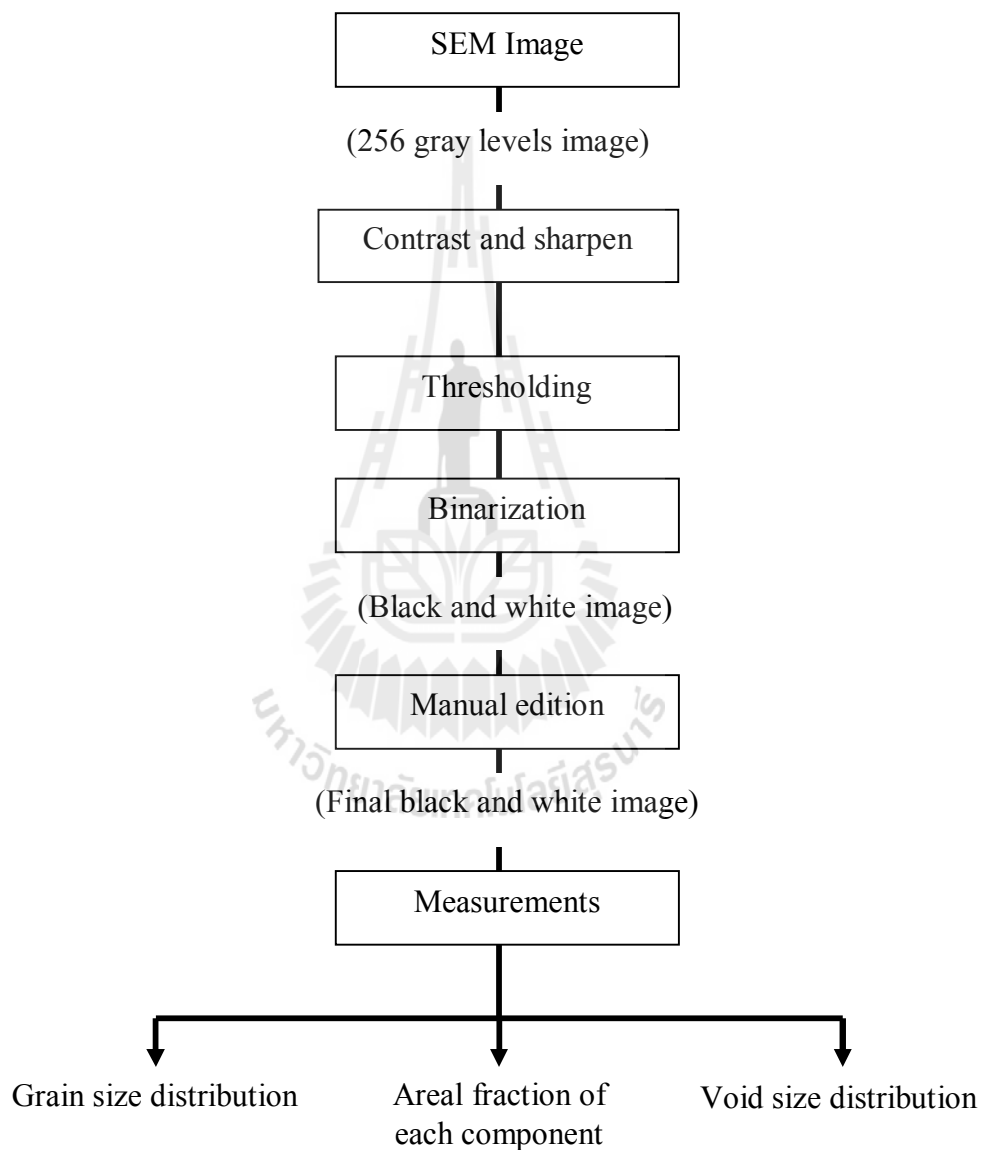
Figure 3.9 Flow chart of image preparation and image analysis procedure
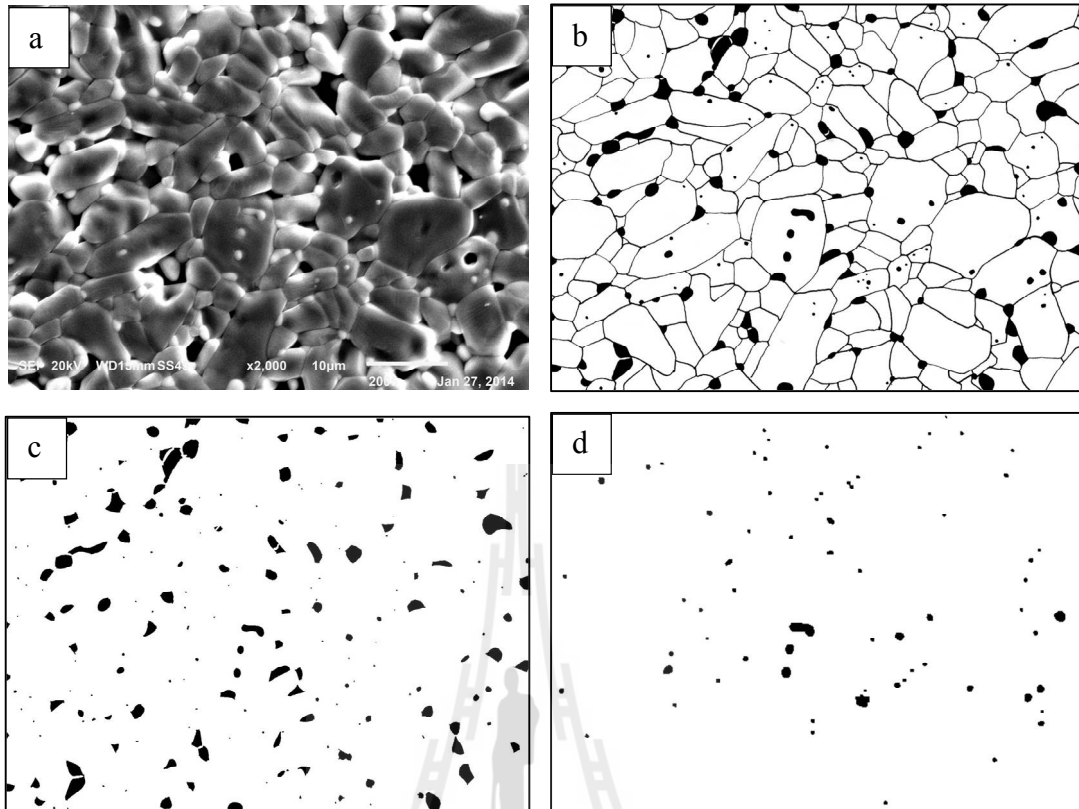
Figure 3.10 Example of phases separation of SEM image of sintered sample

(a) original gray scale SEM image, (b) outline of Al_2O_3grains

(white) and ZrO_2 particles(black), (c) total ZrO_2particles

and (d)ZrO_2 particles embedded inAl_2O_3grains.

3.4.4.2 Grain size distribution

The distribution of grain sizes was measured, after detection of boundaries of all grains in the binary image of i-component in terms of the Heywood, is the equivalent of diameter of circle that has the same area as projected area $D_{eq,i,j}$as follows:

$$D_{eq_{,i,j}} = \sqrt{\frac{4 \cdot A_{i,j}}{\pi}}$$
(3.10)

where $A_{i,j}$ is the area of the j-object of i-component.

3.4.4.3 Areal fraction of component

The percentage of i-component in the sintered sample was computed as an areal fraction, A_i:

$$A_i = \frac{\sum_{j=1}^{N} A_{i,j}}{A_t} \tag{3.11}$$

where N = total number of objects of i–component.

A_t = total analyzing area of the binary image.

3.4.4.3 Void size distribution

The spatial distribution of grains or phases is an important microstructure characteristic of sintered composite, which is closely related to the mechanical properties. Here, an existence probability function of circular voids of size, d_{void}, fitted in the interspaces among grains was used to express the uniformity of grain distribution. For this purpose, the large number of circles of various sizes was randomly positioned all over the binary image of the cross section of the sintered sample. Then, the existence probability of void of certain size was estimated as the proportion of the number of successfully arranged circles to that of the total trials. The void circle was assumed to be arranged successfully in the intergrain space, if it did not overlap grains or touch grain boundaries, as shown in Figure 3.10. For every size of the void circle, 300,000 trials were made to position circle all over the image to measure the spatial distance between grains of zirconia. The results of this process will express the uniformity of zirconia grains distribution in alumina matrix.

Figure 3.11 Illustration of measurement of grain and void size distributions

The spatial distribution of ZrO_2 in Al_2O_3 matrix was analyzed using the image analysis software ImageJ. The macro-program was written for this purpose. At first, the size of the circle was chosen. Then, the loop counter variable was set to 1 and trails started. The coordinates of the circle center were generated using a random number generator.The circle was positioned on the image and the image area covered by circle was checked on existence of black pixels (grains). If no black pixels were detected than the number of successfully arranged circles was increased by one. Then, the next circle of the same size was generated until the loop counter reaches the specified number of trials (100,000). The existence probability of void of chosen size was calculated as the ratio of successfully arranged voids to the number of trials. Thereafter the procedure repeated for circles of various sizes.The illustration of void size distribution measurement is shown in Figure 3.11.
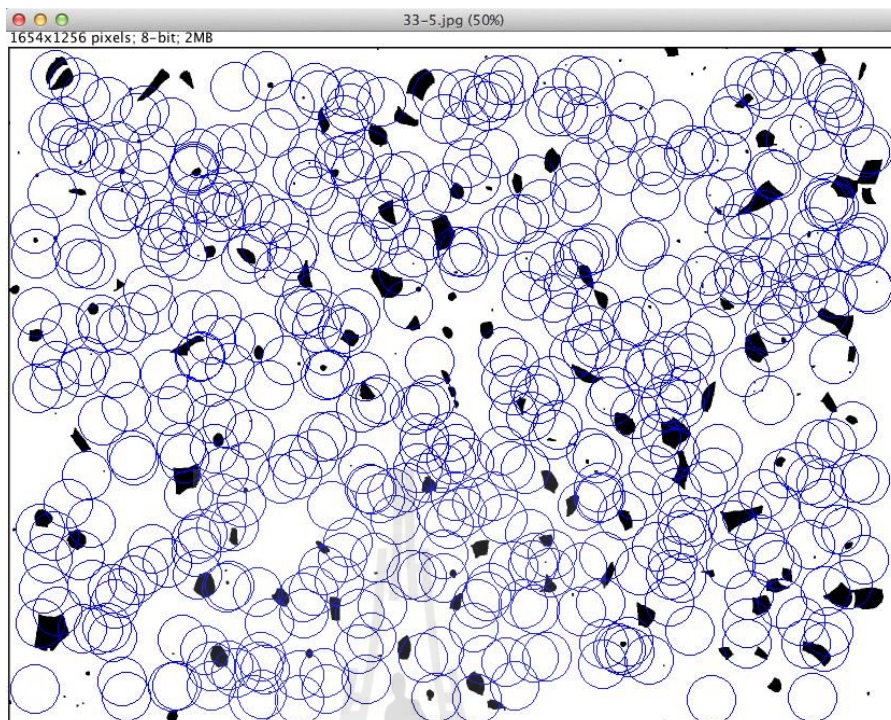
Figure 3.12 Illustration of circular voids generatedby macro-program

To evaluate the uniformity of ZrO_2 particles distribution in the sintered samples, the void sizes distribution data from image analysis were approximatedby the polynomial regression equation:

$$p = c_0 + c_1.d_{void}^1 + c_2.d_{void}^2 + c_3.d_{void}^3 + c_4.d_{void}^4$$

$$+c_5.d_{void}^5 + c_6.d_{void}^6 \qquad (3.12)$$

where p is the probability distribution, d_{void} is the void diameter and c is regression coefficients

The regression coefficients were calculated using the regression data fit software (www.arachnoid.com/polysolve). Then,the void diameter corresponding to the 50% probability, $d_{void,50}$, was calculated by numerical solution ofnonlinear equation (3.13) using Solver function in MicrosoftExcel.

$$p = 0.5 = c_1 . d_{void,50}^1 + c_2 . d_{void,50}^2 + c_3 . d_{void,50}^3$$

$$+ c_4 . d_{void,50}^4 + c_5 . d_{void,50}^5 + c_6 . d_{void,50}^6 \tag{3.13}$$

Here, $d_{void,50}$is the point at which the slope is calculated.To find the slope of approximation curveby the equation (3.13) at the point $d_{void,50}$regression coefficientsc_i and $d_{void,50}$ were substituted in Eq. (3.14) as

$$slope = \frac{dp}{dd} = c_1 + 2 \cdot c_2 d_{void,50} + 3 \cdot c_3 \cdot d_{void,50}^2 + \cdots .$$

$$+ i \cdot c_i \cdot d_{void,50}^{i-1} \tag{3.14}$$

Figure 3.13illustrates the results of evaluation ofuniformity of spatial distribution of ZrO_2 particles in Al_2O_3 matrix of sintered sample.
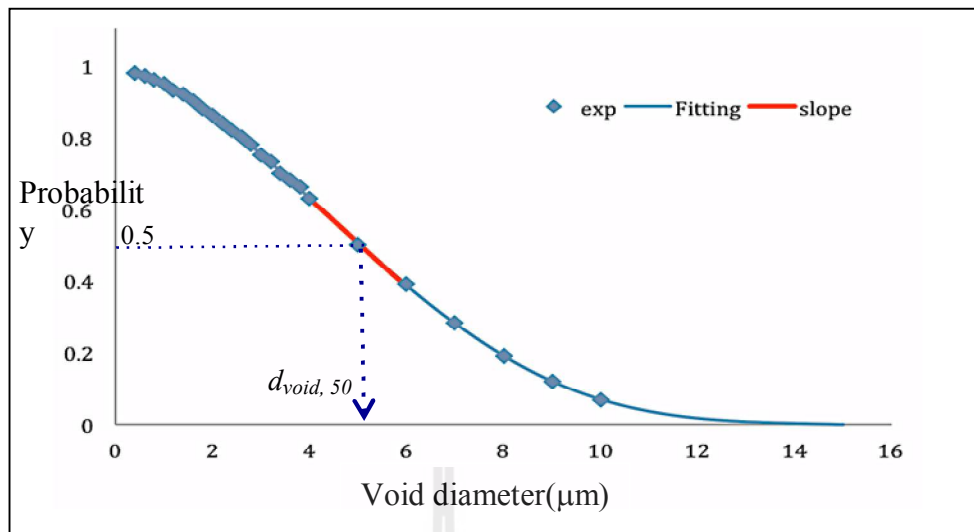
Figure 3.13 Illustration of evaluation of uniformity distributions
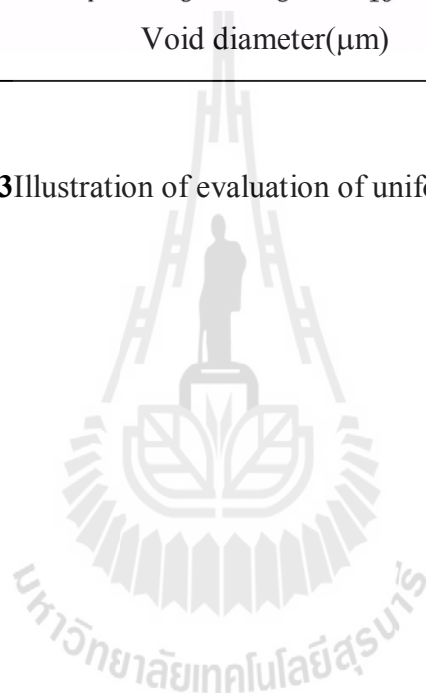
CHAPTER IV

RESULTS AND DISCUSSION

4.1 Effect of Zrpropoxide concentration on phase composition

Al$_2$O$_3$/ZrO$_2$ micro/nano composites have been prepared via powder alkoxide mixture method at various Zrpropoxide solution concentrations. The composite composition was fixed at 90wt% ofalumina and 10wt% of zirconia using Zrpropoxide solution. The effect of the concentration of Zrpropoxide solution on the phase composition was investigated.

4.1.1 Phase composition of composite powder

The X-ray diffraction (XRD) analysis was carried out to confirm the presence of a single phase of α-Al$_2$O$_3$ at 2θ = 35.153 (JCPDS No. 46-1212), the tetragonal ZrO$_2$ phases at 2θ = 30.223 (JCPDS No. 79-1769) and the monoclinic ZrO$_2$ phases at 2θ = 28.213 (JCPDS No. 89-9066)with all samples (Schehl et al.,2002).The TOPAS program was used for analyzed the quantitative of various phase composition of sintered composite. XRD patterns of synthesized (90wt%)Al$_2$O$_3$/(10wt%)ZrO$_2$powder are shown in Figure 4.1. The XRD analysis of everysampleconfirms the presence of the diffraction peak of a single phase of α-Al$_2$O$_3$and the absence of diffraction peaks of tetragonal/monoclinic ZrO$_2$ phases. Therefore, the formation of ZrO$_2$ from Zrpropoxidedid not take place during drying of composite powder at 120°C. However,

the diffraction peaks of the tetragonal and monoclinicZrO_2 phases were detected in every samples of composite powder calcined at 850°C for 2 hours as shown in Figure 4.2. The results indicate that the concentration of Zrpropoxide influences on the phase composition ofcalcined composite powder. The total 10wt% of ZrO_2 in composite materials exhibited the monoclinic ZrO_2 phase increases with an increase in Zrpropoxide concentration while the tetragonal phase significantly declines at higher concentration of Zrpropoxide.
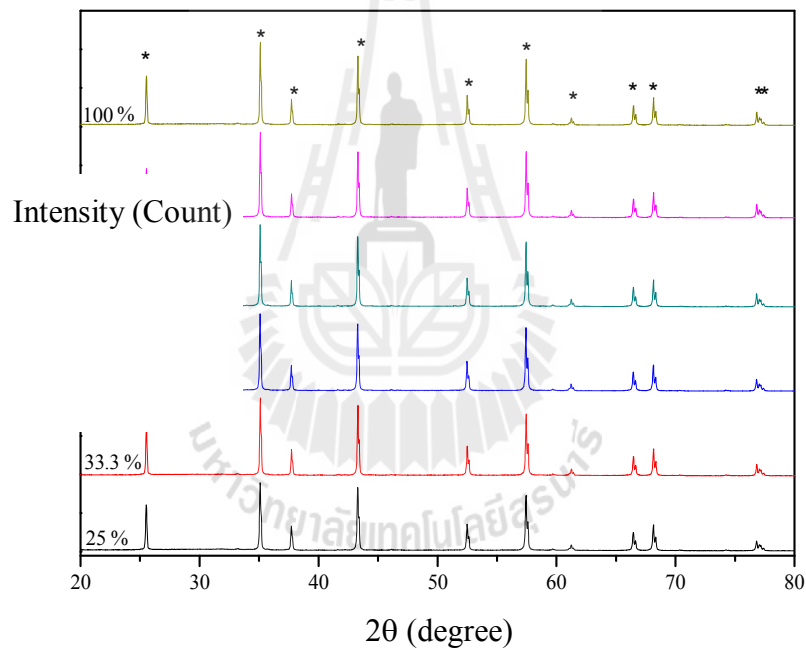
Figure 4.1XRD patterns of (90wt%)Al_2O_3/(10wt%)ZrO_2 Micro/Nano

composite synthesized powder: $* = \alpha\text{-}Al_2O_3$.
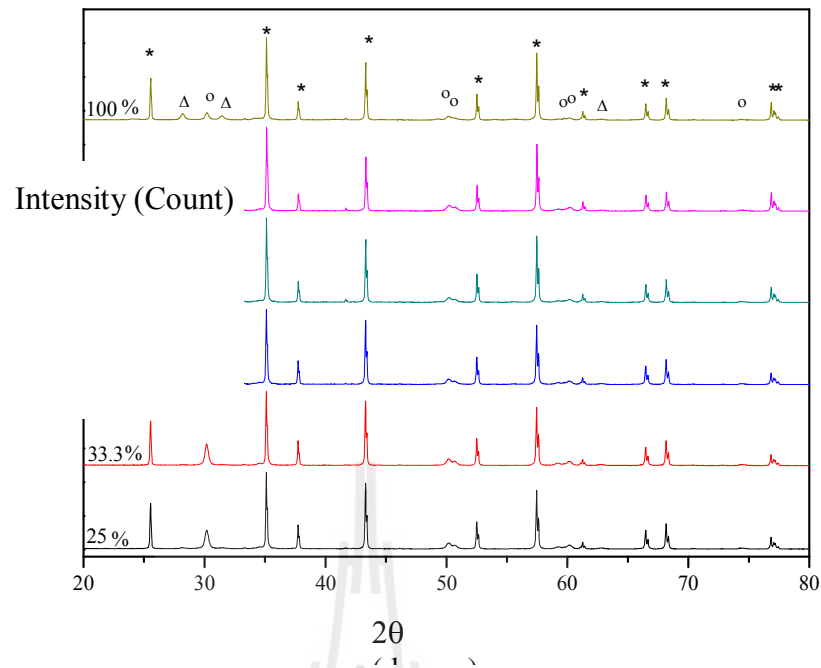
Figure 4.2 XRD patterns of $(90wt\%)Al_2O_3/(10wt\%)ZrO_2$ Micro/Nano composite

calcined powder: $\Delta = m\text{-}ZrO_2$; $o = t\text{-} ZrO_2$; $* = \alpha\text{-}Al_2O_3$.

4.1.2 Phase composition of sintered composite

Figure 4.3 shows the XRD patterns of $(90wt\%)Al_2O_3/(10wt\%)ZrO_2$ composite sintered at 1600°C.The diffraction peaks of the $\alpha\text{-}Al_2O_3$ and the tetragonal and monoclinic ZrO_2 can be detected as shows on this figure. The monoclinic ZrO_2 phase slightly increaseswhile the tetragonal phase decreases with increasingZrpropoxideconcentration. However, sample with 75wt% concentration of Zrpropoxide the intensity of tetragonal ZrO_2 rises. The XRD results indicated Zrpropoxide concentration influenceson the ZrO_2 phase composition of samples sintered at 1600°C.
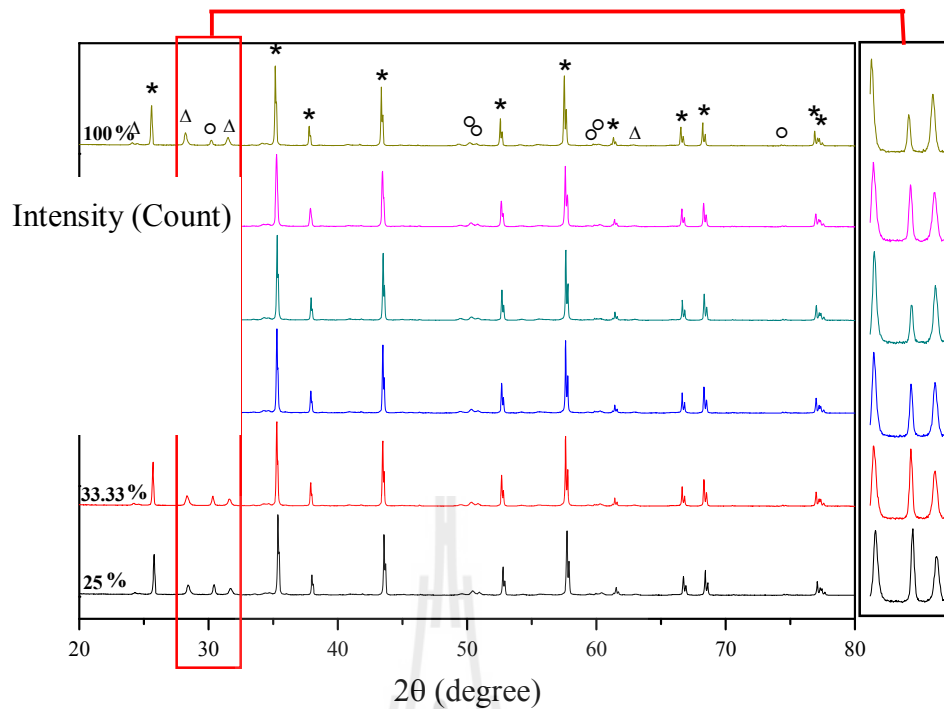
Figure 4.3 XRD patterns of (90wt%)Al$_2$O$_3$/(10wt%)ZrO$_2$ micro/nano composites

sintered at 1600°C: Δ = m-ZrO$_2$; o = t- ZrO$_2$; * = α-Al$_2$O$_3$.

The XRD patterns of composite samples sintered at 1650°C are shown in Figure 4.4. The sintered composites consist α-Al$_2$O$_3$ and both of tetragonal and monoclinic ZrO$_2$ phases. However, the tetragonal ZrO$_2$ phase intensities were slightly lower in comparison with those of composite samples sintered at 1600°C. This is because the transformation rate of zirconia phase depends on the particle sizes (Stevens, 1986). While ZrO$_2$ particles were larger at high sintering temperature (grain growth) the transformation rate of the tetragonal ZrO$_2$ phase decreases. However, the effect of Zrpropoxide concentration on phase composition of samples sintered at 1650°C was exhibited with similar trend samples sintered at lower temperature, i.e. the tetragonal ZrO$_2$ decrease with increasing of Zrpropoxide concentration and sample with 75wt% concentration of Zrpropoxide also increased as same as samples sintered at 1600°C.
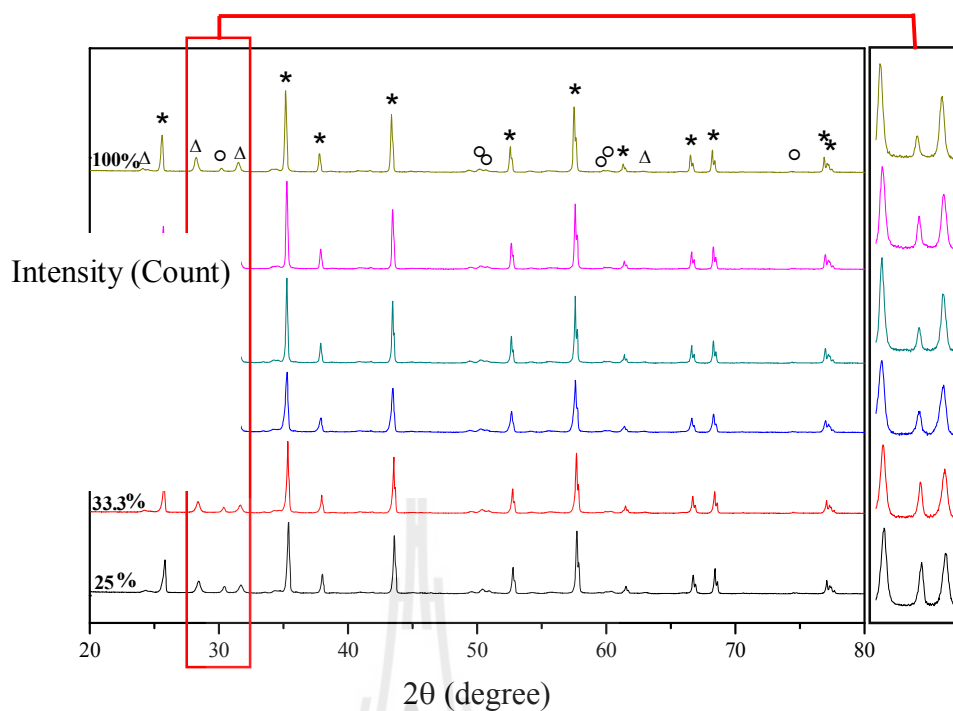
Figure 4.4 XRD patterns of $(90wt\%)Al_2O_3/(10wt\%)ZrO_2$ micro/nano composites sintered at 1650^oC: $\Delta = m\text{-}ZrO_2$; $o = t\text{-}ZrO_2$; $* = \alpha\text{-}Al_2O_3$

The phase composition of samples sintered at 1700°C is shown in Figure 4.5. The phase compositions of these samplesare similar to the compositions of samples sintered at 1600°C and 1650°C. The higher concentration of Zrpropoxide provided the lower intensity of tetragonal ZrO_2. Therefore, composite samples sintered atdifferent sintering temperaturesshowsimilar behavior on variation ofZrpropoxide concentration.
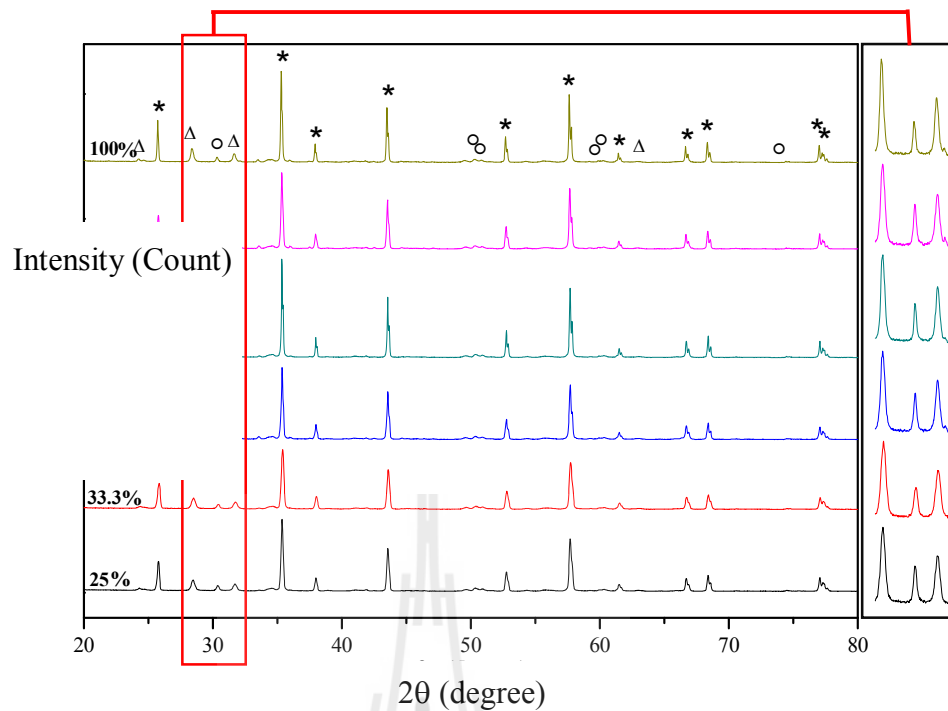
Figure 4.5 XRD patterns of (90wt%)Al_2O_3/(10wt%)ZrO_2 micro/nano composites sintered at 1700^oC: Δ = m-ZrO_2; o = t- ZrO_2; * = α-Al_2O_3.

The XRD results of sintered samples confirmed that the concentration of Zrpropoxide and sintering temperature influence on the ZrO_2 phase composition. The monoclinic ZrO_2 is the predominant phase and the tetragonal ZrO_2 phase decreases with increasing of Zrpropoxide concentration except for the sample with 75wt% concentration. This might be because of the good dispersion of Zrpropoxide in colloidal alumina that provides fine particles of ZrO_2 in Al_2O_3 matrix and effects to ZrO_2 in tetragonal phase. In addition, sintering at high temperature results in the low amount of tetragonal phase. To confirm the quantity of each phases, we used TOPAS program.

The XRD results of samples with the same concentration of Zrpropoxide 25wt% sintered at various sintering temperatures are shown in Fig. 4.6. The results confirmed that the sintering temperature affects to the intensity of ZrO_2 phases. The peak intensity of tetragonal phase decreases with increasing of sintering temperature for samples sintered at 1600°C and 1650°C. However, the intensity of tetragonal ZrO_2 for sample sintered at 1700°C did not differ much compared to the sample sintered at 1650°C. This is because of ZrO_2 grain growth at high sintering temperature and the larger amount of ZrO_2 is normally in monoclinic phase than in tetragonal phase with larger grain(Stevens, 1986).
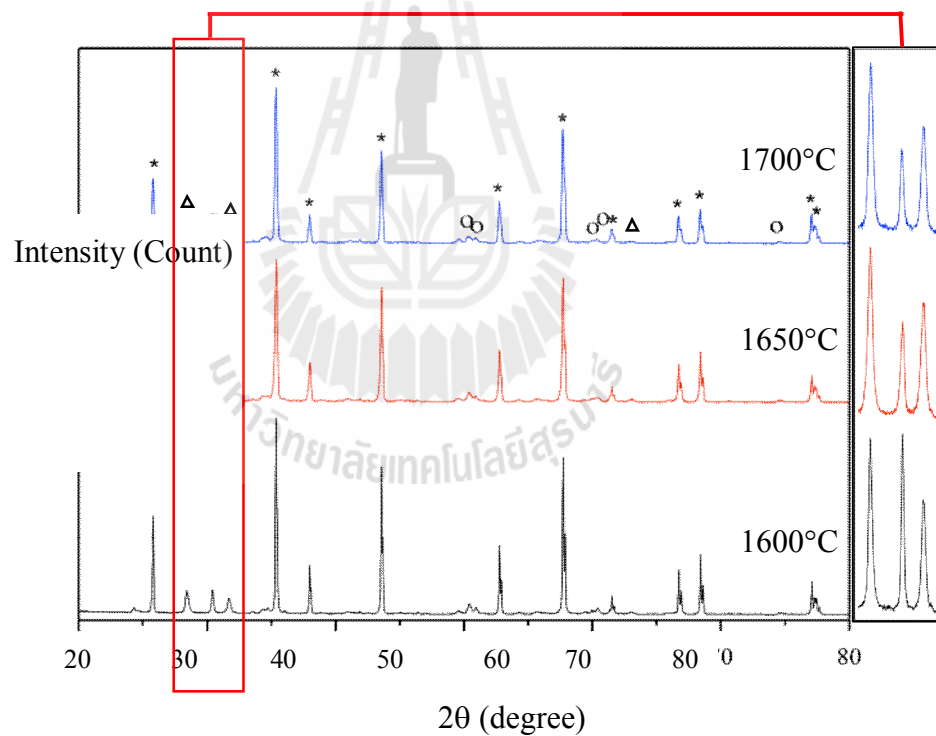
Figure 4.6 XRD patterns of (90wt%)Al_2O_3/(10wt%)ZrO_2 micro/nano compositeswith

25wt% Zrpropoxide concentration sintered at various sintering temperature:

Δ = m-ZrO_2; o = t- ZrO_2; $*$ = α-Al_2O_3

As results of XRD analysis, phase compositions of various sintered composites were quantitative analyzed using TOPAS program. The percentage of various phases are summarized in Table. 4.1. Quantitative results confirmed the phase composition of sintered composites with various Zrpropoxide concentrations. The composite materials had a weight percent composition of $90 \pm 1.5\%$ alumina and $10 \pm 1.5\%$ zirconia. The compositions of sintered composites follow the specified values of 90wt% Al_2O_3 and 10wt% ZrO_2 (Tuan et al. 2002). However, the results show the fluctuation variation of percentage of Al_2O_3 and ZrO_2 because of homogeneity of composites. The phase composition of composite samplesare affected by Zrpropoxide concentration, i.e. at high Zrpropxide concentration the amount of tetragonal zirconia phase decreases while monoclinic zirconia phase rises. The only exception is the sample with 75wt% of Zrpropoxide. The variations of the phase composition of sintered composites with Zrpropoxide concentration show similar behavior for different sintering temperatures. The high content of tetragonal ZrO_2 was obtained with samples sintered at low temperature and low concentration of Zrpropoxide because the monoclinic phase of ZrO_2 dominates over the tetragonal phase at higher sintering temperature (Sachin et al. 2015).
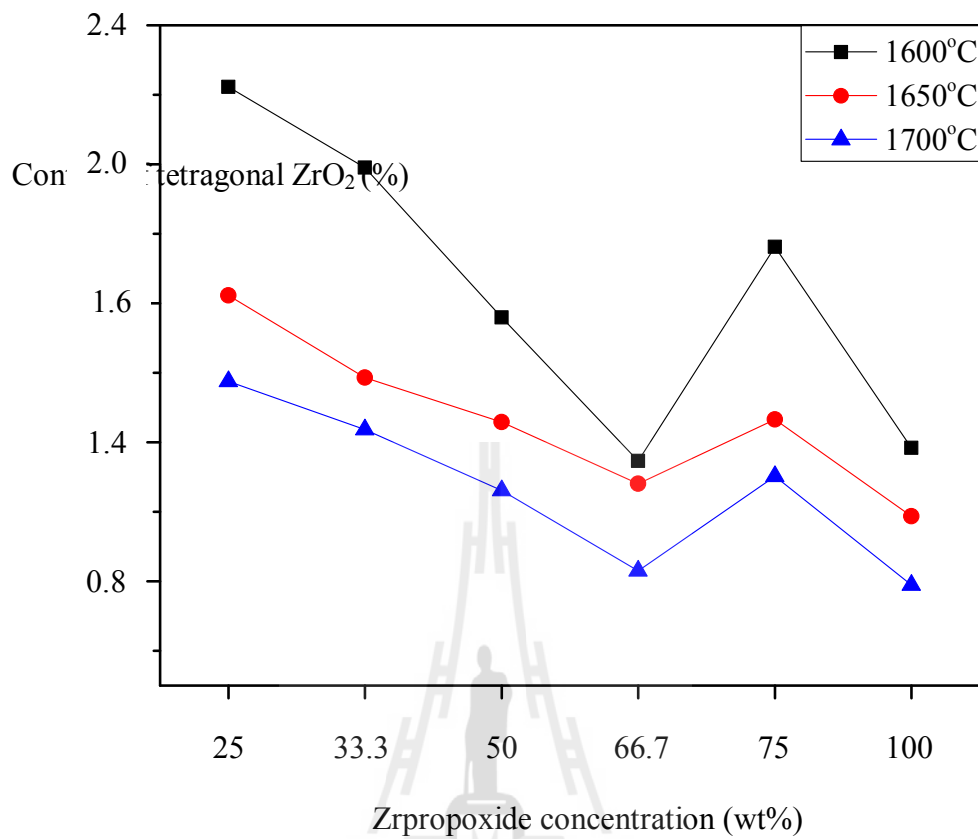
Figure 4.7 Content of tetragonal ZrO_2 as function of Zrpropoxide concentration at various

sintering temperatures

Table 4.1 Results of quantitative analysis of phase composition of sintered

(90wt%)Al_2O_3/(10wt%)ZrO_2 composites

Sintering temperature	Zrpropoxide concentration (wt%)	Alumina (%)	m-ZrO_2 (%)	t-ZrO_2 (%)	Total ZrO_2 (%)
1600°C	25	91.15	6.62	2.22	8.85
	33.3	91.27	6.74	1.99	8.73
	50	91.37	7.06	1.56	8.63
	66.7	91.59	7.26	1.14	8.41
	75	91.12	7.12	1.76	8.88
	100	91.17	7.65	1.18	8.83
1650°C	25	90.63	7.75	1.62	9.37
	33.3	90.61	7.80	1.38	9.39
	50	90.91	7.83	1.26	9.09
	66.7	91.25	7.67	1.08	8.75
	75	90.78	7.95	1.26	9.22
	100	90.96	8.05	0.98	9.04
1700°C	25	90.77	7.89	1.37	9.27
	33.3	90.66	8.10	1.24	9.34
	50	90.56	8.38	1.06	9.44
	66.7	91.11	8.06	0.83	8.89
	75	91.07	7.83	1.10	8.93
	100	91.01	8.20	0.79	8.99

4.2 Effect of sintering temperature on the characteristics of sintered composites

4.2.1 Density of composite

The bulk densities of the composite of 90wt% Al_2O_3 and 10wt% ZrO_2 sintered at various sintering temperatures are shown in Table 4.2. The highest density of composite with $3.82\pm0.027g/cm^3$ was obtained with samples sintered at 1700°C and $3.62\pm0.031g/cm^3$ with samples sintered at 1650°C. The bulk density of sintered composite increases with increasing of sintering temperature due to the high densification rate of compact powder at higher temperature.Furthermore, the samples of various concentration of Zrpropoxide sintered at 1700°C and 1650°C differ only on $\pm$ 0.1 g/cm^3. However, the bulk density of samples sintered at 1600°C differ significantly with various Zrpropoxide concentration. The samples synthesized using 100wt% Zrpropoxide were 0.4 g/cm^3 denser than those produced using 25wt% solution. This might be related to the thermal stress during sintering process and variation of phase composition of samples sintered at 1600°C with Zrpropoxide concentration. High concentration of Zrpropoxide provided high amount of monoclinic ZrO_2 phase with larger volume that pushed to another grain and created micro crack at grain boundaries because they are not as strong as boundaries in samples sintered at higher sintering temperature. Moreover, the diffusion rate is lower in samples sintered at 1600°C than that in simples sintered at 1650°C and 1700°C.

Table 4.2 Bulk densities of sintered (90wt%)Al_2O_3/(10wt%)ZrO_2 composites

Zrpropoxide concentration (wt%)	Bulk density (g/cm^3)		
	1600°C	1650°C	1700°C
25	2.75 ±0.023	3.57 ±0.049	3.82 ±0.027
33.3	2.89 ±0.031	3.50 ±0.143	3.76 ±0.033
50	2.98 ±0.033	3.59 ±0.029	3.79 ±0.028
66.7	3.05 ±0.036	3.54 ±0.027	3.77 ±0.067
75	3.07 ±0.033	3.56 ±0.017	3.74 ±0.089
100	3.14 ±0.018	3.62 ±0.031	3.80 ±0.018

The bulk densities ofsintered composite were compared to the theoretical density of 90wt%Al_2O_3 and 10wt%ZrO_2 calculated by Eq. 3.3. The relative densities of (90wt%)Al_2O_3/(10wt%)ZrO_2micro/nano composites are summarized in Table 4.3. The relative density of sample with low concentration of 25wt% Zrpropoxide concentration sintered at 1700°C was reached to highest value with 92.12±0.66 %. However, the results of bulk density were not significantly different for samples with various concentration of Zrpropoxide because of composition of the composite was fixed at 90wt% Al_2O_3 and 10wt% ZrO_2.

Table 4.3 Relative densities of sintered (90wt%)Al_2O_3/(10wt%)ZrO_2 composites

Zrpropoxide concentration (wt%)	Relative density (%)		
	1600°C	1650°C	1700°C
25	66.35±0.57	86.05±1.20	92.12±0.66
33.3	69.65 ±0.86	84.30±3.45	90.61±0.81
50	71.90±0.80	86.62±0.71	91.33±0.68
66.7	73.53±0.88	85.33±0.66	90.90±1.01
75	74.07±0.81	85.90±0.41	90.15±0.45
100	75.62±0.43	87.33±0.77	91.70±0.43

Figure 4.8 shows the relative density of Al_2O_3/ZrO_2 Micro/Nano composite related to the density of 90%Al_2O_3 and 10%ZrO_2Thesample with the highest density of 92.12 ±0.66% was obtained with 25% Zrpropoxide concentration at sintering temperature of 1700°C. This is because, the wide size distribution (Figure 4.10) and relatively uniform spatial distribution(Figure 4.16)of ZrO_2 particles as well as the high diffusion rate of particlesfacilitates compaction of the composites during sintering at high temperature. The density of composite increased with the increasing of sintering temperature. However, the increase of sintering temperature on 50°C from 1600°C to 1650°C resulted in increase of density of sintered sample around 14%. On the other hand, as for the samples sintered at 1700°C, the densities are increasingonly on ~5% from those at 1650°C. This is because, even the diffusion rate of particles is high,the densification rate declines at high sintering temperature as the samples sintered at 1650°C are already of quite high density.
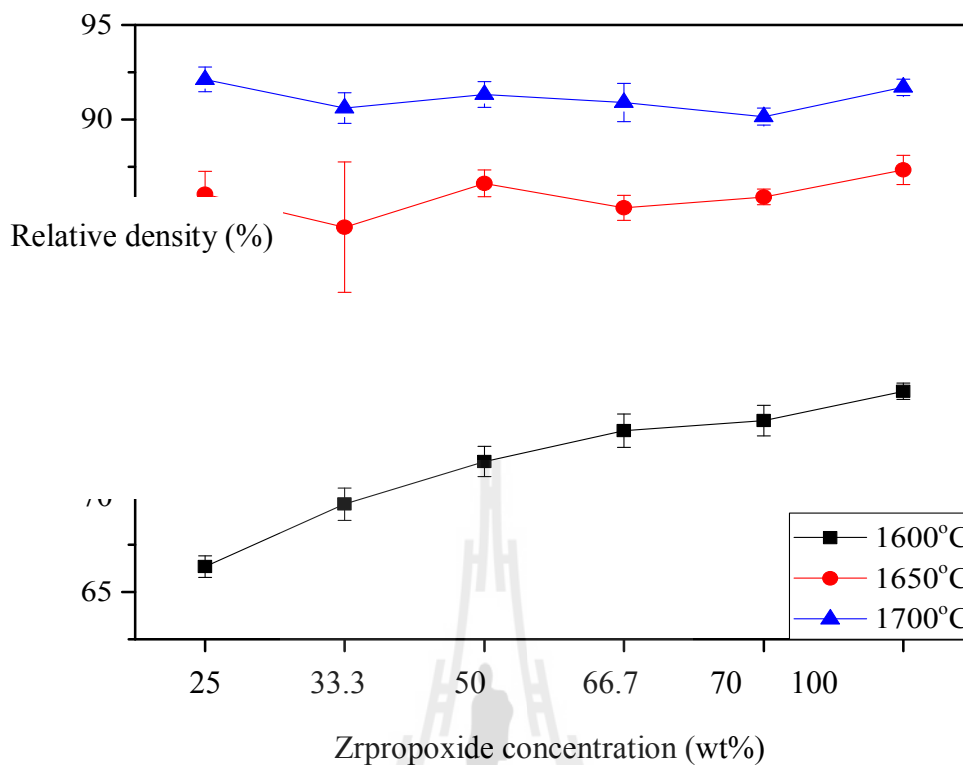
Figure 4.8 Relative densities of $(90wt\%)Al_2O_3/(10wt\%)ZrO_2$ micro/nano composites sintered at 1600^oC, 1650^oC and 1700^oC

Therefore, the concentration of Zrpropoxide did not significantly influenceon the relative density of composite sintered at high sintering temperature because the composition of sintered composite was fixed. The variations of relative density of composite were happened due to homogeneity of composite and fabrication procedure.

4.2.2 Microstructure

Figure 4.9shows the SEM micrographs of cross-sections of Al_2O_3/ZrO_2Micro/Nano composite prepared by powder-alkoxide mixture method and sintered at 1600°C, 1650°C and 1700°C.The images were taken at a magnification of X2,000. Thecomposite microstructure shows ZrO_2 (brighter phase) distributed in Al_2O_3 matrix (darker phase) both at grain boundaries and embedded in the aluminagrain. The most of zirconia grains are located at grain boundaries of Al_2O_3. The changes in microstructure of Al_2O_3/ZrO_2 Micro/Nano composite correspond to the variation of relative density of sintered composite.

The microstructure of composites which were densified to ~ 66-75% relative density during sintering at 1600°C exhibited a lot of open pores of various sizes that distributed all over the image (Figure 4.9(a)). This sintering temperature istoo low to influence on the diffusion rate of Al_2O_3 grains to close open pores. Thus, the results of microstructure analysis are correlated with densification results.

Figure 4.9(b) illustrates the microstructure of composite samples sintered at 1650°C and densified to ~ 84-87% relative density. The image shows compaction of Al_2O_3 and ZrO_2 grainsin accordance with the value of relative density. The increase of sintering temperature on 50°Ceffected to the reduction of open pores, thus, providing better densification of materials than sample sintered at 1600°C. However, open pores still remained in the sample sintered at 1650°C and could be influenced to mechanical properties of materials.

Figure 4.9(c) illustrates the microstructure of sample sintered at 1700°C.The highest density of sintered composite was obtained with samples sintered at 1700°C with ~90-92% relative density. The SEM micrograph shows dense microstructure of composite. The ZrO_2 particles are located at the inter grain space and intra grain of Al_2O_3 matrix. The composite exhibited smaller amount of open pores to yield the higher density in comparison with one sintered at low temperature.
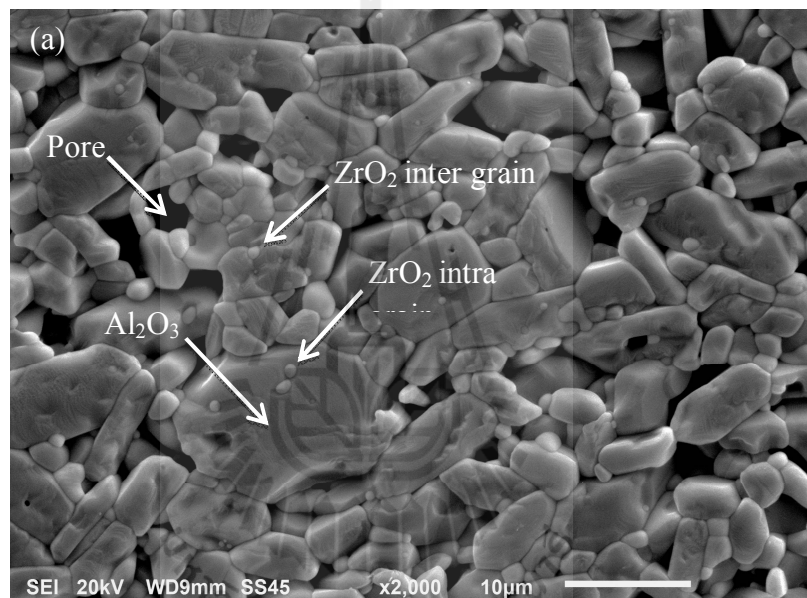
Figure 4.9(a) Scanning electron microscope images of (90wt%)Al_2O_3/(10wt%)ZrO_2 micro/nanocomposites sintered at 1600°C
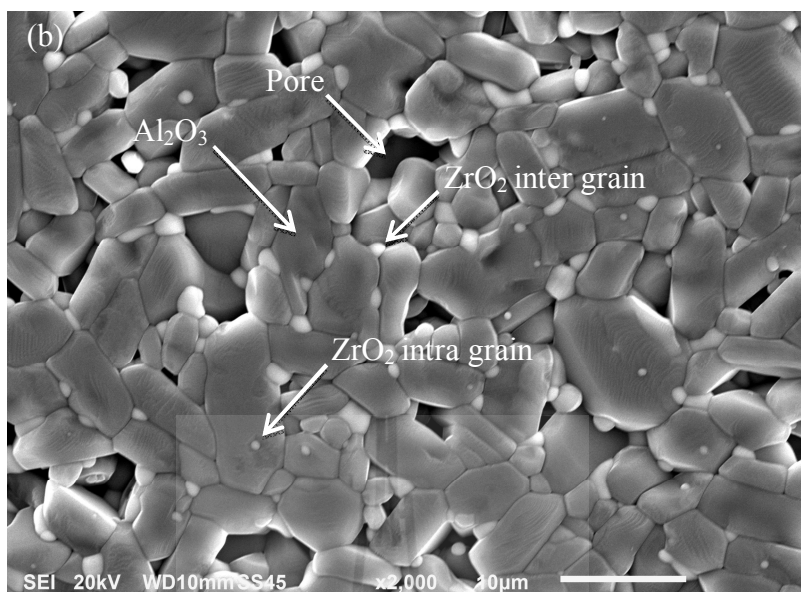
Figure 4.9(b) Scanning electron microscope images of $(90wt\%)Al_2O_3/(10wt\%)ZrO_2$

micro/nanocomposites sintered at $1650^{\circ}C$
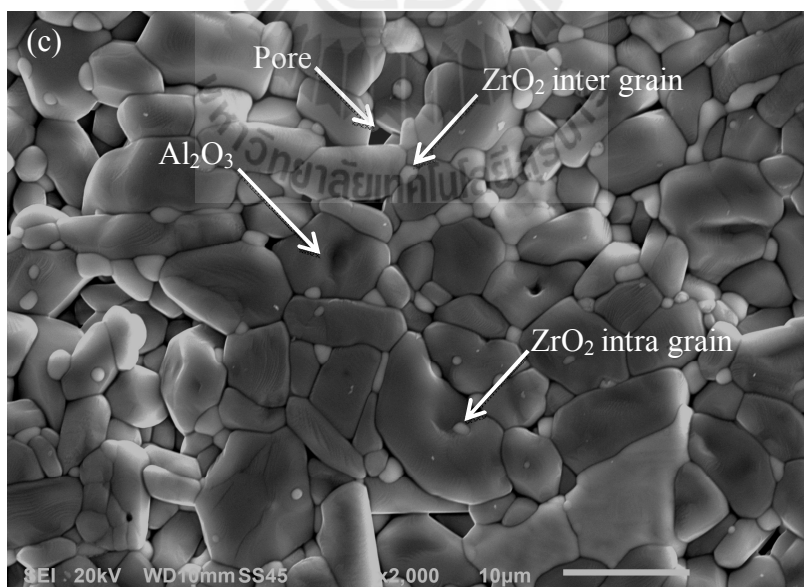
Figure 4.9(c) Scanning electron microscope images of

$(90wt\%)Al_2O_3/(10wt\%)ZrO_2$ micro/nanocomposites sintered at $1700^{\circ}C$

Here, it can be concluded that the sample of the highest density was sintered at 1700°C. Furthermore, ZrO_2 particles located within Al_2O_3 grains and at the grain boundaries were of rounded shape with wide size distribution. In addition, ZrO_2 located at the Al_2O_3 grain boundaries was in the form of agglomerated particles. The particles size distributions of ZrO_2illustrated in Figures 4.10 and 4.11 were determined by image analysis ofsamples sintered at 1700°C.The results show ZrO_2 grains having a wide size distribution with ZrO_2 located at the Al_2O_3 grain boundaries in the size range of 300 - 8500 nm (0.3 - 8.5 μm) considered to 90% of ZrO_2 grain are less than 2000 nm (2 μm) and ZrO_2 grains of broad size distribution with sizes of 40 to 3500 nm (0.04 - 3.5 μm) distributed intra grain of Al_2O_3. The Zrpropoxide concentrations did not significantly affect to the grain size distribution of ZrO_2. The microstructure of the composite was governed by the combination of the sintering temperature with interaction between grains, pores and phase transformation from tetragonal to monoclinic zirconia (Harmid et al., 2008).
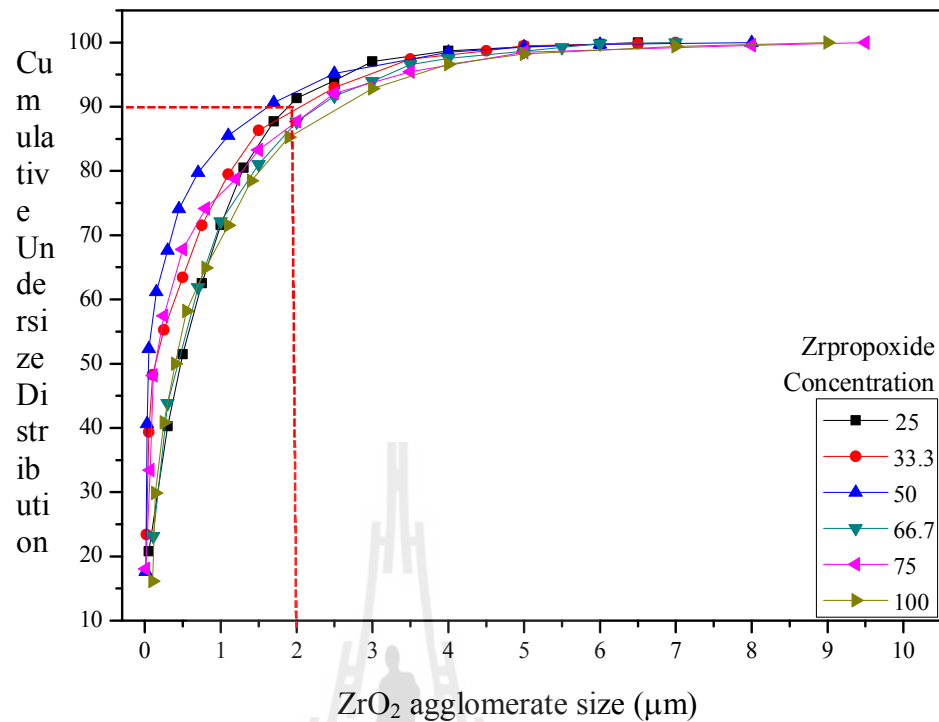
Figure 4.10 ZrO_2 size distributions in Al_2O_3 matrix

Figure 4.11illustratesthesizedistributionof ZrO_2grainslocatedintra grain of Al_2O_3. ZrO_2 grains in samples with various concentration of Zrpropoxide were of the same size range, except the sample with 100wt% concentration of Zrpropoxide which demonstrated a bit larger size of ZrO_2.Nevertheless, 90 % of intra-granular ZrO_2particleswere in the size range of45- 350 nm. A critical size of ZrO_2 particles for phase transformation was reported to be 20 – 50 nm and particles of smaller size exhibited no transformation in the first three testing cycles (Fujio et al., 1997). As ZrO_2 particles synthesized in our experiments are of larger sizes, it is expected that zirconia phase transformation takes place during testing.
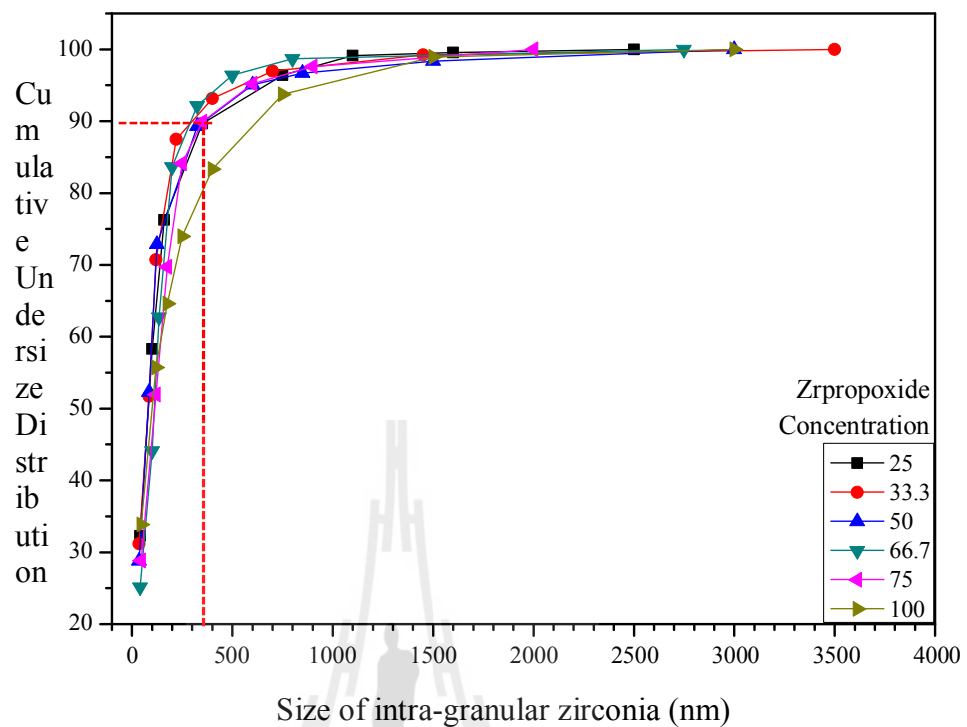
Figure 4.11 ZrO_2 size distributions located intra grain of Al_2O_3

The effected various concentration of Zrpropoxide with Al_2O_3 grain size representedinFigure 4.12. The size of Al_2O_3 grain was shows with wide size distribution in size range of 2.5 − 10μm and illustrated in cluster with various concentration of Zrpropoxide, over 60% Al_2O_3 grain were exhibited with grain growth that larger than starting material of 5 μm Al_2O_3 powder due to high sintering temperature (Mullins, 1986).In addition, the microstructures of sintered composite were shows abnormal grain growth of Al_2O_3.Thus, grains of Al_2O_3 are affected with sintering temperature. However, the concentrations of Zrpropoxide were not effect to Al_2O_3 grain.
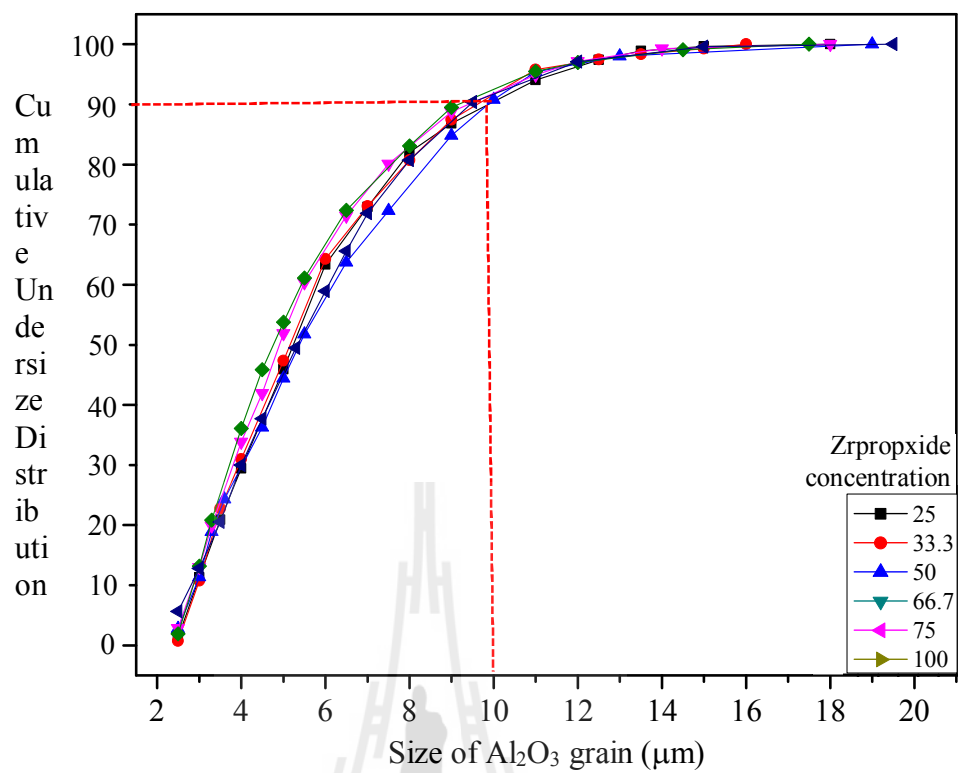
Figure 4.12 Size distributions of Al$_2$O$_3$ grain

4.3 Effect of the Zrpropoxide concentration on uniformity of ZrO$_2$ distribution

The microstructures of sintered composites with various concentrations of Zrpropoxide were analyzed to study theamount and spatial distribution of ZrO$_2$ grains in Al$_2$O$_3$ matrix. The areal fraction and uniformity of distributionof ZrO$_2$reinforcing phase were determined by using the image analysis software (ImageJ). The size distribution of voidsamong ZrO$_2$ grains was measured and parameters of distribution curves were calculated to characterize the distribution uniformity.Figure 4.13 shows microstructure of compositessintered at 1700°C with various concentrations of Zrpropoxide in ethanol solution (a) 25, (b) 33.3, (c) 50, (d) 66.7, (e) 75 and (f) 100wt%. Samplessintered at 1700°C were used to determinethe distribution of ZrO$_2$ because the microstructure of sintered sample shows clearly both of Al$_2$O$_3$ and ZrO$_2$ grains.
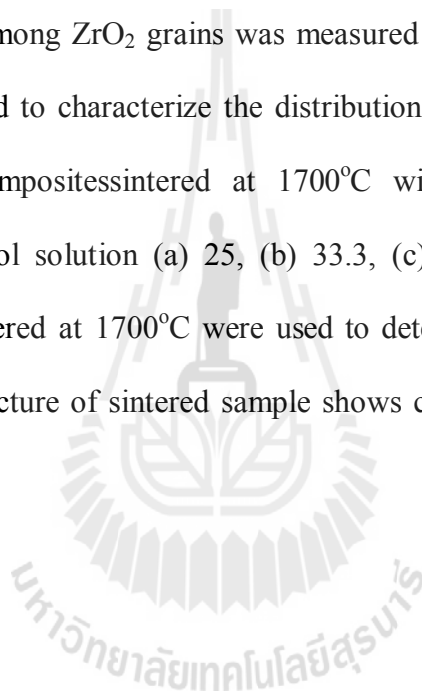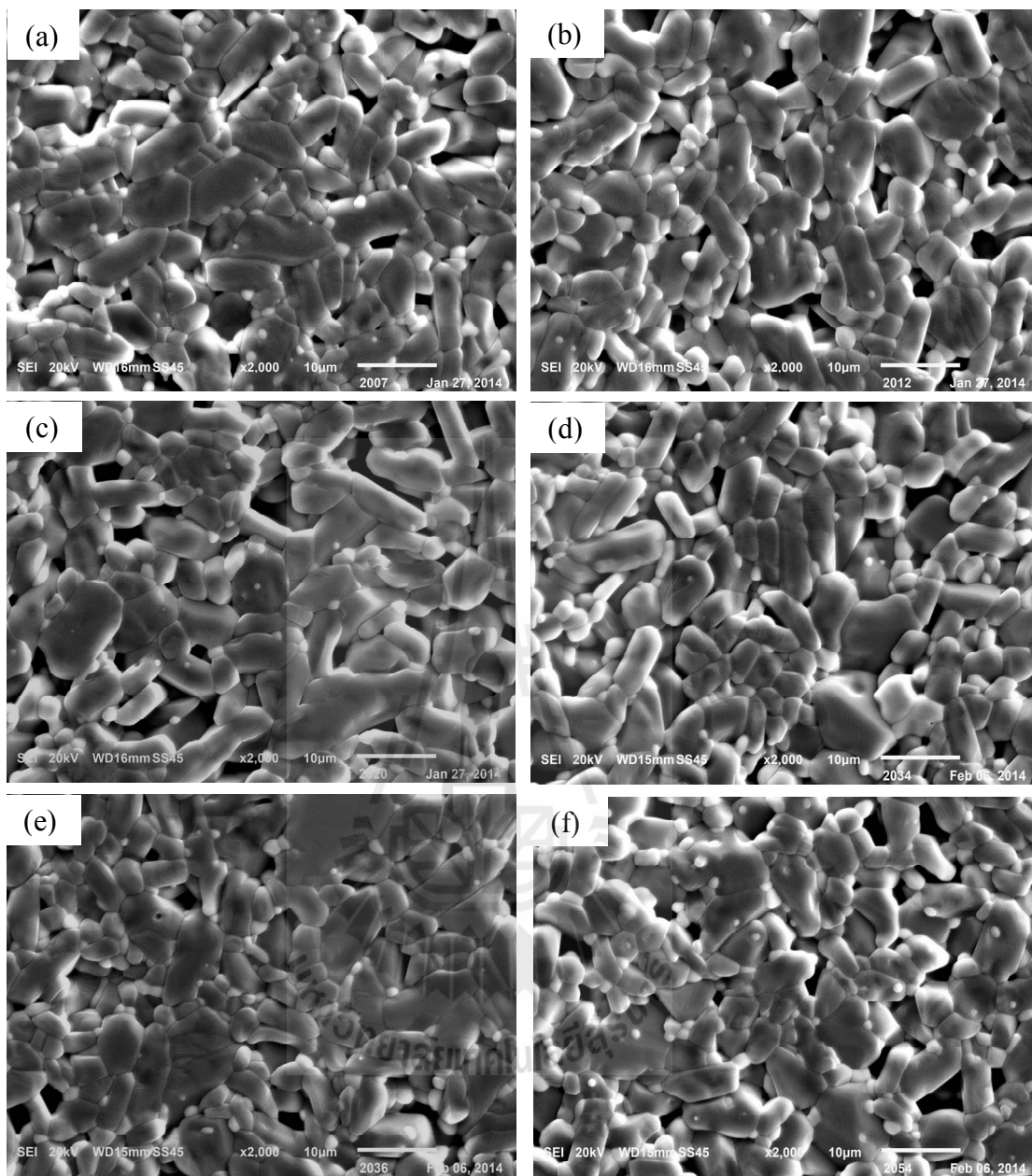
Figure 4.13SEM photographs of composite sintered at 1700°C with various Zr

propoxide concentrations : (a) 25 (b) 33.3 (c) 50 (d) 66.7

(e) 75 (f) 100wt%
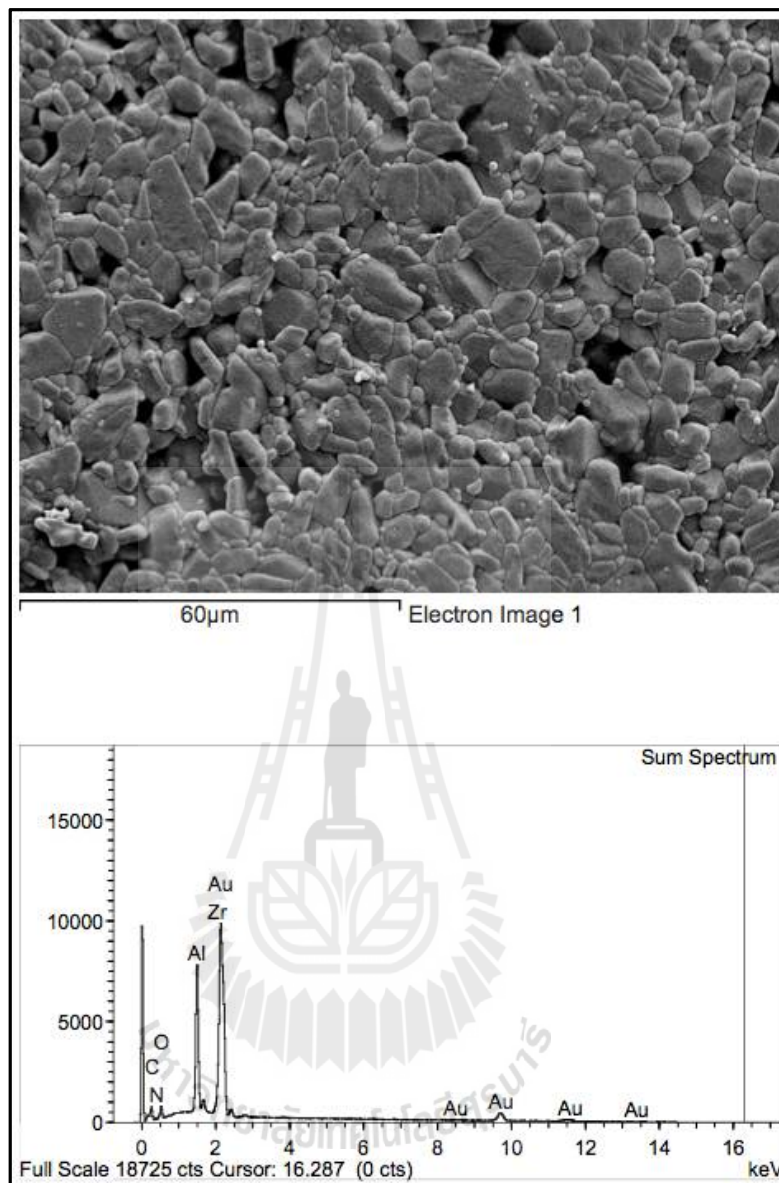
Figure 4.14EDX mapping of (90wt%)Al$_2$O$_3$/(10wt%)ZrO$_2$ micro/nano

composite material

Thedistribution of ZrO$_2$in the sintered materialswas confirmed by EDX

analysis shown in Figure 4.14. The result confirmed the composition of sintered

composite. The sintered samples exhibited both components of alumina (Al$_2$O$_3$)and

zirconia (ZrO$_2$)phase on microstructure.

4.3.1 Areal fraction of ZrO_2

The areal fraction of theZrO_2 reinforcingphase in Al_2O_3matrix was measured as a ratio of the area occupied by black pixels to the total image areausing the image analysis program. The result shows the difference in the areal fractions of ZrO_2 phasewhich is correlated to the Zrpropoxide concentration as presented in Figure 4.15.The areal fractions of ZrO_2 phase incomposite materials with 25, 33.3 and 50wt% concentration of Zrpropoxideare in the range of 3.9 - 4.5 arealfraction andareal fraction of those samples decrease with increasing of Zrpropoxide concentration. However, the areal fraction ofZrO_2 phasein samples with Zrpropoxide concentration over 50wt% increases with increasing Zrpropoxide concentration. The highest areal fraction of ZrO_2 phase of 6.23 percentage was obtained with 100wt% Zrpropoxide. Furthermore, theZrO_2phase with value of areal fraction 0.52-0.69 which is located in theAl_2O_3grains influences on the toughness of material. The highest areal fraction of ZrO_2 embedded in Al_2O_3grain was obtained with the sample 66.7wt% concentration of Zrpropoxide (Chevalier et al., 2005) and the areal fraction of ZrO_2become high at high concentration of Zrpropoxide. The results of areal fraction measurementof $ZrO_2$are summarized in Table 4.4.In addition, the areal fractions of ZrO_2 differ from ZrO_2 content in Al_2O_3 matrixmeasured by XRD in Table 4.1.This is partially because of limiting resolution of SEM images used for image analysis as well as due to the random choice of cross-sectional areas for image analysis in the composite body that might have nonhomogeneous distribution of ZrO_2 in some areas.
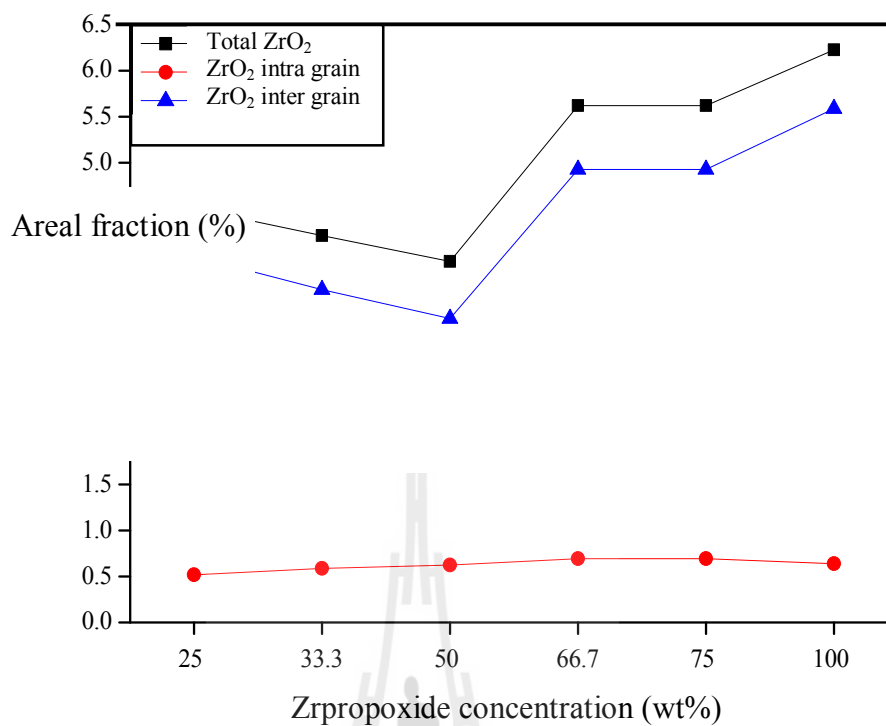
Figure 4.15 Effect of Zrpropoxide concentration on the areal fraction of ZrO_2

in Al_2O_3 matrix

Table 4.4 Areal fraction of ZrO_2 in Al_2O_3 matrix

Zrpropoxide concentration (wt%)	Areal fraction (%)		
	Total ZrO_2	ZrO_2 inter grain	ZrO_2 intra grain
25	4.50	3.98	0.52
33.3	4.21	3.62	0.59
50	3.93	3.30	0.62
66.7	5.62	4.93	0.69
75	5.59	4.90	0.69
100	6.23	5.59	0.64

4.3.2 Uniformity of spatial distribution of ZrO_2

The uniformity of spatial distribution of $ZrO_2$was determined both for total zirconia inter and intra granular particles and only for intra granular particles in sintered samples with various Zrpropoxide solutionconcentrations. The distribution curves of inter and intra granular zirconia particles are shown in Figure 4.16.

Table 4.5 Slope and$d_{void, 50}$of ZrO_2 grain in Al_2O_3 matrix

Zrpropoxide concentration (wt%)	Total ZrO_2 in Al_2O_3 matrix		Intra ZrO_2 in Al_2O_3 matrix	
	Absolute value of Slope	$d_{void, 50}(\mu m)$	Absolute value of Slope	$d_{void, 50}(\mu m)$
25	0.21	2.79	0.12	5.04
33.3	0.23	2.29	0.14	4.42
50	0.25	2.11	0.14	4.12
66.7	0.21	2.55	0.11	5.62
75	0.24	2.24	0.16	3.49
100	0.20	2.71	0.11	5.23

The results of calculation of the slope and $d_{void,50}$for distribution curves of both total ZrO_2 and intra ZrO_2in alumina matrixare summarized in Table 4.5**.** The high absolute value of the slope is an indication of the uniform distribution of ZrO_2grainsin Al_2O_3matrix. The high uniformity of total ZrO_2distribution was obtained for sample with 50wt% of Zrpropoxide concentration. This is possiblebecause of the stable surface charge of zirconium precursor at 50wt% of Zrpropoxide thatprovidesuniform dispersion of zirconium precursor in solution. On the other hand, considering the mechanical properties of this sample, the flexural strength, hardness and toughnessvalues are in the middle group of all samples.The high amount of

monoclinic zirconia phase is believed to be mainly responsible for high strength and the high amount of tetragonal zirconia phase for high toughness for these samples.
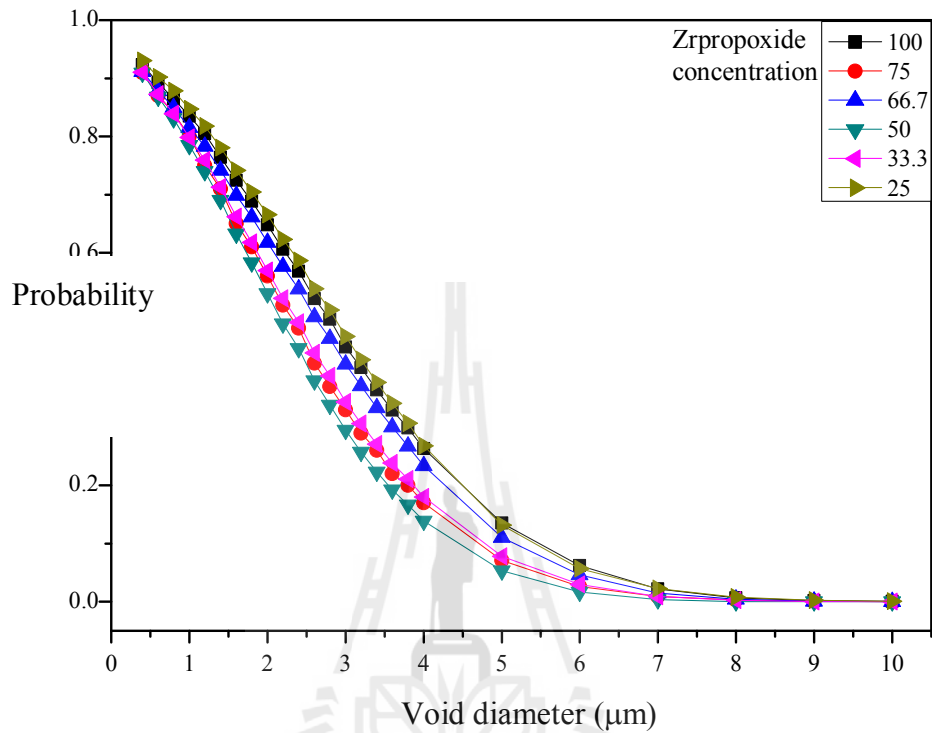
Figure 4.16 Effect of Zrpropoxide concentration on void size distribution of total ZrO_2 grains in Al_2O_3 matrix

Results of ZrO_2 distribution intra grains of $Al_2O_3$are shown in Figure 4.17. The uniformity of ZrO_2grain distributionin Al_2O_3matrix as stronger materialis expected to influence the mechanical properties of the sintered composite material. Moreover, the mechanical properties such as toughness could vary depending on the phase composition of ZrO_2 that provides theresidual stress field responsible for the toughening mechanism of materials. The uniformity of spatial distribution of ZrO_2 embedded in Al_2O_3 grains was illustrated byvalues of slope and$d_{void, 50}$ as mentioned before.The results indicate that the spatial distributions of ZrO_2 embedded in Al_2O_3 grain arewider than those of the total ZrO_2 in Al_2O_3 matrix. The most

uniformdistribution of intra grainZrO$_2$wasobtained forthe sample with 75wt% of Zrpropoxide concentration and that of both inter and intra grain ZrO$_2$ for 50wt% sample. The results shown in Figs. 4.16 and 4.17indicatethat there is a relationship between Zrpropoxideconcentrations and uniformity distribution of ZrO$_2$. The high uniformity distribution of ZrO$_2$wasobtained with samples 75 and 50wt% of Zrpropoxide concentration. However, the mechanical properties of material aredepending on several parameters such as phase composition, areal fraction and distribution of ZrO$_2$. Thus, the results of the analysis on uniformity of ZrO$_2$distribution in Al$_2$O$_3$ matrix indicated that the phase composition of ZrO$_2$ more influenced on the mechanical properties of sintered composite than thedistribution uniformity.
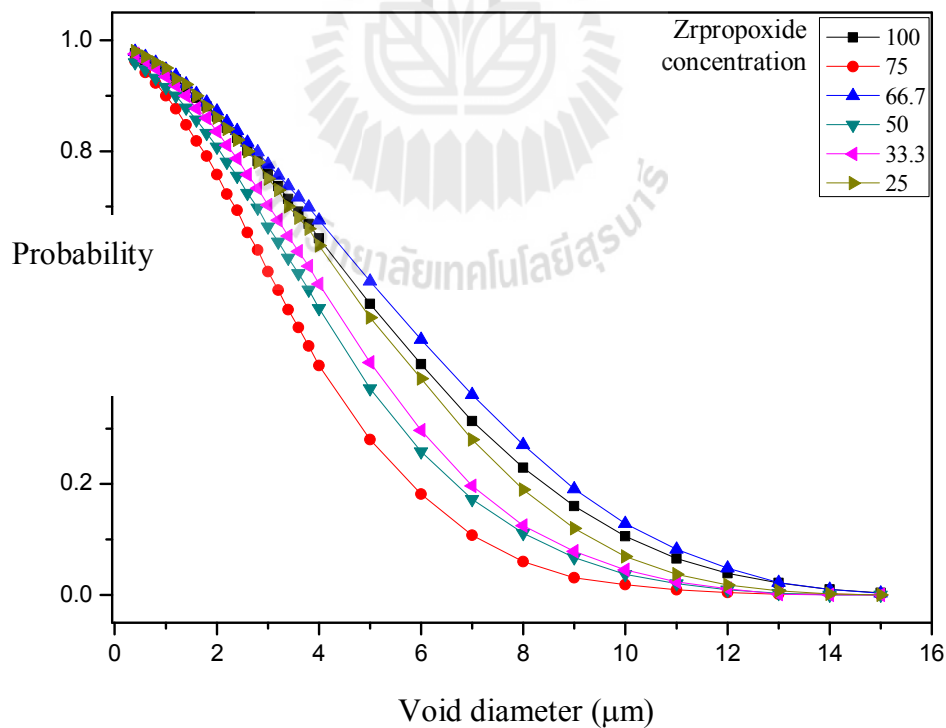
Figure 4.17 Effect of Zrpropoxide concentration on void size distribution of intra

ZrO$_2$ grains in Al$_2$O$_3$ matrix

Nevertheless,the uniformity becomes the second important parameter that influenced to the mechanical properties of the sintered composite. For example, the sample with 50wt% of Zrpropoxideexhibited higher distribution uniformity of ZrO_2 particles, and low areal fraction and lower amount of tetragonal ZrO_2 phase than sample with 33.3wt%. The sample with 50wt% of Zrpropoxide demonstrated the higher toughness than the sample with 33.3wt% concentration of Zrpropoxide at various sintering temperatures, even we expected an opposite results as toughness usually decreases with an increase of tetragonal ZrO_2 phase. Thus, we can explain the high toughness of the sample with 50wt% of Zrpropoxide concentration by high uniformity of ZrO_2 distribution. This sample shows the highest value of uniformity of all, inter and intra granular, ZrO_2 particles and the second highest value of uniformity of intra granular ZrO_2 distribution.The distribution uniformity mainly influenceson toughness because the distributed ZrO_2 particles provide residual stress field to improve materialtoughness.Thus, it can be concluded that the uniformity of spatial distribution of ZrO_2 particles shows the influence on mechanical properties of composites even not as strong as ZrO_2 phase composition.

4.4 Effect ofZrpropoxide concentration on mechanical properties of sintered composite

Table 4.6 summarized the results of measurement offlexural strength of sintered, Vickers hardness and fracture toughness $K_{1C}$of sintered composite. The results show that mechanical properties of materials improved with increasing sintering temperature. The samples with high concentration of Zrpropoxide solution exhibitedhigh strength and hardnessbecausethe high monoclinic ZrO_2content provides the strength and hardness, while the high fracture toughness was measured for samples with low concentration of Zrpropoxide. The higheststrength and hardness of sintered composite were obtained forthe samplewith 100wt% of Zrpropoxide concentration sintered at 1700°C. On the other hand, the highest toughness of materials was obtained with the sample contained 25wt% of Zrpropoxide in solution because of the high amount of tetragonal ZrO_2phase and high uniformityof ZrO_2 particles distribution. The samples of high strength and hardness (100wt%) and high toughness (25wt%), the uniformity of ZrO_2 distribution is not the predominant factor influencing to the mechanical properties of composite materials.

Table 4.6 Mechanical properties of sintered composite.

Sintering temperature (°C)	Zrpropoxides olution concentration (wt%)	Flexural strength (MPa)	Vickers hardness (GPa)	Fracture toughness K_{1C}(MPa$^{1/2}$)
1600°C	25	404.66 ±49.05	2.06±0.20	5.57 ±0.19
	33.3	503.67±9.84	2.06±0.06	4.51 ±0.14
	50	554.91 ±66.70	2.86±0.05	4.58 ±0.88
	66.7	659.79 ±44.46	3.27±0.04	4.45 ±0.13
	75	634.81 ±47.17	3.18±0.06	3.57 ±0.39
	100	674.44 ±21.58	3.55±0.07	3.58 ±0.15
1650°C	25	638.47 ±63.42	5.96±0.49	9.23 ±0.52
	33.3	650.53 ±11.29	6.34±0.12	8.03 ±0.15
	50	617.70 ±16.24	7.10±0.28	8.56 ±0.49
	66.7	700.89±14.31	7.52±0.51	8.49 ±1.83
	75	693.93 ±31.64	6.21±0.32	7.39 ±0.48
	100	707.63 ±8.15	7.24±0.03	7.68 ±1.02
1700°C	25	1089.10 ±36.63	9.04±0.25	13.06 ±1.23
	33.3	1091.07 ±42.05	10.30 ±0.12	8.91 ±0.17
	50	1135.50 ±109.64	9.82 ±0.67	10.49 ±0.80
	66.7	1369.45 ±108.09	11.12±0.60	9.87 ±0.59
	75	1304.90 ±168.34	10.63 ±0.10	10.04 ±1.80
	100	1437.77 ±108.07	13.96±0.43	8.92 ±0.40

4.4.1 Flexural strength

The results of flexural strength measurements ofAl_2O_3/ZrO_2 Micro/Nano composites at room temperature are shown in Figure 4.18as a function of Zrpropoxide concentrationand sintering temperature. Results demonstratedthat the flexural strength of samples tends to increasewith increasing of Zrpropoxide concentration because the high amount of monoclinic ZrO_2phase was obtained at high concentration of Zrpropoxide, asconfirmed by XRD results.The similar trends were observed at various sintering temperatures. However, the flexural strength values for samples with 50wt% and 75wt% concentration of Zrpropoxide solution were slightly lower than those for samples of other compositions. The highvalues of flexural strengthwere obtained with samples of 100wt% concentration of Zrpropoxide at various sintering temperatures. The sample sintered at 1700°C showed the highest flexural strength of 1437 MPa because of high density, phase composition (high amount of monoclinic phase) and areal fraction of ZrO_2 phase.Al_2O_3/ZrO_2 composite exhibits higher mechanical properties than both monolithic alumina and zirconia ceramics. The bending strength of 1075 MPa was reached with alumina/zirconia composite sintered at 1510 °C (Sarraf et al., 2008).Sommer et al. 2012 reported that the bending strength strongly depends on zirconia content and reaches of 1288 MPa at 24% of ZrO_2 with sample hot pressed at 1475°C under 50 MPa axial load. This study revealed that the gain in the flexural strength of Al_2O_3/ZrO_2 Micro/Nano composite samples with an increase in sintering temperature on 50°C from 1650°C to 1700°C is more than three times of strength gain by rising sintering temperature from 1600°C to 1650°C. Therefore, the results of flexural strength indicated that the higher concentration of Zrpropoxide solution and higher sintering temperature contribute to

the enhanced strength of materials due to the high areal fraction of ZrO_2 and high content of monoclinic ZrO_2 phase with good densification of material.
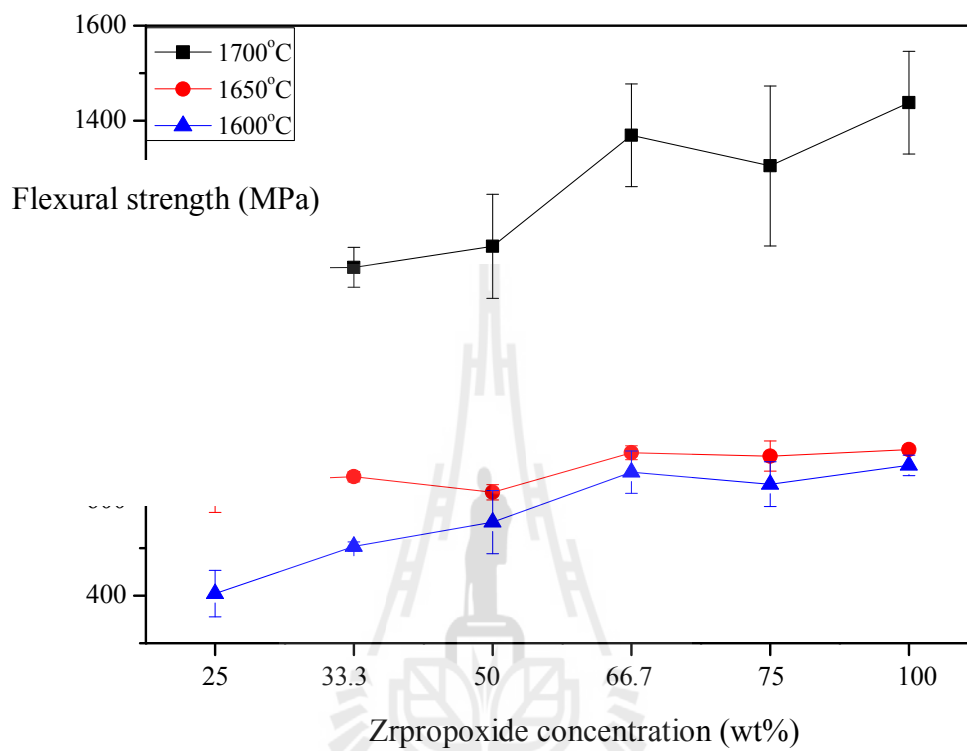
Figure 4.18 Effect of Zrpropoxide concentrations on flexural strength of sintered composite

4.4.2 Vickers hardness

Figure 4.19 illustrates the indented Vickers hardness of compositessintered at various sintering temperatures. The SEM images taken at the same magnificationdemonstrate clearly that indention sizes differ for each sintering temperature. The indentation size was measured using image analysis software (ImageJ) and the hardness of sintered composite was expressed by Eq. (3.6). The high hardness was obtained withsamples sintered at 1700°C.Moreover, withSEM imagesconfirmed the difference in density of sintered compositeswith sintering temperature that influenced to the hardness of materials. Furthermore, the crack paths did not appear by indented Vickers hardness testing.
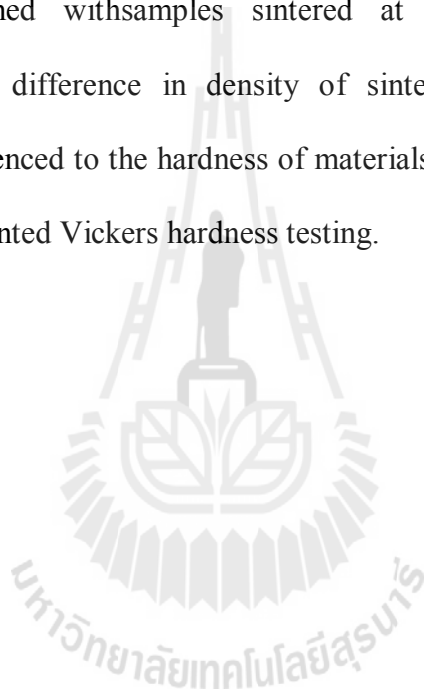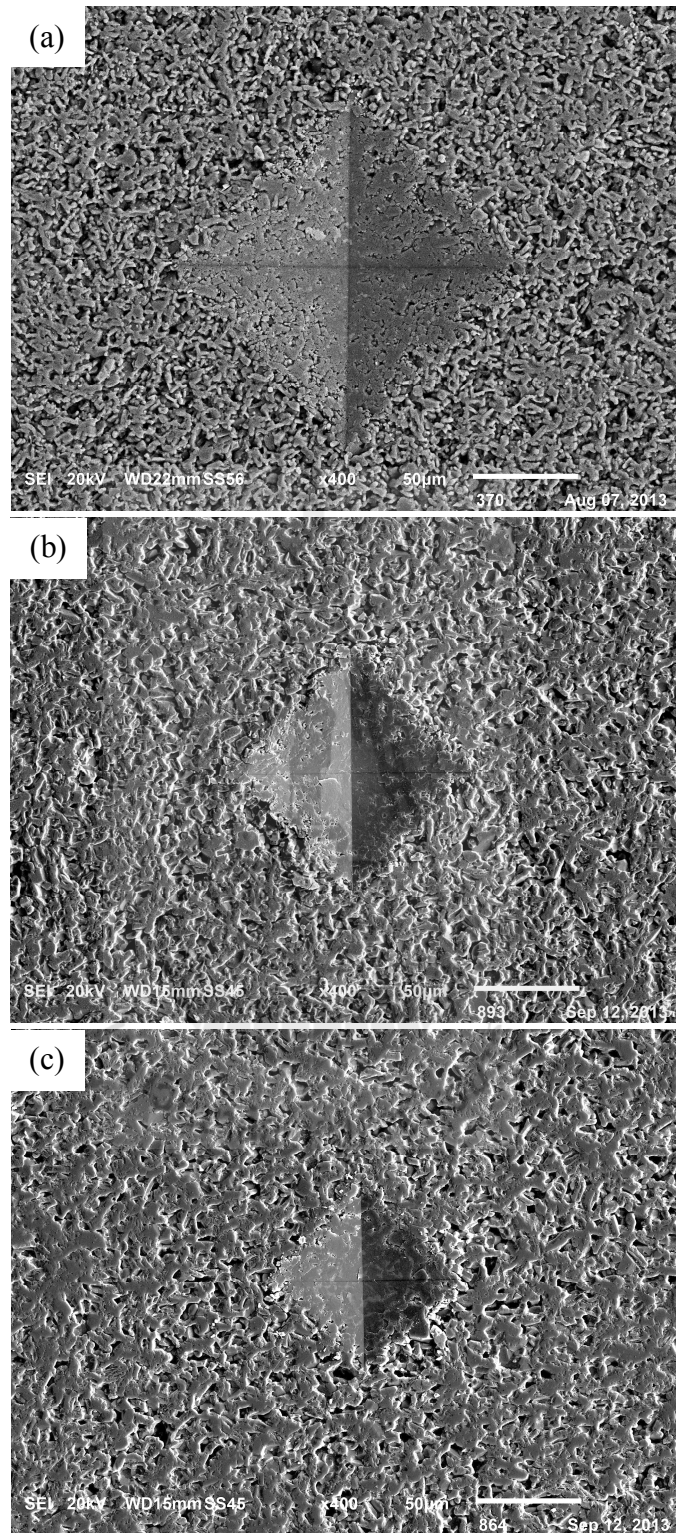
Figure 4.19 Indented Vickers hardness of composites sintered at various sintering

temperatures. (a) 1600°C,(b) 1650°C and(c) 1700°C

The results of hardnessmeasurement of(90wt%)Al_2O_3/(10wt%)ZrO_2 micro/nano composite samples at room temperatureare shown in Figure 4.20 as a function of Zrpropoxide concentration and sintering temperature.The Vickers hardness results for samples of all compositions sintered at 1600°C, 1650°C and 1700°C show that an increase of sintering temperature on 50°Cfrom 1600°C to 1650°C and from 1650°Cto 1700°C leads to the improvement in hardness of materials on approximately 4.00GPa. Thus, the increasing sintering temperature is effective forhardness enhancement of composite material. This behavior could be explainedby the relationship between the density and hardness of sintered samples. Moreover, hardness data show an increase in trend with the increasing of Zrpropoxide concentration. However, the low hardness valueswere measured for sampleswith 75wt% concentration of Zrpropoxide at all sintering temperaturessimilar to the flexural strength results. In addition, samples sintered at 1700°C exhibited $\approx$ 50% increase in hardness of samples with lowest and highest concentration of Zrpropoxide. The highest hardness value of 13.96 GPa obtained for the sample with 100wt% concentration of Zrpropoxide sintered at 1700°C was slightly lower than the Vickers hardness of the Al_2O_3-ZrO_2 ceramics with micro-nano structure of 14-15 GPa reported by Gong et al., 2004, because of the low densification of material. In addition, the hardness values of composite sintered at 1700°C in this study was higher than the hardness in the range of 6.0-7.2 GPa measured by Maiti and Sil, 2010 for pure alumina samples.The mechanical properties of compositesin this study as flexural strength and hardness exhibited with similar trends. These mechanical properties were governed by the phase composition of ZrO_2.The monoclinic zirconia phase is great for hardness with larger grain size (Liu et al., 2011). Considering the phase composition

by XRD analysis, the enhancement of hardness could be related to the increase of monoclinic phase and corresponding decrease of tetragonal phase when increasing of Zrpropoxide solution concentration.
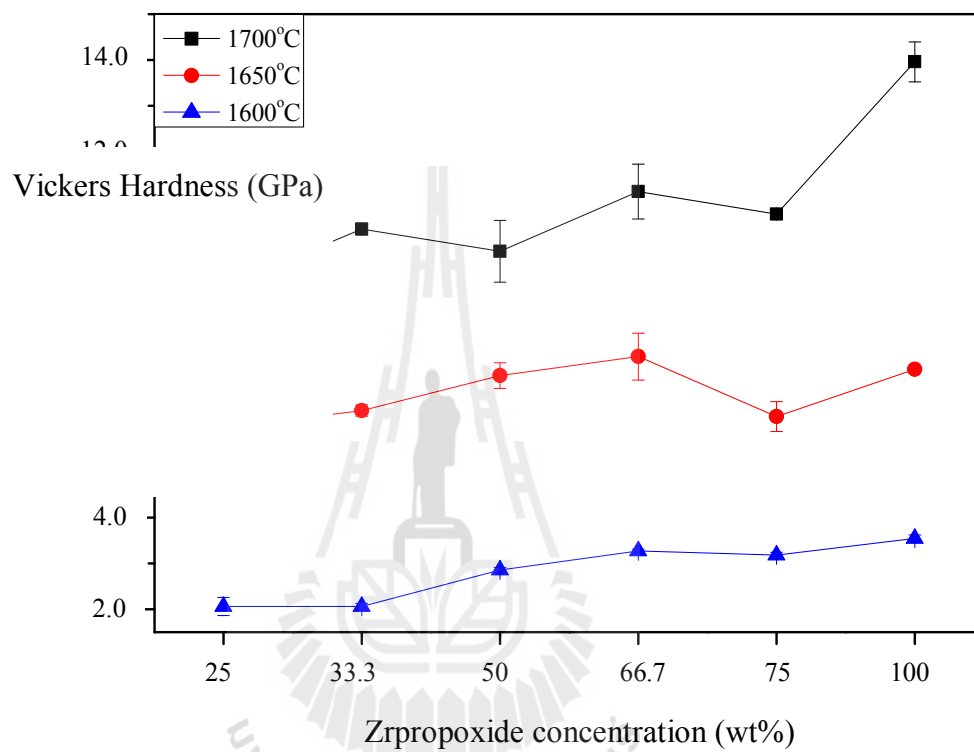
Figure 4.20 Effect ofZrpropoxide concentrations on Vickers hardness of sintered

composite

4.4.3 Fracture toughness

The Single-Edge-Notched-Beam (SENB) toughness was measured according to Tuan et al.(2002) and Wang et al. (2007). The variations of fracture toughness with concentration of Zrpropoxide show similar trends for samples sintered at various temperatures, as illustratedin Figure 4.21.
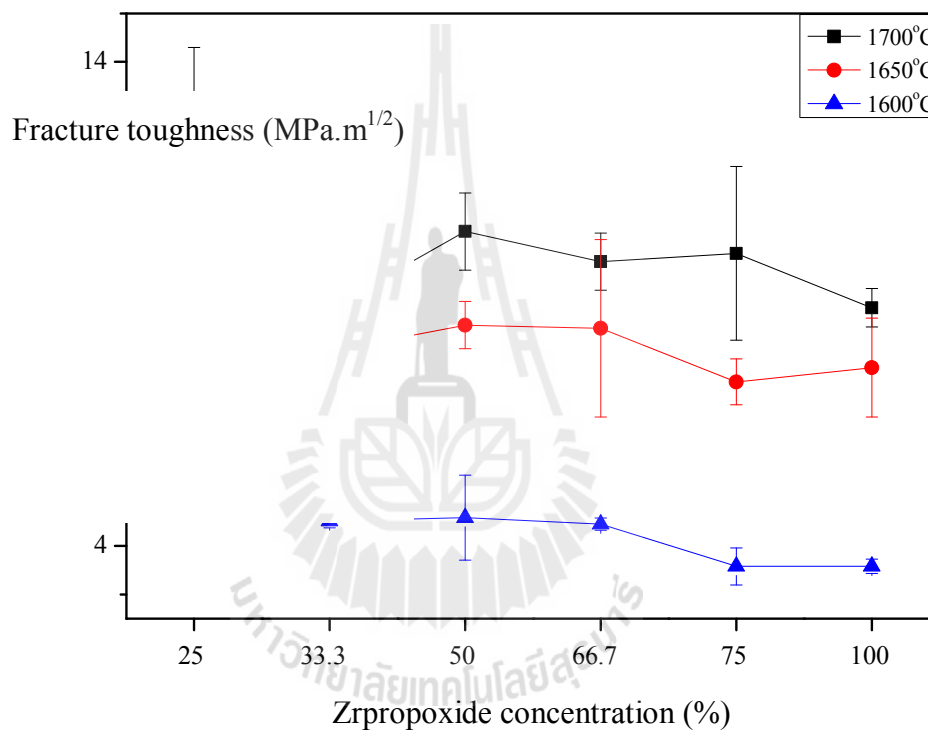
Figure 4.21 Effect ofZrpropoxide concentration on fracture toughness of

sintered composite

The highest toughness reached to 14.22 MPa.m$^{1/2}$ for the sample of 25% Zrpropoxideconcentration sintered at 1700°C. The highest toughness value was obtained with samples of 25wt% concentration of Zrpropoxide for every sintering temperature. The toughening of materials decreased with increasing of Zrpropoxideconcentration. However, the toughness of sample with 33.3wt% Zrpropoxidewas slightly lower than that of sample with 50wt% due to the lower uniformity of spatial distribution of ZrO_2 particles in 33.3wt% sample as explained on page 83. The fracture toughness results are in accordance with the phase composition of materials that the tetragonal zirconia decreased with increasing of Zrpropoxide solution concentration. High toughness of composite was obtained with high amount of tetragonal ZrO_2 (Cahn et al, 1993). As well known, the toughening potential of Al_2O_3/ZrO_2 Micro/Nano composite areproviding by both tetragonal ZrO_2 and monoclinic ZrO_2 phase composition. However, the higher amount of tetragonal ZrO_2 is advantages to improve toughness of materials (Tuan et al., 2002). That is the reason why,the toughness value of the sample with 25wt% concentration of Zrpropoxide was high compared to other samples with various Zrpropoxide concentration.The high intensity of tetragonal ZrO_2 corresponding to ZrO_2 phase composition was observed at low concentration of Zrpropoxideaccording to XRD results. However, we also need to consider that the high areal fraction of ZrO_2 is one of confirmed reasons of improving the toughness of materials.The ZrO_2 areal fractions in Al_2O_3matrix were measured by image analysis using ImageJ software as shown in Figure 4.14. The samples with 66.7 and 75wt% Zrpropoxide concentration have high ZrO_2 areal fraction but lowamount of tetragonal ZrO_2phase. Therefore, our results confirmed that the amount of tetragonal ZrO_2 phase more strongly influences the fracture toughness of Al_2O_3/ZrO_2 Micro/Nano composite than the areal fraction of ZrO_2. As the results, high

toughening of composite material was obtained with high amount of tetragonal ZrO_2 phase in samples with low concentration of Zrpropoxide sintered at high sintering temperature.

CHAPTER V

CONCLUSIONS

The(90wt%)Al_2O_3/(10wt%)ZrO_2 micro/nano composite material was fabricatedvia powder alkoxide mixture method.Themicrostructure of sintered composites and mechanical properties were investigated for various Zrpropoxide concentrations in ethanol mixture and sintering temperatures. Particularly, the effects of zirconia phase compositions and uniformity of zirconia distribution were explored in relation to the mechanical properties of composites.Thefollowing conclusions have been draw from this study.

5.1 Effect of Zrpropoxide concentration

1.The concentration of Zrpropoxide in the solutionhas been found to have significant influence to the phase composition of sintered composite materials.The tetragonal ZrO_2 phase declines while monoclinic one rises at higher Zrpropoxide concentration.

2.The uniform spatial distributions of ZrO_2 particles in Al_2O_3 matrix were obtained with sample 75 and 50wt% of Zrpropoxide concentration because high stable of surface charge of zirconium precursor in ethanol solution.

3. Zrpropoxidesolution concentrations did not have significant effect onthe relative density of sintered compositesbecause the composition of composite materials was fixed at Al_2O_3 90wt% and ZrO_2 10wt%. The highest relative

density of 91.70% was obtained with the sample 25wt% of Zrpropoxide concentration sintered at 1700°C due tothe wide size distribution andhigh amounts of tetragonal and total ZrO_2phase with relatively uniform spatial distribution of ZrO_2 particles as well as the high diffusion rate of particlesat high sintering temperature.

4. The samples with 25wt% concentration of Zrpropoxideprovided high amounts of tetragonal and total ZrO_2 phase that archived highest toughness of samples with various sintering temperature.

5.2   Effect of sintering temperature

1. The samples of high density were sinteredat 1700°C for 4 hours. However, the grain sizes become bit larger during sintering at high temperature. The denser microstructure was obtained at 1700°C of sintering temperature due to the higher diffusion rate of Al_2O_3 and ZrO_2 particles.

2.The flexural strength of sintered composite was found to increase with increasing sintering temperature. The rise in the sintering temperature on 50°C from 1650°C to 1700°C resulted in an increase of the flexural strength of sintered composite over ~500 MPa ormore than three times of strength gain obtained by rising the sintering temperature from 1600°C to 1650°C, due to the higher diffusion rate at higher sintering temperature.

3.The increasein sintering temperature is effective inenhancing hardness of sintered composite. The rise of sintering temperature on 50°C from 1600°C to 1650°C and from 1650°Cto 1700°C leads to an increasein the materialhardness on almost 4.00GPa due to higher density of material.

4. The toughening of materials increases with increasingsintering temperature. The highest toughness of 13.06 ±1.23 MPa$^{1/2}$was obtained with the sample sintered at 1700°C with 25wt% of Zrpropoxide concentration. In addition, the fracture toughness results were corresponding to the phase composition of materials and uniformity of spatial distribution of ZrO_2 particles in alumina matrix.

5.3 Microstructure characteristics

1. Thesintered composites of high density withlarge Al_2O_3grainswere obtained at high sintering temperature at 1700°C. ZrO_2particles exhibitedwith spherical shape and wide size distribution located in Al_2O_3 grains and at the grain boundaries.

2. The areal fraction of $ZrO_2$was increased with increasing of Zrpropoxide concentration. The sample with 25wt% Zrpropoxide concentrationwas of high toughness and of low areal fraction of ZrO_2. This is because the high amount of tetragonal ZrO_2 phase was obtained at low concentration of Zrpropoxide, as confirmed by XRD results.

3.The high uniformity distributions of ZrO_2 were obtained with samples 75 and 50wt% of Zrpropoxide concentration owing to the uniform dispersion of zirconium precursor in solution as a result of the stable surface charge.

In summary,the (90wt%)Al_2O_3/(10wt%)ZrO_2 Micro/Nano composite were successfully prepared via powder-alkoxide mixture.It was found that theZrpropoxide concentration and sintering temperature are influenced to the mechanical properties of the composites. The amount of tetragonal zirconia decreased and monoclinic increased with increasing Zrpropoxideconcentration. The microstructure of composites demonstrated zirconia particles of the spherical shape with wide size

distribution both embedded in Al_2O_3 grains and located at the grain boundaries. The high mechanical properties such as hardness and strength were obtained with concentratedZrpropoxidesolution at high sintering temperature. The high toughness was measured for the samples with dilute of Zrpropoxide solution.

The outcome of this research is expected to be useful for the production of $(90wt\%)Al_2O_3/(10wt\%)ZrO_2$ composites material to be associated with better mechanical properties and longer lifetime.

As the result of this study, the following recommendation could be suggested for the future research development:

The mechanical properties of composite materials obtained via colloidal method using Zrpropoxidecan befurtherimproved by controlling the size distribution and orientation of reinforcing particles.To use the composite material for implant applications, the wear resistance should be measured and the biocompatibility testing should be conducted.

REFFERENCES

Ali, S., Rasoul, S., Zahra, K. (2012). Effect of organic dispersants on structural and mechanical properties of Al_2O_3/ZrO_2 composites.**Materials Research Bulletin**.Vol.47: 4210-4215.

Bimal P. S., Ruben M.,Chika T., Masayoshi F., Minoru T. (2005). Stability of dispersions of colloidal alumina particles in aqueous suspensions.**Journal of Colloid and Interface Science**. Vol.291: 181-186.

Calderon-Moreno, J.M. and Schehl, M. (2004).Microstructure after super plastic creep of alumina-zirconia composites prepared by powder alcoxide mixtures, **Journal of the European Ceramic Society**. Vol.24: 393-397.

Chevalier, J.,Taddei, P.,Gremillard, L., Deville, S.,Fantozzi, G.,Bartolome, J.F.,Pecharroman, C., Moya, J.S., Diaz, L.A., Torrecillas, R., Affatato, S. (2011) Reliability assessment in advanced nanocomposite materials for orthopedic application.**Journal of Mechanical Behavior Biomedical Materials**. Vol.4: 303-314.

Chevalier, J. and Gremillar, L.(2009). Ceramics for medical applications: A picture for the next 20 years. **Journal of the European Ceramic Society**. Vol.29: 1245-1255.

Claussen, N. (1976). Fracture toughness of Al_2O_3 with an unstabilized ZrO_2 dispersed phase.**Journal of American Ceramic Society**.Vol.59:49-51.

De Azaa, A.H.,Chevaliera,J.,Fantozzia,G.,Schehlb, M.,Torrecillas,R. (2002). Crack growth resistance of alumina, zirconia and zirconia toughened alumina ceramics for joint prostheses, **Biomaterials**. Vol.23: 937-945.

Francisco A.T. et al. (2009). Correlation between microstructure and mechanical preperties of Al_2O_3/ZrO_2nanocomposites.**Ceramics International**. Vol.35: 741-745.

Fujio, A., Seiichi, M., Koichi, Y.(1997).Tetragonal to monoclinic transformation and microstructural evolution in ZrO_2–9.7mol% MgO during cyclic heating and cooling.**Journal of Materials Science.**Vol.32: 513-522.

Gong J., Miao H., Hu B. (2004). Compositional dependence of hardness of (Ce,Y)-TZP/Al_2O_3 composites. **Materials Science and Engineering**. A 372: 207–212

Guanwei, L., Zhipeng, X., Yin, W. (2011). Fabrication and mechanical properties of homogeneous zirconia toughned alumina ceramics via cyclic solution infiltration and in situ precipitation.**Materials and Design**. Vol.32: 3340-3347.

Hamid, S., Reinhard, H., Martin, M. (2008).Fine-grained Al_2O_3-ZrO_2 composites by optimization of the processing parameters.**ScriptaMaterialia**.Vol.59: 155-158.

Hang, W., Prem, P., Giuseppe, I., Albert, J. F.(2007). Fracture toughness comparison of three test methods with four dental porcelains.**Dental Materials**. Vol.23: 905-910.

Sarraf H.,Herbigc R.,Maryska M. (2008). Fine-grained Al_2O_3–ZrO_2 composites by optimization of the processing parameters. **ScriptaMaterialia.** Vol. 59: 155–158

Horovistiz, A.L., and Muccillo, E.N.S. (2011). Quantification of microstructural

features in gadolinia-doped ceriacontaining co-additives by digital image analysis.**Journal of the European Ceramic Society.**Vol.31: 1431-1438.

Kangwantrakool, S., Golman, B., Shinohara, K. (2003). Quantitative Characterization of Microstructure of WC-Co/ TiC-Al$_2$O$_3$ composite materials with Relate to Mechanical properties. **Journal of Chemical Engineering of Japan**. Vol.36, 1: 49-56.

Lawn, B. (1993). Fracture of brittle solid. Cambridge solid state science series 2nd ed. **UK: Cambridge university press.**378.

Ma, W., Wen, L.,Guan, R., Sun, X., Li X. (2008).Sintering densification, microstructure and transformation behavior of Al$_2$O$_3$/ZrO$_2$(Y$_2$O$_3$) composites. **Materials Science and Engineering**. A 477: 100-106.

Maiti K., Sil A. (2010). Relationship between fracture toughness characteristics and morphology of sintered Al$_2$O$_3$ ceramics. **Ceramics International**. Vol.36: 2337-2344.

Maiti K., Sil A. (2011). Microstructural relationship with fracture toughness of undoped and rare earths (Y, La) doped Al$_2$O$_3$-ZrO$_2$ ceramic composites. Ceramics International Vol.37: 2411-2421.

Piconi, C., Maccauro, G. (1999). Review: Zirconia as a ceramic biomaterial. **Biomaterials**.Vol.20: 1-25.

Rafferty, A., Alsebaie, A.M., Olabi, A.G., Prescott, T. (2009). Properties of zirconia-toughened-alumina prepared via powder processing and colloidal processing routes.**Journal of Colloid and Interface Science**.Vol.329: 310-315.

Ramakrishnan, V., Pradip, Malghan, S.G. (1998).The stability of alumina zirconia

suspension.**Colloidal and Surfaces, A: Physicochemical and Engineering Aspects**. Vol.133: 135-142.

Rao, P.G., Iwasa, M., Tanaka, T.,Kondoh I., Inoue, T. (2003). Preparation and mechanical properties of Al_2O_3-15wt.%ZrO_2 composites. **ScriptaMaterialia.**Vol.48: 437-441.

Rimmer,S. (2006). Modern dental ceramics: an overview, **International density SA**. Vol.8: 32-40.

Schehl, M., Diaz, L.A., Torrecillas, R. (2002). Alumina nanocomposites form powder-lakeside mixture. **ActaMeaterialia**. Vol.50: 1125-1139.

Siilva,F. T. da,Zacche, M. A. N.,Amorin,H. S. de.(2007). Influence of different surface treatments on the fracture toughness of a commercial ZTA dental ceramic.**Journal of Materials Research**.Vol.10: 63-68.

Sommer, F., Landfried, R., Kern, F., Gadow, R. (2012). Mechanical properties of zirconia toughened alumina with 10–24 vol.% 1Y-TZP reinforcement.**Journal of the European Ceramic Society.**Vol.32: 4177-4184.

Steven, R. (1986). Zirconia and Zirconia ceramicsseries 2nd ed. **Magnesium Elektron Ltd.**

Suzuki, T. S., Sakka Y., Morita K., Hiraga K. (2002). Ehancedsuperplasticity in a Alumina-comtaining Zirconia prepared by colloidal processing**. Scriptarmaterialia.** Vol.43: 705-710.

Tuan, W.H., Chen, R.Z., Wang, T.C., Cheng, C.H., Kuo, P.S. (2002).Mechanical properties of Al_2O_3/ZrO_2 composites.**Journal of the European Ceramic Society**. Vol.22: 2827-2833.

Wang, J. and Stevens, R. (1989). Review zirconia-toughened alumina (ZTA)

ceramics. **Journal of Materials Science**.Vol.24(10):3421-3440.

Wang, G.,Sarkar,P., Nicholson,P.S. (1997).Influence of Acidity on the Electrostatic Stability of Alumina Suspension in Ethanol.**Journal of American Ceramic Society**. Vol.80: 965.

Wan, J., Zhou, M., Yang, X.S., Dai, C.Y., Zhang, Y., Mao, W.G., Lu, C. (2013). Fracture characteristic of freestanding 8 wt% Y_2O_3-ZrO_2 coating by single edge notch beam and Vickers hardness indentation tests, **Materials Science and Engineering**. A 581: 140-144.

Walia,S. (2009).Restoring esthetics with metal-free ceramics: A case report. Vol.75: 353.

Xianglong, H., Zuozhong, L., Li, F., Wei, W., Jianfeng, C., Chunyu, X., Hong, Z. (2015). Co-precipitated synthesis of Al_2O_3-ZrO_2 composite ceramic nanopowders by precipitant and drying method regulation: A systematic study. Ceramics International. Vol.41: 505-513

Xin, W., Jintao, T., Xuegang, Y., Yan, S., Zifeng, L., Yansheng, Y. (2008). Effect of microstructure on the fracture behavior of micro–nano ZTA composite.**Materials Chemistry and Physics**. Vol.112: 213-217.

Ye, Y., Li J., Zhou H., Chen J. (2008).Microstructure and mechanical properties of yttria-stabilized ZrO_2/Al_2O_3nanocomposite ceramics.**Ceramics International.**Vol.34: 1797-1803.

APPENDIX A

JCPDS-XRD PATTERNS OF α-ALUMINA,

MONOCLINIC AND TETRAGONAL ZIRCONIA

Pattern: PDF 46-1212   Radiation: 1.54060   Quality: Star (*)

Formula	Al2 O3
Name	Aluminum Oxide
Name (mineral)	Corundum, syn
Name (common)	α-2 O3

Lattice:	Rhombo.H.axes	Mol. weight =	101.96
S.G.:	R-3c (167)	Volume [CD] =	254.81
		Dx =	
		Dm =	
		I/Icor =	-1.000

a =	4.75870	alpha =	
b =		beta =	
c =	12.99290	gamma =	
a/b =	1.00000	Z =	6
c/b =	2.73035		

Sample Source Or Locality: The sample is an alumina plate as received from ICDD
General Comments: Unit cell computed from d#o#b#s
Optical Data: A=1.7604, B=1.7686, Sign=-

Structure
Publication: Acta Crystallogr., Sec. B: Structural Science
Detail: volume 49, page 973 (1993)
Primary Reference
Publication: Adv. X-Ray Anal.
Detail: volume 33, page 295 (1990)
Authors: Huang, T., Parrish, W., Masciocchi, N., Wang, P.

Radiation:	CuKa1	Filter:	Not specified
Wavelength:	1.54060	d-spacing:	
SS/FOM:	378.7 (0.0026,25)		

d	2θ	I	h	k	l
3.47975	25.579	45	0	1	2
2.55085	35.153	100	1	0	4
2.37947	37.777	21	1	1	0
2.16542	41.676	2	0	0	6
2.08532	43.356	66	1	1	3
1.96432	46.176	1	2	0	2
1.74007	52.550	34	0	2	4
1.60156	57.497	89	1	1	6
1.54667	59.741	1	2	1	1
1.51506	61.118	2	1	2	2
1.51101	61.300	14	0	1	8
1.40452	66.521	23	2	1	4
1.37372	68.214	27	3	0	0
1.33599	70.420	1	1	2	5
1.27555	74.299	2	2	0	8
1.23915	76.871	29	1	0	10
1.23434	77.226	12	1	1	9
1.19315	80.422	1	2	1	7
1.18973	80.700	2	2	2	0
1.16002	83.217	1	3	0	6
1.14721	84.359	3	2	2	3
1.13864	85.143	1	1	3	1
1.12566	86.363	2	3	1	2
1.12419	86.503	3	1	2	8
1.09903	88.997	9	0	2	10

Pattern: PDF 89-9066 Radiation: 1.54060 Quality: Calculated

Formula	Zr O2
Name	Zirconium Oxide
Name (mineral)	Zirconia, syn
Name (common)	Zirconium dioxide

Lattice:	Monoclinic	Mol. weight =	123.22
S.G.:	P21/c (14)	Volume [CD] =	140.52
		Dx =	
		Dm =	
		I/Icor =	4.970

a =	5.14600	alpha =	
b =	5.20500	beta =	99.100
c =	5.31300	gamma =	
a/b =	0.98866	Z =	4
c/b =	1.02075		

ICSD Collection Code: 089426
Note: Rietveld profile refinement applied
Temperature Factor: ITF
Article Title: Crystal structure of zirconia by Rietveld refinement
Wyckoff Sequence: e3 (P121/C1)
ANX: AX2

Structure
Publication: Sci. China, Ser. A: Math., Phys., Astron.
Detail: volume 42, page 80 (1999)
Authors: Wang, D.-N., Guo, Y.-Q., Liang, K.-M., Tao, K.
Primary Reference
Publication: Calculated from ICSD using POWD-12++

Radiation:	CuKa1	Filter:	Not specified
Wavelength:	1.54060	d-spacing:	
SS/FOM:	379.7 (0.0023,34)		

d	2θ	I	h	k	l
5.08123	17.439	53	1	0	0
3.69495	24.066	102	0	1	1
3.63594	24.462	110	1	1	0
3.16052	28.213	999	-1	1	1
2.84160	31.457	659	1	1	1
2.62306	34.155	265	0	0	2
2.60250	34.433	134	0	2	0
2.54062	35.299	149	2	0	0
2.49737	35.931	25	-1	0	2
2.34243	38.398	7	0	1	2
2.33139	38.587	28	0	2	1
2.31635	38.847	6	1	2	0
2.28315	39.435	10	2	1	0
2.25161	40.011	2	-1	1	2
2.21166	40.766	129	-2	1	1
2.19369	41.115	51	1	0	2
2.17780	41.428	29	-1	2	1
2.02149	44.798	60	1	1	2
1.98890	45.573	58	-2	0	2
1.84747	49.284	123	0	2	2
1.81797	50.139	207	2	2	0
1.80193	50.616	111	-1	2	2
1.78125	51.246	35	-2	2	1
1.69582	54.031	77	3	0	0
1.69582	54.031	77	2	0	2
1.67731	54.677	9	1	2	2
1.66060	55.274	41	2	2	1
1.65766	55.380	86	0	1	3
1.65057	55.639	55	-1	1	3
1.64725	55.761	35	0	3	1
1.64192	55.958	47	1	3	0
1.60908	57.204	73	-3	1	1
1.60908	57.204	73	3	1	0
1.59031	57.943	53	-1	3	1
1.58026	58.346	45	-2	2	2
1.54463	59.827	94	1	3	1
1.53806	60.109	58	-3	0	2
1.51056	61.320	49	1	1	3
1.49462	62.046	60	-2	1	3
1.47856	62.796	88	3	1	1
1.47501	62.964	47	-3	1	2
1.45148	64.105	7	0	2	3
1.44671	64.342	22	-1	2	3
1.44671	64.342	22	0	3	2
1.43278	65.044	5	2	3	0
1.42488	65.450	22	-1	3	2
1.42080	65.662	63	3	2	0
1.42080	65.662	63	2	2	2
1.36082	68.951	11	1	3	2
1.34964	69.604	2	1	2	3
1.33824	70.284	4	-2	2	3
1.33024	70.770	1	3	0	2
1.32410	71.148	19	-3	2	2
1.32150	71.309	25	-1	0	4
1.31153	71.935	8	0	0	4
1.30744	72.196	13	-2	3	2
1.30125	72.594	19	0	4	0
1.30125	72.594	19	2	1	3
1.28490	73.668	7	-3	1	3
1.28086	73.939	4	-1	1	4
1.27031	74.657	16	4	0	0
1.26298	75.166	34	0	4	1
1.26057	75.334	18	1	4	0
1.24468	76.468	17	-4	1	1
1.23676	77.047	2	-1	4	1
1.23409	77.245	5	4	1	0
1.23165	77.426	9	0	3	3
1.22873	77.645	12	-1	3	3
1.22393	78.007	12	1	0	4
1.22159	78.185	8	-4	0	2
1.21423	78.750	6	-2	1	4
1.21423	78.750	6	1	4	1
1.21133	78.975	20	-3	3	1
1.21133	78.975	20	3	3	0
1.19456	80.307	3	2	2	3
1.19144	80.561	3	1	1	4
1.18928	80.737	3	-4	1	2
1.18143	81.386	3	-3	2	3
1.17829	81.649	27	-1	2	4
1.17121	82.249	7	0	2	4
1.16758	82.560	20	1	3	3
1.16570	82.723	12	0	4	2
1.16215	83.031	7	4	1	1
1.16017	83.204	18	-2	3	3
1.15818	83.379	14	2	4	0

d	2θ	I	h	k	l
1.15818	83.379	14	2	4	0
1.15399	83.750	7	-1	4	2
1.15262	83.873	14	3	3	1
1.15093	84.024	9	-3	3	2
1.14995	84.112	11	-4	2	1
1.14851	84.241	11	-2	4	1
1.14158	84.872	16	4	2	0
1.12684	86.250	16	-2	2	4
1.12684	86.250	16	-3	0	4
1.11917	86.988	2	1	4	2
1.11416	87.478	12	2	4	1
1.10756	88.133	14	1	2	4
1.10479	88.411	30	3	1	3
1.10479	88.411	30	-4	2	2
1.10133	88.762	13	-3	1	4
1.09684	89.222	9	2	0	4
1.09029	89.903	20	-4	1	3

Pattern: PDF 79-1769   Radiation: 1.54060   Quality: Calculated

Formula	Zr O2
Name	Zirconium Oxide
Name (mineral)	
Name (common)	

Lattice:	Tetragonal	Mol. weight =	123.22
S.G.:	P42/nmc (137)	Volume [CD] =	67.04
		Dx =	
		Dm =	
		I/Icor =	9.870

a =	3.59570	alpha =	
b =		beta =	
c =	5.18500	gamma =	
a/b =	1.00000	Z =	2
c/b =	1.44200		

ICSD Collection Code: 066787
Note: Rietveld profile refinement applied
Temperature Factor: ITF
Additional Pattern: See PDF 01-079-1771 and PDF 01-088-1007
Article Title: Powder diffraction investigations of plasma sprayed zirconia
Wyckoff Sequence: d b (P42/NMCZ)
ANX: AX2

Structure
Publication: J. Mater. Sci.
Detail: volume 30, page 1621 (1995)
Authors: Bondars, B., Heidemane, G., Grabis, J., Laschke, K., Boysen, H., Schneider, J., Frey, F.
Primary Reference
Publication: Calculated from ICSD using POWD-12++

Radiation:	CuKa1	Filter:	Not specified
Wavelength:	1.54060	d-spacing:	
SS/FOM:	999.9 (0,20)		

d	2θ	I	h	k	l
2.95473	30.223	999	1	0	1
2.59250	34.570	81	0	0	2
2.54254	35.272	124	1	1	0
2.10291	42.975	14	1	0	2
1.81525	50.219	320	1	1	2
1.79785	50.739	171	2	0	0
1.69863	53.935	1	2	0	1
1.55773	59.274	106	1	0	3
1.53588	60.203	200	2	1	1
1.47737	62.852	47	2	0	2
1.36652	68.623	3	2	1	2
1.29625	72.919	15	0	0	4
1.27127	74.592	37	2	2	0
1.21943	78.350	3	1	0	4
1.17729	81.733	64	2	1	3
1.16777	82.544	31	3	0	1
1.15483	83.676	24	1	1	4
1.14143	84.886	17	2	2	2
1.13706	85.289	15	3	1	0

APPENDIX B

STANDARD TEST METHOD FOR FLEXURAL

STRENGHT, VICKER'S HARDNESS AND DENSITY

Designation: C 1161 – 94 (Reapproved 1996)

Standard Test Method for
Flexural Strength of Advanced Ceramics at Ambient Temperature[1]

This standard is issued under the fixed designation C 1161; the number immediately following the designation indicates the year of original adoption or, in the case of revision, the year of last revision. A number in parentheses indicates the year of last reapproval. A superscript epsilon (ε) indicates an editorial change since the last revision or reapproval.

1. Scope

1.1 This test method covers the determination of flexural strength of advanced ceramic materials at ambient temperature. Four-point–¼ point and three-point loadings with prescribed spans are the standard. Rectangular specimens of prescribed cross-section sizes are used with specified features in prescribed specimen-fixture combinations.

1.2 The values stated in SI units are to be regarded as the standard. The values given in parentheses are for information only.

1.3 *This standard does not purport to address all of the safety concerns, if any, associated with its use. It is the responsibility of the user of this standard to establish appropriate safety and health practices and determine the applicability of regulatory limitations prior to use.*

2. Referenced Documents

2.1 *ASTM Standards:*
E 4 Practices for Force Verification of Testing Machines[2]
E 337 Test Method for Measured Humidity with a Psychrometer (The Measurement of Wet- and Dry-Bulb Temperatures)[3]
2.2 *Military Standard:*
MIL-STD-1942 (MR) Flexural Strength of High Performance Ceramics at Ambient Temperature[4]

3. Terminology

3.1 *Definitions:*
3.1.1 *flexural strength*—a measure of the ultimate strength of a specified beam in bending.
3.1.2 *four-point–¼ point flexure*—configuration of flexural strength testing where a specimen is symmetrically loaded at two locations that are situated one quarter of the overall span, away from the outer two support bearings (see Fig. 1).
3.1.3 *three-point flexure*—configuration of flexural strength testing where a specimen is loaded at a location midway between two support bearings (see Fig. 1).

4. Significance and Use

4.1 This test method may be used for material development, quality control, characterization, and design data generation purposes.

4.2 The flexure stress is computed based on simple beam theory with assumptions that the material is isotropic and homogeneous, the moduli of elasticity in tension and compression are identical, and the material is linearly elastic. The average grain size should be no greater than one fiftieth of the beam thickness. The homogeneity and isotropy assumption in the standard rule out the use of this test for continuous fiber-reinforced ceramics.

4.3 Flexural strength of a group of test specimens is influenced by several parameters associated with the test procedure. Such factors include the loading rate, test environment, specimen size, specimen preparation, and test fixtures. Specimen sizes and fixtures were chosen to provide a balance between practical configurations and resulting errors, as discussed in MIL-STD 1942 (MR) and Refs (1) and (2).[5] Specific fixture and specimen configurations were designated in order to permit ready comparison of data without the need for Weibull-size scaling.
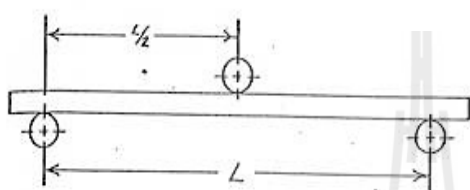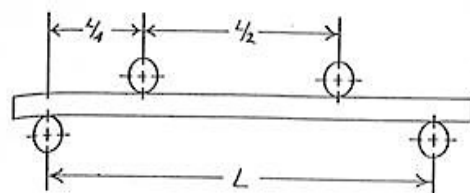
4.4 The flexural strength of a ceramic material is dependent on both its inherent resistance to fracture and the presence of defects. Analysis of a fracture surface, fractography, though beyond the scope of this test method, is highly recommended for all purposes, especially for design data as discussed in MIL-STD-1942 (MR) and Refs (2–5).

5. Interferences

5.1 The effects of time-dependent phenomena, such as stress corrosion or slow crack growth on strength tests conducted at ambient temperature, can be meaningful even for the relatively short times involved during testing. Such influences must be considered if flexure tests are to be used to generate design data.

5.2 Surface preparation of test specimens can introduce machining flaws which may have a pronounced effect on flexural strength. Machining damage imposed during specimen preparation can be either a random interfering factor, or an inherent part of the strength characteristic to be measured. Surface preparation can also lead to residual stresses. Universal or standardized test methods of surface preparation do not exist. It should be understood that final machining steps may or may not negate machining damage

---

[1] This test method is under the jurisdiction of ASTM Committee C-28 on Advanced Ceramics and is the direct responsibility of Subcommittee C28.01 on Properties and Performance.
Current edition approved July 25, 1994. Published February 1995. Originally published as C 1161 – 90. Last previous edition C 1161 – 90.
[2] *Annual Book of ASTM Standards*, Vol 03.01.
[3] *Annual Book of ASTM Standards*, Vol 11.03.
[4] Available from Standardization Documents, Order Desk, Bldg. 4, Section D, 700 Robbins Ave., Philadelphia, PA 19111-5094.

[5] The boldface numbers in parentheses refer to the references at the end of this test method.

{ASTM} C 1161

NOTE—Configuration:
A: L = 20 mm
B: L = 40 mm
C: L = 80 mm

FIG. 1   The Four-Point–¼ Point and Three-Point Fixture
Configuration

TABLE 1   Fixture Spans

Configuration	Support Span (L), mm	Loading Span, mm
A	20	10
B	40	20
C	80	40

TABLE 2   Nominal Bearing Diameters

Configuration	Diameter, mm
A	2.0 to 2.5
B	4.5
C	9.0

TABLE 3   Specimen Size

Configuration	Width (b), mm	Depth (d), mm	Length (L$_r$), min, mm
A	2.0	1.5	25
B	4.0	3.0	45
C	8.0	6.0	90

introduced during the early course or intermediate machining.

6. Apparatus

6.1 *Loading*—Specimens may be loaded in any suitable testing machine provided that uniform rates of direct loading can be maintained. The load-measuring system shall be free of initial lag at the loading rates used and shall be equipped with a means for retaining read-out of the maximum load applied to the specimen. The accuracy of the testing machine shall be in accordance with Practices E 4 but within 0.5 %.

6.2 *Four-Point Flexure*—Four-point–¼ point fixtures (Fig. 1) shall have support and loading spans as shown in Table 1.

6.3 *Three-Point Flexure*—Three-point fixtures (Fig. 1) shall have a support span as shown in Table 1.

6.4 *Bearings*—Three- and four-point flexure:

6.4.1 Cylindrical bearing edges shall be used for the support of the test specimen and for the application of load. The cylinders shall be made of hardened steel which has a hardness no less than HRC 40 or which has a yield strength no less than 1240 MPa (~180 ksi). Alternatively, the cylinders may be made of a ceramic with an elastic modulus between 2.0 and 4.0×10^5 MPa (30–60×10^6 psi) and a flexural strength no less than 275 MPa (~40 ksi). The portions of the test fixture that support the bearings may need to be hardened to prevent permanent deformation. The cylindrical bearing length shall be at least three times the specimen width. The above requirements are intended to ensure that ceramics with strengths up to 1400 MPa (~200 ksi) and elastic moduli as high as 4.8×10^5 MPa (70×10^6 psi) can be tested without fixture damage. Higher strength

and stiffer ceramic specimens may require harder bearings.

6.4.2 The bearing cylinder diameter shall be approximately 1.5 times the beam depth of the test specimen size employed. See Table 2.

6.4.3 The bearing cylinders shall be carefully positioned such that the spans are accurate within ±0.10 mm. The load application bearing for the three-point configurations shall be positioned midway between the support bearing within ±0.10 mm. The load application (inner) bearings for the four-point configurations shall be centered with respect to the support (outer) bearings within ±0.10 mm.

6.4.4 The bearing cylinders shall be free to rotate in order to relieve frictional constraints (with the exception of the middle-load bearing in three-point flexure which need not rotate). This can be accomplished by mounting the cylinders in needle bearing assemblies, or more simply by mounting the cylinders as shown in Figs. 2 and 3. Note that the outer-support bearings roll *outward* and the inner-loading bearings roll *inward*.

6.5 *Semiarticulating–Four-Point Fixture*—Specimens prepared in accordance with the parallelism requirements of 7.1 may be tested in a semiarticulating fixture as illustrated in Fig. 2. The bearing cylinders themselves must be parallel to each other to within 0.015 mm (over their length).

6.6 *Fully Articulating–Four-Point Fixture*—Specimens that are as-fired, heat treated, or oxidized often have slight twists or unevenness. Specimens which do not meet the parallelism requirements of 7.1 shall be tested in a fully articulating fixture as illustrated in Fig. 3.

6.7 The fixture shall be stiffer than the specimen, so that most of the crosshead travel is imposed onto the specimen.

7. Specimen

7.1 *Specimen Size*—Dimensions are given in Table 3 and shown in Fig. 4. Cross-sectional dimensional tolerances are ±0.13 mm for B and C specimens, and ±0.05 mm for A. The parallelism tolerances on the four longitudinal faces are 0.015 mm for A and B and 0.03 mm for C. The two end faces need not be precision machined.

7.2 *Specimen Preparation*—Depending upon the intended application of the flexural strength data, use one of
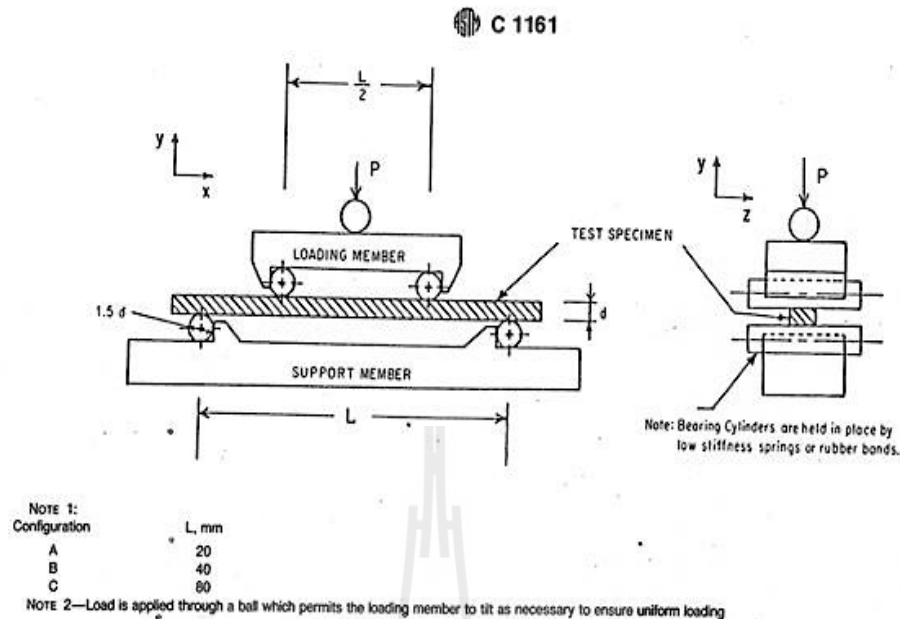
🖭 C 1161

NOTE 1:
Configuration   L, mm

Configuration	L, mm
A	20
B	40
C	80

NOTE 2—Load is applied through a ball which permits the loading member to tilt as necessary to ensure uniform loading

FIG. 2 Schematic of a Semiarticulated Four-Point Fixture Suitable for Flat and Parallel Specimens

the following four specimen preparation procedures:

7.2.1 *As-Fabricated*—The flexural specimen shall simulate the surface condition of an application where no machining is to be used; for example, as-cast, sintered, or injection-molded parts. No additional machining specifications are relevant. An edge chamfer is not necessary in this instance. As-fired specimens are especially prone to twist or warpage and might not meet the parallelism requirements. In this instance, a fully articulating fixture (6.6 and Fig. 3) shall be used in testing.

7.2.2 *Application-Matched Machining*—The specimen shall have the same surface preparation as that given to a component. Unless the process is proprietary, the report shall be specific about the stages of material removal, wheel grits, wheel bonding, and the amount of material removed per pass.

7.2.3 *Customary Procedures*—In instances where a customary machining procedure has been developed that is completely satisfactory for a class of materials (that is, it induces no unwanted surface damage or residual stresses), this procedure shall be used.

7.2.4 *Standard Procedures*—In the instances where 7.2.1 through 7.2.3 are not appropriate, then 7.2.4 shall apply. This procedure shall serve as minimum requirements and a more stringent procedure may be necessary.

7.2.4.1 All grinding shall be done with an ample supply of appropriate filtered coolant to keep workpiece and wheel constantly flooded and particles flushed. Grinding shall be in at least two stages, ranging from coarse to fine rates of material removal. All machining shall be in the surface grinding mode, and shall be parallel to the specimen long axis shown in Fig. 5. No Blanchard or rotary grinding shall be used.

7.2.4.2 The stock-removal rate shall not exceed 0.03 mm (0.001 in.) per pass to the last 0.06 mm (0.002 in.) per face.

Final (and intermediate) finishing shall be performed with a diamond wheel that is between 320 and 500 grit. No less than 0.06 mm per face shall be removed during the final finishing phase, and at a rate of not more than 0.002 mm (0.0001 in.) per pass. Remove approximately equal stock from opposite faces.

7.2.4.3 Materials with low fracture toughness and a greater susceptibility to grinding damage may require finer grinding wheels at very low removal rates.

7.2.4.4 The four long edges of each specimen shall be uniformly chamfered at 45°, a distance of 0.12 ± 0.03 mm as shown in Fig. 4. They can alternatively be rounded with a radius of 0.15 ± 0.05 mm. Edge finishing must be comparable to that applied to the specimen surfaces. In particular, the direction of machining *shall be parallel* to the specimen long axis. If chamfers are larger than the tolerance allows, then corrections shall be made to the stress calculation (1). Alternatively, if a specimen can be prepared with an edge that is free of machining damage, then a chamfer is not required.

7.2.5 *Handling Precautions*—Care should be exercised in storing and handling of specimens to avoid the introduction of random and severe flaws, such as might occur if specimens were allowed to impact or scratch each other.

7.3 *Number of Specimens*—A minimum of 10 specimens shall be required for the purpose of estimating the mean. A minimum of 30 shall be necessary if estimates regarding the form of the strength distribution are to be reported (for example, a Weibull modulus). The number of specimens required by this test method has been established with the intent of determining not only reasonable confidence limits on strength distribution parameters, but also to help discern multiple-flaw population distributions. More than 30 specimens are recommended if multiple-flaw populations are present.

⊕ C 1161
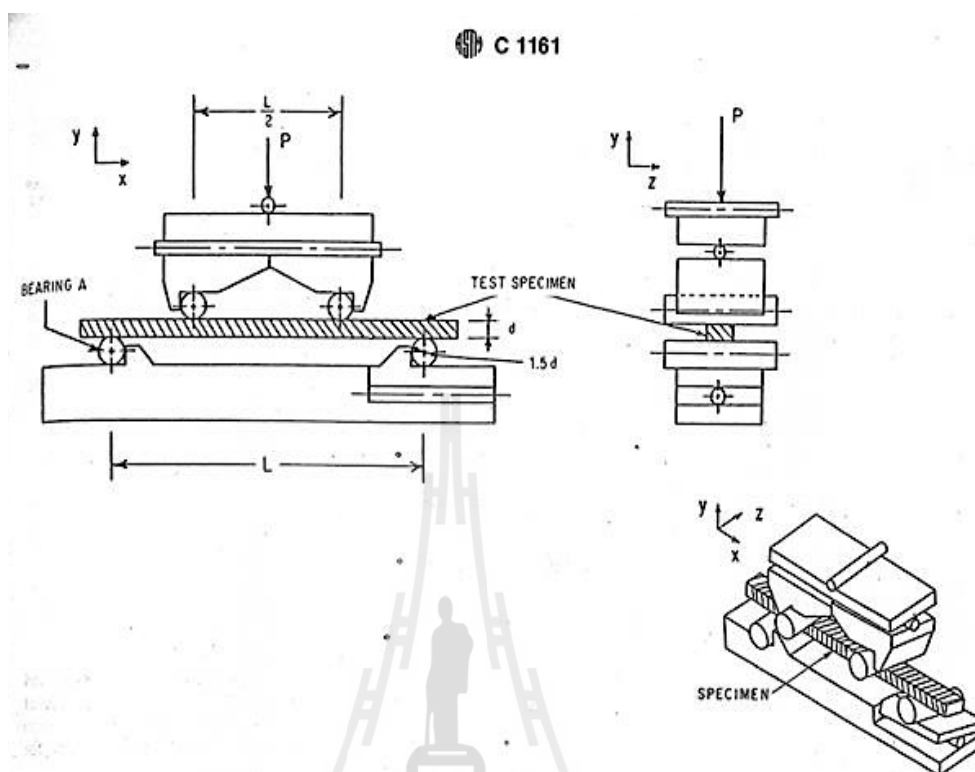
NOTE 1:

Configuration	L, mm
A	20
B	40
C	80

NOTE 2—Bearing A is fixed so that it will not pivot about the x axis. The other three bearings are free to pivot about the x axis.

FIG. 3 Schematic of a Fully Articulating Four-Point Fixture Suitable for Twisted or Uneven Specimens

8. Procedure

8.1 Test specimens on their appropriate fixtures in specific testing configurations. Test specimens Size A on either the four-point A fixture or the three-point A fixture. Similarly, test B specimens on B fixtures, and C specimens on C fixtures. A fully articulating fixture is required if the specimen parallelism requirements cannot be met. An alternative procedure with a D specimen is given in the Appendix.

8.2 Carefully place each specimen into the test fixture to preclude possible damage and to ensure alignment of the specimen in the fixture. In particular, there should be an equal amount of overhang of the specimen beyond the outer bearings and the specimen should be directly centered below the axis of the applied load.

8.3 Slowly apply the load at right angles to the fixture. The maximum permissible stress in the specimen due to initial load shall not exceed 25 % of the mean strength. Inspect the points of contact between the bearings and the specimen to ensure even line loading and that no dirt or contamination is present. If uneven line loading of the specimen occurs, use fully articulating fixtures.

8.4 Mark the specimen to identify the points of load application and also so that the tensile and compression faces can be distinguished. Carefully drawn pencil marks will suffice.

8.5 Put cotton, crumbled tissues, or other appropriate material around specimen to prevent pieces from flying out of the fixtures upon fracture. This step may help ensure operator's safety and preserve primary fracture pieces for subsequent fractographic analysis.

8.6 *Loading Rates*—The crosshead rates are chosen so that the strain rate upon the specimen shall be of the order of $1.0 \times 10^{-4} \ s^{-1}$.

8.6.1 The strain rate for either the three- or four-point-¼ point mode of loading is as follows:

$$\dot{\epsilon} = 6 \ ds/L^2$$

where:

$\dot{\epsilon}$ = strain rate,

TABLE 4 Crosshead Speeds for Displacement-Controlled Testing Machine

Configuration	Crosshead Speeds, mm/min
A	0.2
B	0.5
C	1.0

307

Designation: C 1327 – 96a

Standard Test Method for
Vickers Indentation Hardness of Advanced Ceramics[1]

This standard is issued under the fixed designation C 1327; the number immediately following the designation indicates the year of original adoption or, in the case of revision, the year of last revision. A number in parentheses indicates the year of last reapproval. A superscript epsilon (ε) indicates an editorial change since the last revision or reapproval.

1. Scope

1.1 This test method covers the determination of the Vickers indentation hardness of advanced ceramics.

1.2 *This standard does not purport to address all of the safety concerns, if any, associated with its use. It is the responsibility of the user of this standard to establish appropriate safety and health practices and determine the applicability of regulatory limitations prior to use.*

2. Referenced Documents

2.1 *ASTM Standards:*
E 4 Practices for Force Verification of Testing Machines[2]
E 177 Practice for Use of the Terms Precision and Bias in ASTM Test Methods[3]
E 380 Practice for Use of the International System of Units (SI) (the Modernized Metric System)[3]
E 384 Test Method for Microhardness of Materials[2]
E 691 Practice for Conducting an Interlaboratory Study to Determine the Precision of a Test Method[3]
2.2 *European Standard:*
CEN ENV 843-4 Advanced Technical Ceramics, Monolithic Ceramics, Mechanical Properties at Room Temperature, Part 4: Vickers, Knoop and Rockwell Superficial Hardness[4]
2.3 *Japanese Standard:*
JIS R 1610 Testing Method for Vickers Hardness of High Performance Ceramics[5]
2.4 *ISO Standard:*
ISO 6507/2 Metallic Materials—Hardness test—Vickers test—Part 2: HV0.2 to less than HV5[6]

3. Terminology

3.1 *Definition:*
3.1.1 *Vickers hardness number (HV), n*—the number obtained by dividing the applied load in kilograms-force by the surface area of the indentation in square millimetres computed from the mean of the measured diagonals of the indentation. It is assumed that the indentation is an imprint of the undeformed indenter.

4. Summary of Test Method

4.1 This test method describes an indentation hardness test using a calibrated machine to force a pointed, square base, pyramidal diamond indenter having specified face angles, under a predetermined load, into the surface of the material under test and to measure the surface-projected diagonals of the resulting impression after removal of the load.

NOTE 1—A general description of the Vickers indentation hardness test is given in Test Method E 384. The present method is very similar, has most of the same requirements, and differs only in areas required by the special nature of advanced ceramics. This test method also has many elements in common with standards ENV 843-4 and JIS R 1610, which are also for advanced ceramics.

5. Significance and Use

5.1 For advanced ceramics, Vickers indenters are used to create indentations whose surface-projected diagonals are measured with optical microscopes. The Vickers indenter creates a square impression from which two surface-projected diagonal lengths are measured. Vickers hardness is calculated from the ratio of the applied load to the area of contact of the four faces of the undeformed indenter. (In contrast, Knoop indenters are also used to measure hardness, but Knoop hardness is calculated from the ratio of the applied load to the projected area on the specimen surface.)

5.2 Vickers indentation hardness is one of many properties that is used to characterize advanced ceramics. Attempts have been made to relate Vickers indentation hardness to other hardness scales, but no generally accepted methods are available. Such conversions are limited in scope and should be used with caution, except for special cases where a reliable basis for the conversion has been obtained by comparison tests.

5.3 Vickers indentation diagonal lengths are approximately 2.8 times shorter than the long diagonal of Knoop indentations, and the indentation depth is approximately 1.5 times deeper than Knoop indentations made at the same load.

5.4 Vickers indentations are influenced less by specimen surface flatness, parallelism, and surface finish than Knoop indentations, but these parameters must be considered nonetheless.

5.5 Vickers indentations are much more likely to cause cracks in advanced ceramics than Knoop indentations. The cracks may influence the measured hardness by fundamentally altering the deformation processes that contribute to the formation of an impression, and they may impair or preclude measurement of the diagonal lengths due to excessive damage at the indentation tips or sides.

5.6 A full hardness characterization includes measure-

---

[1] This test method is under the jurisdiction of ASTM Committee C-28 on Advanced Ceramics and is the direct responsibility of Subcommittee C28.01 on Properties and Performance.
Current edition approved Dec. 10, 1996. Published February 1997. Originally published as C 1327 – 96. Last previous edition C 1327 – 96.
[2] *Annual Book of ASTM Standards*, Vol 03.01.
[3] *Annual Book of ASTM Standards*, Vol 14.02.
[4] Available from European Committee for Standardization, Brussels, Belgium.
[5] Available from Japanese Standards Association, Tokyo, Japan.
[6] Available from International Standards Organization, Geneva, Switzerland.

C 1327

ments over a broad range of indentation loads. A comprehensive characterization of this type is recommended but is beyond the scope of this test method, which measures hardness at a single, designated load.

6. Interferences

6.1 Cracking from the indentation tips can interfere with determination of tip location and thus the diagonal length measurements.

6.2 Cracking or spalling around the Vickers impression may occur and alter the shape and clarity of the indentation, especially for coarse-grained ceramics whereby grains may cleave and dislodge. The cracking may occur in a time-dependent manner (minutes or hours) after the impression is made.

6.3 Porosity (either on or just below the surface) may interfere with measuring Vickers hardness, especially if the indentation falls directly onto a large pore or if the indentation tip falls in a pore.

6.4 At higher magnifications in the optical microscope, it may be difficult to obtain a sharp contrast between the indentation tip and the polished surface of some advanced ceramics. This may be overcome by careful adjustment of the lighting as discussed in Test Method E 384.

7. Apparatus

7.1 *Testing Machines:*

7.1.1 There are two general types of machines available for making this test. One type is a self-contained unit built for this purpose, and the other type is an accessory available to existing microscopes. Usually, this second type is fitted on an inverted-stage microscope. Descriptions of the various machines are available (1–3).[7]

7.1.2 Design of the machine should be such that the loading rate, dwell time, and applied load can be set within the limits set forth in 10.5. It is an advantage to eliminate the human element whenever possible by appropriate machine design. The machine should be designed so that vibrations induced at the beginning of a test will be damped out by the time the indenter touches the sample.

7.1.3 The calibration of the balance beam should be checked monthly or as needed. Indentations in standard reference materials may also be used to check calibration when needed.

7.2 *Indenter:*

7.2.1 The indenter shall meet the specifications for Vickers indenters. See Test Method E 384. The four edges formed by the four faces of the indenter shall be sharp. Chamfered edges (as in Ref (4)) are not permitted. The tip offset shall be not more than 0.5 μm in length.

7.2.2 Figure 1 shows the indenter. The depth of the indentation is 1/7 the length of the diagonal. The indenter has an angle between opposite faces of 136° 0 min (±30 min).

7.2.3 The diamond should be examined periodically; and if it is loose in the mounting material, chipped, or cracked, it shall be replaced.

[7] The boldface numbers in parentheses refer to the list of references at the end of this test method.
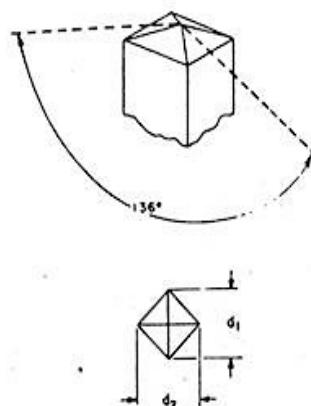

FIG. 1 Vickers Indenter

NOTE 2—This requirement is from Test Method E 384 and is especially pertinent to Vickers indenters used for advanced ceramics. Vickers indenters are often used at high loads in advanced ceramics in order to create cracks. Such usage can lead to indenter damage. The diamond indenter can be examined with a scanning electron microscope, or indents can be made into soft copper to help determine if a chip or crack is present.

7.3 *Measuring Microscope:*

7.3.1 The measurement system shall be constructed so that the length of the diagonals can be determined with errors not exceeding ±0.0005 mm.

NOTE 3—Stage micrometres with uncertainties less than this should be used to establish calibration constants for the microscope. See Test Method E 384. Ordinary stage micrometres, which are intended for determining the approximate magnification of photographs, may be too coarsely ruled or may not have the required accuracy and precision.

7.3.2 The numerical aperture (NA) of the objective lens shall be between 0.65 and 0.90.

NOTE 4—The apparent length of a Vickers indentation will increase as the resolving power and NA of a lens increases. The variation is much less than that observed in Knoop indentations, however (2, 5, 6). The range of NA specified by this test method corresponds to 40 to 100x objective lenses. The higher power lenses may have higher resolution, but the contrast between the indentation tips and the polished surface may be less.

7.3.3 A filter may be used to provide monochromatic illumination. Green filters have proved to be useful.

8. Preparation of Apparatus

8.1 *Verification of Load*—Most of the machines available for Vickers hardness testing use a loaded beam. This beam shall be tested for zero load. An indentation should not be visible with zero load, but the indenter should contact the sample. Methods of verifying the load application are given in Practices E 4.

8.2 *Separate Verification of Load, Indenter, and Measuring Microscope*—Procedures in Test Method E 384, Section 14, may be followed.

8.3 *Verification by Standard Reference Materials*—Standard reference blocks, SRM No. 2831, of tungsten carbide that are available from the National Institute of Standards

and Technology[8] can be used to verify that an apparatus produces a Vickers hardness within ±5 % of the certified value.

9. Test Specimens

9.1 The Vickers indentation hardness test is adaptable to a wide variety of advanced ceramic specimens. In general, the accuracy of the test will depend on the smoothness of the surface and, whenever possible, ground and polished specimens should be used. The back of the specimen shall be fixed so that the specimen cannot rock or shift during the test.

9.1.1 *Thickness*—As long as the specimen is over ten times as thick as the indentation depth, the test will not be affected. In general, if specimens are at least 0.50 mm thick, the hardness will not be affected by variations in the thickness.

9.1.2 *Surface Finish*—Specimens should have a ground and polished surface. The roughness should be less than 0.1 µm rms. However, if one is investigating a surface coating or treatment, one cannot grind and polish the specimen.

Note 5—This requirement is necessary to ensure that the surface is flat and that the indentation is sharp. Residual stresses from polishing are of less concern for most advanced ceramics than for glasses or metals. References (7) and (8) report that surfaces prepared with 1 µm or finer diamond abrasive had no effect on measured ceramic hardness. Hardness was only affected when the surface finish had an optically resolvable amount of abrasive damage (7). (Extra caution may be appropriate during polishing of transformation toughening ceramics, such as some zirconias, since the effect upon hardness is not known.)

10. Procedure

10.1 *Specimen Placement*—Place the specimen on the stage of the machine so that the specimen will not rock or shift during the measurement. The specimen surface shall be clean and free of any grease or film.

10.2 *Specimen Leveling:*

10.2.1 The surface of the specimen being tested shall lie in a plane normal to the axis of the indenter. The angle of the indenter and specimen surface should be within 2° perpendicular.

Note 6—Greater amounts of tilting produce nonuniform indentations and invalid test results. A 2° tilt will cause an asymmetrical indentation which is just noticeable, and will cause a 1 % error in hardness (9).

10.2.2 If one leg of a diagonal is noticeably longer than the other leg of the same diagonal, resulting in a deformed indentation, misalignment is probably present and should be corrected before proceeding with any measurements. See Test Method E 384.

10.2.3 Leveling the specimen is facilitated if one has a leveling device.[9]

10.3 *Magnitude of Test Load*—A test load of 9.81 N (1 kgf) is specified. If another load is used because of a special

requirement, or due to cracking problems at 9.81 N, then the reporting procedure of 12.6 shall be used.

10.4 *Clean the Indenter*—The indenter shall be cleaned prior to and during a test series. A cotton swab with ethanol, methanol, or isopropanol may be used. Indenting into soft copper also may help remove debris.

Note 7—Ceramic powders or fragments from the ceramic test piece can adhere to the diamond indenter.

10.5 *Application of Test Load:*

10.5.1 Start the machine smoothly. The rate of indenter motion prior to contact with the specimen shall be 0.015 to 0.070 mm/s. If the machine is loaded by an electrical system or a dash-pot lever system, it should be mounted on shock absorbers which damp out all vibrations by the time the indenter touches the specimen.

Note 8—This rate of loading is consistent with Test Method E 384.

10.5.2 The time of application of the full test load shall be 15 s (±2) unless otherwise specified. After the indenter has been in contact with the specimen from this required dwell time, raise it carefully off the specimen to avoid a vibration impact.

10.5.3 The operator shall not bump or inadvertently contact the test machine or associated support (for example, the table) during the period of indenter contact with the specimen.

10.6 *Spacing of Indentations*—Allow a distance of at least four diagonal lengths between the centers of the indentations as illustrated in Fig. 2. If there is cracking from the indentations, the spacing shall be increased to at least five times the length of the cracks, as shown in Fig. 2.

10.7 *Acceptability of Indentations:*

10.7.1 If there is excessive cracking from the indentation tips and sides, or the indentation is asymmetric, the indent shall be rejected for measurement. Figure 3 provides guid-
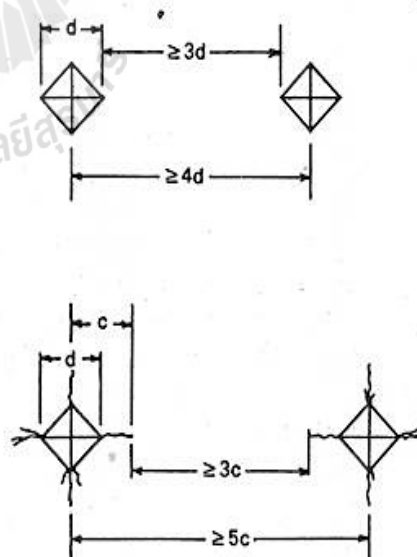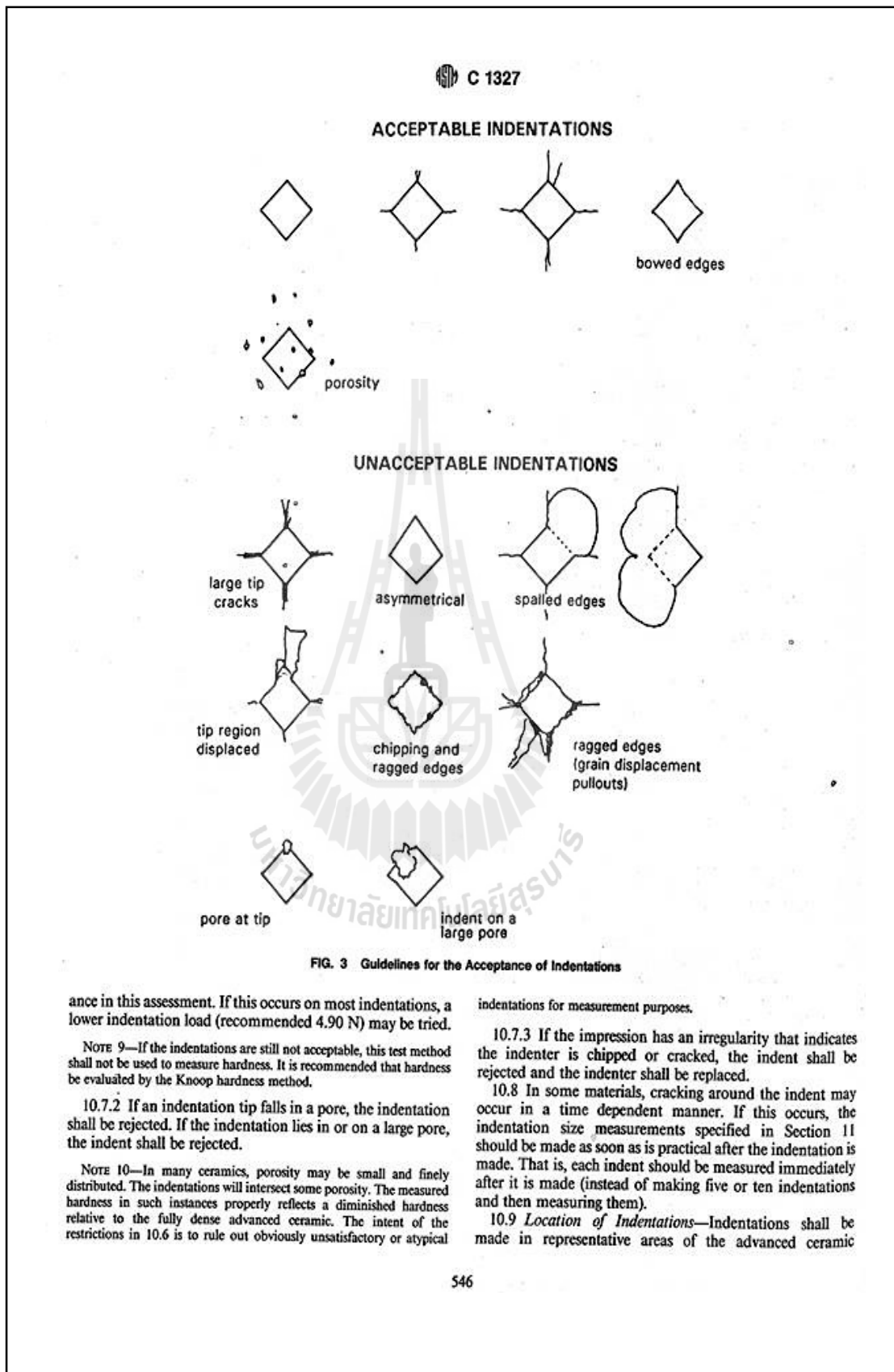
FIG. 2 Closest Permitted Spacing for Vickers Indentations

FIG. 3 Guidelines for the Acceptance of Indentations

ance in this assessment. If this occurs on most indentations, a lower indentation load (recommended 4.90 N) may be tried.

NOTE 9—If the indentations are still not acceptable, this test method shall not be used to measure hardness. It is recommended that hardness be evaluated by the Knoop hardness method.

10.7.2 If an indentation tip falls in a pore, the indentation shall be rejected. If the indentation lies in or on a large pore, the indent shall be rejected.

NOTE 10—In many ceramics, porosity may be small and finely distributed. The indentations will intersect some porosity. The measured hardness in such instances properly reflects a diminished hardness relative to the fully dense advanced ceramic. The intent of the restrictions in 10.6 is to rule out obviously unsatisfactory or atypical

indentations for measurement purposes.

10.7.3 If the impression has an irregularity that indicates the indenter is chipped or cracked, the indent shall be rejected and the indenter shall be replaced.

10.8 In some materials, cracking around the indent may occur in a time dependent manner. If this occurs, the indentation size measurements specified in Section 11 should be made as soon as is practical after the indentation is made. That is, each indent should be measured immediately after it is made (instead of making five or ten indentations and then measuring them).

10.9 *Location of Indentations*—Indentations shall be made in representative areas of the advanced ceramic

546

🌐 C 1327

microstructure. They shall not be restricted to high density regions if such regions exist.

10.10 *Number of Indentations*—For homogeneous and fully dense advanced ceramics, at least five and preferably ten acceptable indentations shall be made. If the ceramic is multiphase, not homogeneous, or not fully dense, ten acceptable indentations shall be made.

11. Measurement of Indentation

11.1 The accuracy of the test method depends to a very large extent on this measurement, as follows:

11.1.1 If the measuring system contains a light source, take care to use the system only after it has reached equilibrium temperature. This is because the magnification of a microscope depends on the tube length.

11.1.2 Calibrate the measuring system carefully with an accurate and precision stage micrometer or with an optical grating.

11.1.3 Adjust the illumination and focusing conditions carefully as specified in Test Method E 384 to obtain the optimum view and clarity of the impression. Proper focus and illumination are critical for accurate and precise readings. Both indentation tips shall be in focus at the same time. Do not change the focus once the measurement of the diagonal length has begun.

NOTE 11—The lighting intensity and the settings of the field and aperture diaphragms can have a noticeable effect upon the apparent location of the tips in Vickers indentations. Consult the manufacturer's guidelines for optimum procedures. Additional information is presented in Test Method E 384. In general, the field diaphragm can be closed so that it barely enters or just disappears from the field of view. The aperture diaphragm can be closed in order to reduce glare and sharpen the image, but it should not be closed so much as to cause diffraction that distorts the edges of the indentation.

NOTE 12—Uplift and curvature of the sides of the impressions may be substantial in impressions in advanced ceramics, which may cause the sides of the impression to be slightly out of focus. The tips of the impression shall be focused on for measurement of the indentation diagonals. It may be helpful to focus on a small microstructural feature on the flat specimen surface just beyond the indentation tips.

11.1.4 If either a measuring microscope or a filar micrometer eyepiece is used, always rotate the drum in the same direction to eliminate backlash errors.

11.1.5 Follow the manufacturer's guidelines for the use of crosshairs or graduated lines. To eliminate the influence of the thickness of the line, always use the same edge of the crosshair or graduation line. CAUTION—Serious systematic errors can occur due to improper crosshair usage. Procedures vary considerably between different equipment. In nearly all instances, the crosshairs should not be placed entirely over or fully cover the indentation tip as shown in Fig. 4a. The indentation tip should be just visible in the fringe of light on the side of the crosshair or graduated line as shown in Fig. 4b or 4c. In some measuring systems with twin crosshairs, the measurement is made with the inside edge of the two lines as shown in Fig. 4b. In other measuring systems, particularly those with a single moveable crosshair, the measurement is made with the same side of the crosshair as shown in Fig. 4c.

11.1.6 Read the two diagonals of the indent to within 0.00025 mm and determine the average of the diagonal lengths.

11.1.7 Use the same filters in the light system at all times. Usually a green filter is used.

11.1.8 For transparent or translucent ceramics, where contrast is poor, the specimen may be coated (for example, a gold/palladium coating) to improve the measurability of the indents (4). Such coatings shall be less than 50 nm thick and shall be applied after the indentations have been made. Never indent into coatings made to enhance visibility.

12. Calculation

12.1 Vickers hardness may be calculated and reported either in units of GPa (12.2) or as Vickers hardness number (12.3).

12.2 The Vickers hardness with units of GPa is computed as follows:

$$HV = 0.0018544\ (P/d^2) \tag{1}$$

where:

P = load, N, and
d = average length of the two diagonals of the indentation, mm.

NOTE 13—This computation and set of units are in accordance with the recommendations of Practice E 380.

12.3 The Vickers hardness number is computed as follows:

$$HV = 1.8544\ (P/d^2) \tag{2}$$

where:

P = load, kgf, and
d = average length of the two diagonals of the indentation, mm.

NOTE 14—This computation is consistent with Test Method E 384.

Alternately, the Vickers hardness number also may be computed as follows:

$$HV = (0.102)(1.8544)(P/d^2) \tag{3}$$

where:

P = load, N, and
d = average length of the two diagonals of the indentation, mm.

NOTE 15—This computation is consistent with ISO 6507/2, ENV 843-4, and JIS R 1610.

NOTE 16—Equations 2 and 3 compute the Vickers hardness number, which is a dimensionless number; for example, $HV = 1500$. HV formerly had been assigned units of kgf/mm^2. Equations 2 and 3 produce the same Vickers hardness number.

NOTE 17—The factor 0.102 in Eq 3 becomes necessary through the introduction of the SI unit newton for the test force instead of kilogram-force to avoid changing the value of the Vickers hardness number from its traditional units.

12.4 The mean hardness, $\overline{HV}$, is:
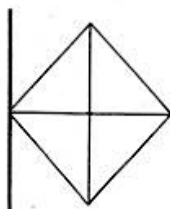
$$\overline{HV} = \frac{\Sigma\ HV_n}{n} \tag{4}$$

where:

HV_n = HV obtained from nth indentation and
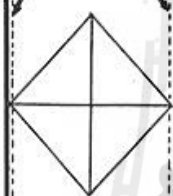n = number of indentations.

12.5 The standard deviation, S, is:

$$S = \sqrt{\frac{\Sigma\ (\overline{HV} - HV_n)^2}{n-1}} \tag{5}$$

C 1327

(a) INCORRECT. Crosshair completely covers the tip.
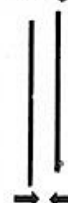
(b) CORRECT. Double crosshair measurement system, whereby the indentation is intended to be measured between two crosshairs or measuring lines. Indentation tips should be on the inside edge (in the fringe) of each crosshair. The measuring system is zeroed by bringing the inside measuring line inside edges together as shown on the right.
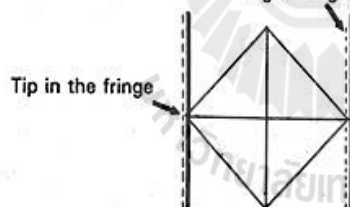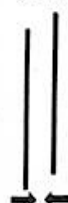
(c) CORRECT. Single crosshair and some double crosshair measurement systems. The indentation tip is on the same side of the crosshair line(s). The measuring system is zeroed with the tip on the same side of one line for a single crosshair system, or with both lines superimposed in a double crosshair system as shown on the right.

FIG. 4. Crosshair Measurement Systems

12.6 The hardness symbol *HV* shall be supplemented by a number indicating the test force used, expressed in newtons multiplied by 0.102 (and therefore equal to the test force expressed in kilograms-force), and optionally a number indicating the duration of test force applications in seconds. So, for example, *HV*1/15 means the Vickers hardness for an applied test force of 9.81 N (1 kgf) applied for 15 s at full load.

13. Report

13.1 The report shall include the following information:

13.1.1 Mean *HV*,
13.1.2 Test load,
13.1.3 Duration of test load,
13.1.4 Standard deviation,
13.1.5 Test temperature and humidity,
13.1.6 Number of satisfactory indentations measured, as well as the total number of indents made,
13.1.7 Surface conditions and surface preparation,
13.1.8 Thermal history of the sample,
13.1.9 The extent of cracking (if any) observed, and
13.1.10 Deviations from the specified procedures, if any.

14. Precision and Bias

14.1 The precision and bias of microhardness measurements depend on strict adherence to the stated test procedure and are influenced by instrumental and material factors and indentation measurement errors.

14.2 The consistency of agreement for repeated tests on the same material is dependent on the homogeneity of the material, repeatability and reproducibility of the hardness tester, and consistent, careful measurements of the indents by a competent operator.

14.3 Instrumental factors that can affect test results include accuracy of loading, inertia effects, speed of loading, vibrations, the angle of indentation, lateral movement of the indenter or sample, indentation, and indenter shape deviations. Results are particularly sensitive to vibration or impact, which will produce larger indents and lower apparent hardness results.

14.4 The largest source of error or uncertainty in hardness usually arises from the error and uncertainty in the measurement of the diagonal length.

14.4.1 The harder the material, the smaller the indent size is. Therefore, hardness uncertainties are usually greater for harder materials.

14.4.2 Diagonal length measurement errors include inaccurate calibration of the measuring device, inadequate resolving power of the objective, insufficient magnification, operator bias in sizing the indents, poor image quality, and nonuniform illumination. These can contribute to both bias and precision errors.

14.4.3 The numerical aperture (NA) of the objective lens determines the maximum useful magnification and the resolving power of the microscope. The higher the NA of the lens, the longer the indentation will appear. This limited resolution leads to a bias error since the microscope is not able to resolve the exact tip and thus leads to underestimates

TABLE 1 Precision of Diagonal Length Measurements Estimated from an Interlaboratory Round Robin Project (10, 11)

Load, P (N)	Number of Laboratories	Average Diagonal Length, d (µm)	Within-Laboratory Repeatability		Between-Laboratory Reproducibility	
			Expanded Uncertainty[C] (µm)	Coefficient of Variation, %	Expanded Uncertainty[C] (µm)	Coefficient of Variation, %
9.81[A]	10	34.52	0.56	0.58	2.94	3.05
9.81[B]	8	34.57	0.62	0.64	2.70	2.79

[A] Indentations made by organizing laboratory. Outlier results from one laboratory deleted.
[B] Indentations made by participating laboratories. Outlier results from two laboratories deleted. One other laboratory did not do this part of the exercise.
[C] Coverage factor of 2.8, corresponding to a 95 % confidence interval.

of the true length. The theoretical shortening is estimated to be λ/2NA, where λ is the wavelength of the light used (2, 5). Experimental evidence indicates that actual shortening is less than this, but the use of different NA objective lenses will contribute to a reproducibility (between-laboratory) uncertainty of less than ±0.2 µm (5, 6). (This error is substantially less for Vickers indentations than for Knoop indentations.)

14.5 A round robin was conducted to evaluate the suitability of tungsten carbide-cobalt specimens as standard hardness test blocks (10, 11). The results of this eleven-laboratory round robin can be used to evaluate the precision of Vickers hardness measurements for a hard material (~15 GPa) that does not pose difficult measuring problems. Within-laboratory repeatability and between-laboratory reproducibility were evaluated in accordance with Practices E 177 and E 691. The results are listed in Table 1, which shows the repeatability and reproducibility in measured diagonal lengths. The hardness repeatability interval when expressed as a percentage is double the diagonal-length repeatability interval. Participants read five indents made at 9.81 N at the organizing laboratory, and also made and measured five of their own indents at the same load. The within-laboratory hardness repeatabilities were 1.2 and 1.3 % (coefficient of variation, COV), respectively. The between-laboratory hardness reproducibilities were 6.1 and 5.6 % (COV), respectively. The reproducibility estimates were made after deleting one or two outlier sets as noted in Table 1. The reproducibility uncertainty includes both the hardness measurement uncertainty and the variations in hardness (±2.8 %, COV) of the eight blocks used in the round robin.

15. Keywords

15.1 advanced ceramics; cracks; indentation; microscope; Vickers hardness

⊕ C 1327

REFERENCES

(1) Small, L., *Hardness Theory and Practice (Part I: Practice)*, Service Diamond Tool Co., Ann Arbor, MI, 1960, pp. 241–243.

(2) Mott, B. W., *Micro-Indentation Hardness Testing*, Butterworth's Scientific Publications, London, 1956.

(3) Blau, P. J., "Methods and Applications of Microindentation Hardness Testing," *Applied Metallography*, Vander Voort, G. F., ed., Van Nostrand-Reinhold, 1986, pp. 123–138.

(4) Clinton, D. J., and Morrell, R., "Hardness Testing of Ceramic Materials," *Material Chemistry and Physics*, Vol 17, 1987, pp. 461–473.

(5) Brown, A. R. G., and Ineson, E., "Experimental Survey of Low-Load Hardness Testing Machines," *Journal of Iron and Steel Institute*, Vol 169, 1951, pp. 376–388.

(6) Gahm, J., "Neurere Erkinntnisse zur Mikro-Härte," (New Results on Microhardness), Verein Deutscher Ingenieure-Berichte (*Society of German Engineers, Reports*), Nr 160, 1972, pp. 25–41.

(7) Naylor, M. G. S., and Page, T. F., "Microhardness, Friction and Wear of SiC and Si_3N_4 Materials as a Function of Load, Temper-ature and Environment," Third Annual Technical Report, October 1981, Cambridge University, England.

(8) Thibault, N. W., and Nyquist, H. L., "The Measured Hardness of Hard Substances and Factors Affecting Its Determination," *Transactions of the American Society of Metals*, Vol 38, 1947, pp. 271–330.

(9) Mulhearn, T. O., and Samuels, L. E., "The Errors Introduced into Diamond Pyramid Hardness Testing by Tilting the Specimen," *Journal of Iron and Steel Institute*, August 1955, pp. 354–359.

(10) Gettings, R. J., Quinn, G. D., Ruff, A. W., and Ives, L. K., "Development of Ceramic Hardness Reference Materials," *New Horizons for Materials*, Proceedings of the 8th World Congress on Ceramics, Florence, Italy, July 1994, Vincenzini, P., ed., Techna, Faenza, 1995, pp. 617–624.

(11) Gettings, R. J., Quinn, G. D., Ruff, A. W., and Ives, L. K., "Hardness Standard Reference Materials (SRM) for Advanced Ceramics," *Verein Deutscher Ingenieure Reports*, 1194, 1995, pp. 255–264.

ASTM Designation: C 373 – 88 (Reapproved 1994)

Standard Test Method for
Water Absorption, Bulk Density, Apparent Porosity, and Apparent Specific Gravity of Fired Whiteware Products[1]

This standard is issued under the fixed designation C 373; the number immediately following the designation indicates the year of original adoption or, in the case of revision, the year of last revision. A number in parentheses indicates the year of last reapproval. A superscript epsilon (ε) indicates an editorial change since the last revision or reapproval.

1. Scope

1.1 This test method covers procedures for determining water absorption, bulk density, apparent porosity, and apparent specific gravity of fired unglazed whiteware products.

1.2 *This standard does not purport to address all of the safety concerns, if any, associated with its use. It is the responsibility of the user of this standard to establish appropriate safety and health practices and determine the applicability of regulatory limitations prior to use.*

2. Significance and Use

2.1 Measurement of density, porosity, and specific gravity is a tool for determining the degree of maturation of a ceramic body, or for determining structural properties that may be required for a given application.

3. Apparatus and Materials

3.1 *Balance,* of adequate capacity, suitable to weigh accurately to 0.01 g.

3.2 *Oven,* capable of maintaining a temperature of 150 ± 5°C (302 ± 9°F).

3.3 *Wire Loop, Halter, or Basket,* capable of supporting specimens under water for making suspended mass measurements.

3.4 *Container*—A glass beaker or similar container of such size and shape that the sample, when suspended from the balance by the wire loop, specified in 3.3, is completely immersed in water with the sample and the wire loop being completely free of contact with any part of the container.

3.5 *Pan,* in which the specimens may be boiled.

3.6 *Distilled Water.*

4. Test Specimens

4.1 At least five representative test specimens shall be selected. The specimens shall be unglazed and shall have as much of the surface freshly fractured as is practical. Sharp edges or corners shall be removed. The specimens shall contain no cracks. The individual test specimens shall weigh at least 50 g.

5. Procedure

5.1 Dry the test specimens to constant mass (Note) by heating in an oven at 150°C (302°F), followed by cooling in a desiccator. Determine the dry mass, D, to the nearest 0.01 g.

NOTE—The drying of the specimens to constant mass and the determination of their masses may be done either before or after the specimens have been impregnated with water. Usually the dry mass is determined before impregnation. However, if the specimens are friable or evidence indicates that particles have broken loose during the impregnation, the specimens shall be dried and weighed after the suspended mass and the saturated mass have been determined, in accordance with 5.3 and 5.4 In this case, the second dry mass shall be used in all appropriate calculations.

5.2 Place the specimens in a pan of distilled water and boil for 5 h, taking care that the specimens are covered with water at all times. Use setter pins or some similar device to separate the specimens from the bottom and sides of the pan and from each other. After the 5-h boil, allow the specimens to soak for an additional 24 h.

5.3 After impregnation of the test specimens, determine to the nearest 0.01 g the mass, S, of each specimen while suspended in water. Perform the weighing by placing the specimen in a wire loop, halter, or basket that is suspended from one arm of the balance. Before actually weighing, counterbalance the scale with the loop, halter, or basket in place and immerse in water to the same depth as is used when the specimens are in place. If it is desired to determine only the percentage of water absorption, omit the suspended mass operation.

5.4 After the determination of the suspended mass or after impregnation, if the suspended mass is not determined, blot each specimen lightly with a moistened, lint-free linen or cotton cloth to remove all excess water from the surface, and determine the saturated mass, M, to the nearest 0.01 g. Perform the blotting operation by rolling the specimen lightly on the wet cloth, which shall previously have been saturated with water and then pressed only enough to remove such water as will drip from the cloth. Excessive blotting will introduce error by withdrawing water from the pores of the specimen. Make the weighing immediately after blotting, the whole operation being completed as quickly as possible to minimize errors due to evaporation of water from the specimen.

6. Calculation

6.1 In the following calculations, the assumption is made that 1 cm³ of water weighs 1 g. This is true within about 3 parts in 1000 for water at room temperature.

6.1.1 Calculate the exterior volume, V, in cubic centimetres, as follows:

$$V = M - S$$

⊛ C 373

6.1.2 Calculate the volumes of open pores V_{OP} and impervious portions V_{IP} in cubic centimetres as follows:

$$V_{OP} = M - D$$
$$V_{IP} = D - S$$

6.1.3 The apparent porosity, P, expresses, as a percent, the relationship of the volume of the open pores of the specimen to its exterior volume. Calculate the apparent porosity as follows:

$$P = [(M - D)/V] \times 100$$

6.1.4 The water absorption, A, expresses as a percent, the relationship of the mass of water absorbed to the mass of the dry specimen. Calculate the water absorption as follows:

$$A = [(M - D)/D] \times 100$$

6.1.5 Calculate the apparent specific gravity, T, of that portion of the test specimen that is impervious to water, as follows:

$$T = D/(D - S)$$

6.1.6 The bulk density, B, in grams per cubic centimetre, of a specimen is the quotient of its dry mass divided by the exterior volume, including pores. Calculate the bulk density as follows:

$$B = D/V$$

7. Report

7.1 For each property, report the average of the values obtained with at least five specimens, and also the individual values. Where there are pronounced differences among the individual values, test another lot of five specimens and, in addition to individual values, report the average of all ten determinations.
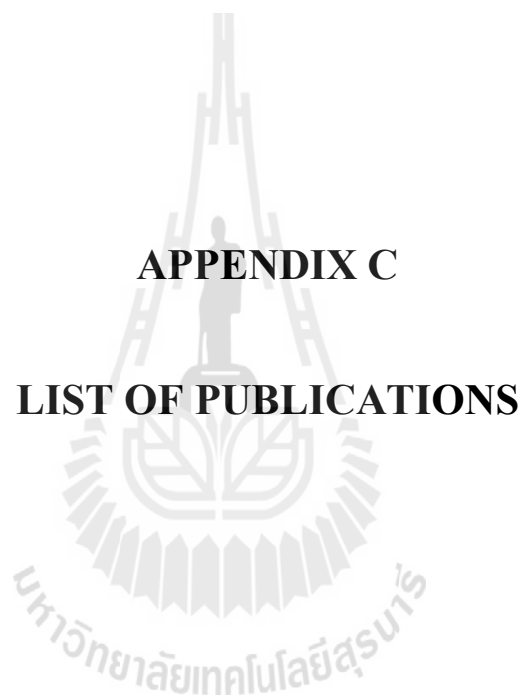
8. Precision and Bias

8.1 This test method is accurate to ±0.2 % water absorption in interlaboratory testing when the average value recorded by all laboratories is assumed to be the true water absorption. The precision is approximately ± 0.1 % water absorption on measurements made by a single experienced operator.

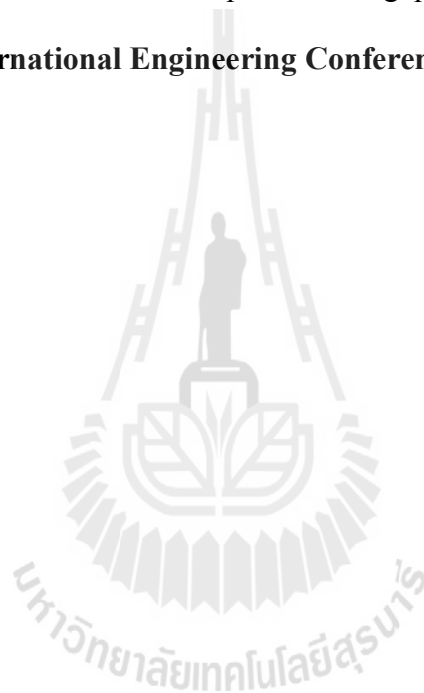**APPENDIX C**

LIST OF PUBLICATIONS

ListofPublications

WathunBoonsorn,SukasemWatcharamaisakuland Boris Golman.(2014).Fabrication of
Al$_2$O$_3$/ZrO$_2$ micro/nano composites using powder alkoxide
mixtures.**Advanced Materials Research Vols. 931-932: 132-136.**

WathunBoonsorn,SukasemWatcharamaisakuland Boris Golman.(2014). Fabrication
of Al$_2$O$_3$/ZrO$_2$ micro/nano composites using powder alkoxide mixtures.**The
5th KKU International Engineering Conference**.27-29/ March/ 2014.

Fabrication of Al$_2$O$_3$/ZrO$_2$ micro/nano composites using powder alkoxide mixtures

W. Boonsorn[1, a], S. Watcharamaisakul[1, b*] and B. Golman[2, c]

[1]School of Ceramic Eng., Suranaree Univ of Techn., Nakhon-Ratchasima, Thailand, 30000
[2]School of Chemical Eng., Suranaree Univ of Techn., Nakhon-Ratchasima, Thailand, 30000

[a]boonsorn.w@gmail.com, [b]sukasem@sut.ac.th, [c]golman@sut.ac.th

Keywords: Al$_2$O$_3$/ZrO$_2$ composite, Micro/Nano composite, colloidal process

Abstract. Al$_2$O$_3$/ZrO$_2$ composites have been investigated as the bio-inert material. In the present work Al$_2$O$_3$/ZrO$_2$ Micro/Nano composites were prepared by colloidal method. The effects of the concentration of zirconium propoxide and the sintering temperature were studied on the distribution of ZrO$_2$ nano-grains in Al$_2$O$_3$ matrix and mechanical properties of composites. XRD patterns for all compositions showed a single phase of α-Al$_2$O$_3$, and the tetragonal and monoclinic ZrO$_2$ phases. Samples sintered at 1650°C demonstrated the high bulk density with value of 86-92% of theoretical density. ZrO$_2$ nano-grains were dispersed within Al$_2$O$_3$ grain and the grain boundary. The sample of the highest flexural strength of 710 MPa was synthesized using 100% Zr propoxide solution and sintered at 1650° C. The flexural strength was found to increase with increasing the concentration of Zr propoxide and sintering temperature.

Introduction

In recent years, all-ceramic systems have been developed for metal-free dental restorations due to their excellent esthetics, enhanced reproducibility and improved biocompatibility as compared to the porcelain fused to metal or even gold ones [1-3]. The alumina base system is promising for achieving the objective of restorations. Alumina/Zirconia composites were generally developed for orthopedic and structural ceramic applications such as ceramic joint prostheses, femoral heads, acetabular cups for total hip replacement and dental implants due to their advantageous mechanical properties. The relationship between mechanical properties of composites and the clinical performance of implants are influenced by various factors. The reliability and lifetime of orthopedic implants were improved by the use of materials possessing high fracture toughness and mechanical strength [4]. Zirconia has three crystallographic phases: monoclinic, tetragonal and cubic. The cubic phase is the most stable one at high temperature, but the monoclinic and tetragonal phases are metastable and the phase transformation can be induced by variation of temperature and stress. The tetragonal-to-monoclinic phase transformation of zirconia in alumina matrix could be responsible for the superior crack growth resistance in the micro/nano composite by enhancement of the residual stress field to inhibit crack propagation.

A modified colloidal method was utilized for synthesis of nanostructured composite powder [5,6]. A stable suspension of alumina powder was doped with a dilute solution of zirconium alkoxide and dried to form composite powder involving a zirconium precursor layer coated on alumina particle. Subsequently, zirconia nanoparticles were formed and grew on the surface of alumina grains during thermal treatment.

The mechanical properties of sintered material depend largely on their microstructure, such as the pore size, crack length, grain size, existence of agglomerates, etc. In this work, the effects of zirconium propoxide concentration used in the colloidal method and sintering temperature were investigated on the dispersion of zirconia nano-grains in alumina matrix and mechanical properties of Al$_2$O$_3$/ZrO$_2$ micro/nano composites.

Materials and Experimental Procedures

The Al_2O_3/ZrO_2 Micro/Nano composite powder was prepared via colloidal method. The composition was fixed at 90 wt.% of alumina and 10wt% of zirconia [5]. α-Alumina 5 micron powder (A-5M, ACC product) and ethanol absolute (99.9% purity, VWR BDH Prolabo, UK) with a weight ratio of 1:3 were mixed by ball milling. Acetic acid (100% purity, VWR BDH Prolabo, UK) was used to adjust the pH of colloidal alumina to 7.1 monitored using pH meter (Model Inlab Expert Pro ISM, Mettler Toledo, Switzerland) in order to improve the suspension stability. Wang et al. [10] reported the isoelectric point at pH 7.1 for alumina particles suspended in ethanol. Zirconium solution was prepared by mixing zirconium IV propoxide (70 wt% solution in 1-propanol) (33397-2, Sigma-Aldrich, Ireland), and ethanol in various ratios, as shown in Table 1.

Table 1 Zr alkoxide solution ratio

Sample ID	Zr alkoxide : Ethanol Ratio in solution (weight)		Concentration of Zr alkoxide solution (%)
	Zr alkoxide	Ethanol	
100	1	-	100
75	3	1	75
66.7	2	1	66.7
50	1	1	50
33.3	1	2	33.3
25	1	3	25

The slurry was prepared by the dropwise addition of colloidal alumina into zirconium solution under stirring. The slurry was dried at 70°C to remove ethanol by evaporation. The powder was calcined at 850°C for 2 hrs in air. Finally, Al_2O_3/ZrO_2 Micro/Nano composite powder was deagglomerated and sieved to less than 45 micron. Al_2O_3/ZrO_2 Micro/Nano composite powder mixed with 0.5 wt.% PVA was pre-formed at 150 MPa by using a uniaxial press and then consolidated by the cold isostatic pressing at 350 MPa in order to improve the green strength of samples. The CIPed composites were sintered at 1600°C and 1650°C for 4 hrs in an electric furnace.

The phase composition of powder and sintered composites were investigated by means of X-ray diffraction (XRD) using Bruker D2 Advance with CuKα step scan mode (5s/0.2° 2θ;) in the 20-80° 2θ range. Archimedes' method was utilized for measurement of the bulk density of sintered composites. The flexural strength of sintered samples was determined by the three-point bending method using Universal Testing Machine (UTM, UH-100A Shimadzu, Japan) with 20 mm of span length. The microstructure of sintered specimens was analyzed on the fracture surface using Scanning Electron Microscopy (SEM, JEOL JSM6010LV, Japan).

Results and Discussion

XRD patterns of Al_2O_3/ZrO_2 Micro/Nano composite materials sintered at 1600° C and 1650° C are shown in Fig. 1. The XRD analysis confirms the presence of a single phase of α-Al_2O_3, and the tetragonal and monoclinic ZrO_2 phases in all samples after calcination. The results indicates that the concentration of zirconium solution influences on the phase composition as the monoclinic ZrO_2 phase increases while the tetragonal decreases at high concentration of zirconium propoxide.
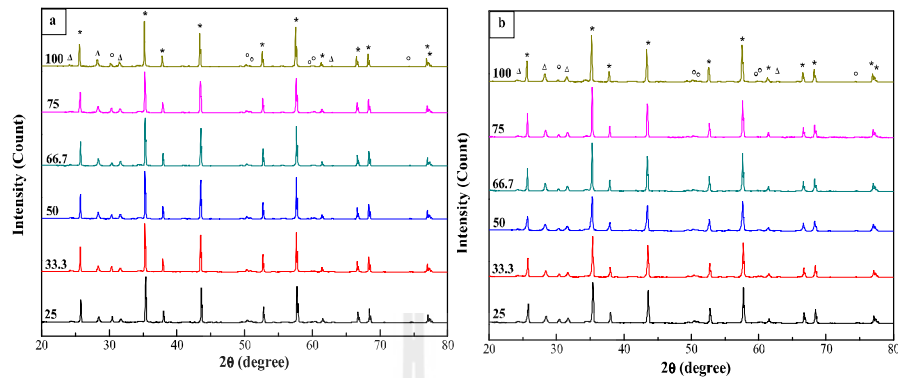
Fig. 1. XRD patterns of Al_2O_3/ZrO_2 micro/nano composites sintered at (a) 1600^oC and (b) 1650^oC
$\Delta = m\text{-}ZrO_2$; $o = t\text{-}ZrO_2$; $* = \alpha\text{-}Al_2O_3$.

Figure 2 shows the bulk density of composites sintered at 1600^oC and 1650^oC. The composites sintered at 1650^oC were densified to 86-92% of theoretical density while sintered at 1600^oC were 68-78% for various concentrations of Zr propoxide. The higher density materials were obtained with higher concentration solution.
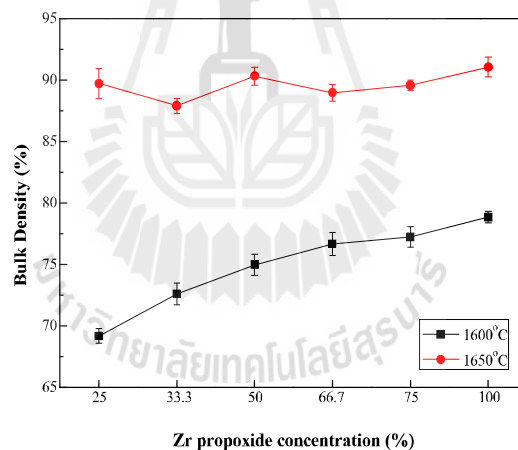

Fig. 2. Effect of Zr propoxide concentration on bulk density of sintered composites.

The flexural strength of sintered composites increased with increasing the concentration of zirconia propoxide, as illustrated in Fig. 3. However, the flexural strength of composites sintered at 1650^oC slightly decreased for the samples of 50% and 75% of Zr propoxide. Nevertheless, the highest flexural strength of 710 MPa was obtained with a sample prepared at highest Zr propoxide concentration of 100% and sintered at 1650^oC.
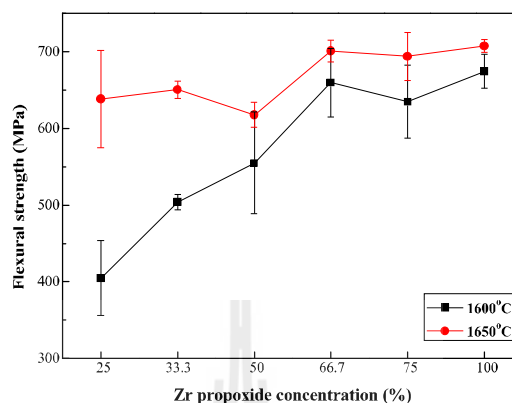
Fig. 3. Effect of Zr propoxide concentration on flexural strength of sintered composites.

SEM observations indicate the formation of dense composite with large Al_2O_3 grains and low porosity at high sintering temperature, which corresponds to the high value of theoretical density. ZrO_2 particles of spherical shape and wide size distribution were located within Al_2O_3 grains and the grain boundary, as shown in Fig. 4. As a result, the high flexural strength was obtained with a sample of low porosity sintered at $1650^{\circ}C$.
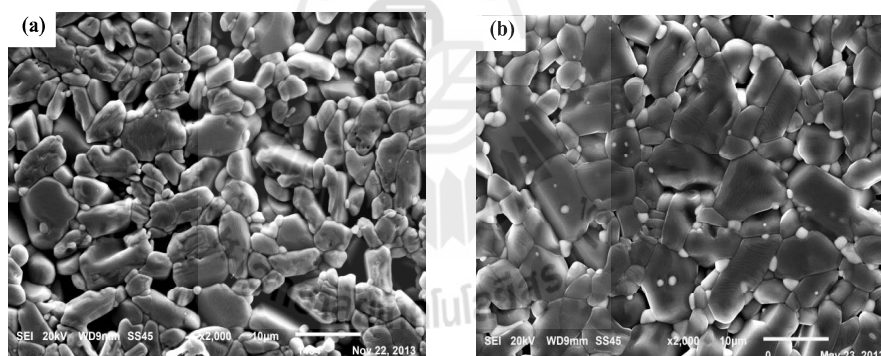

Fig. 4. Scanning electron microscope images of Al_2O_3/ZrO_2 micro/nano composites sintered at (a) $1600^{\circ}C$ and (b) $1650^{\circ}C$.

Conclusions

Al_2O_3/ZrO_2 micro/nano composites with ZrO_2 nanoparticles embedded into Al_2O_3 micro grains were successfully prepared by using powder-alkoxide mixture of various concentrations of zirconium propoxide. The concentration of zirconium propoxide in the solution and the sintering temperature has been found to have a significant effect on the phase composition and bulk density of sintered composite material. The results showed that the amount of tetragonal ZrO_2 phase declines and monoclinic one rises at higher zirconium propoxide concentration. It was confirmed that increasing the sintering temperature from $1600^{\circ}C$ to $1650^{\circ}C$ results in an increase in bulk density on 15%. The grain growth was observed for samples sintered at $1650^{\circ}C$. Zirconia particles in alumina grain were appeared of the spherical shape with wide size distribution. The sample of high density and flexural strength were obtained at high sintering temperature and Zr propoxide concentration.

References

[1] S. Rimmer, Modern dental ceramics: an overview, International density SA. 8 (2006) 32-40.

[2] S. Walia, Restoring esthetics with metal-free ceramics: A case report. 75 (2009) 353.

[3] F. T. da Siilva, M. A. N. Zacche, H. S. de Amorin, Influence of different surface treatments on the fracture toughness of a commercial ZTA dental ceramic, Mat. Res. 10 (2007) 63-68.

[4] J. Chevalier, P. Taddei, L. Gremillard, S. Deville, G. Fantozzi, J.F. Bartolome, C. Pecharroman, J.S. Moya, L.A. Diaz, R. Torrecillas, S. Affatato, Reliability assessment in advanced nanocomposite materials for orthopedic application, J. Mechanical Behavior Biomedical Materials. 4 (2011) 303-314.

[5] J. Chevalier, L. Gremillar, Ceramics for medical applications: A picture for the next 20 years, J. Eur. Ceram. Soc. 29 (2009) 1245-1255.

[6] W.H.Tuan, R.Z. Chen, T.C. Wang, C.H. Cheng, P.S. Kuo, Mechanical properties of Al_2O_3/ZrO_2 composites, J. Eur. Ceram. Soc. 22 (2002) 2827-2833.

[7] A. Rafferty, A.M. Alsebaie, A.G. Olabi, T. Prescott, Properties of zirconia-toughened-alumina prepared via powder processing and colloidal processing routes, J. Colloid Interface Sci. 329 (2009) 310-315.

[8] A.H. De Azaa, J. Chevaliera, G. Fantozzia, M. Schehlb, R. Torrecillas, Crack growth resistance of alumina, zirconia and zirconia toughened alumina ceramics for joint prostheses, Biomaterials. 23 (2002) 937-945.

[9] J.M. Calderon-Moreno, M. Schehl, Microstructure after super plastic creep of alumina-zirconia composites prepared by powder alcoxide mixtures, J. Eur. Ceram. 24 (2004) 393-397.

[10] G. Wang, P Sarkar, P.S. Nicholson, Influence of Acidity on the Electrostatic Stability of Alumina Suspension in Ethanol, J. Am. Ceram. 80 (1997) 965.

BIOGRAPHY

WathunBoonsorn was born on November 3rd, 1982 in Nakhonratchasima Province, Thailand. He graduated in Bachelor Degree in Ceramics Industry Design from King Mongkut's Institute of Technology North Bangkok in 2004. After graduation, he earned a Master Degree, from Department of Ceramics, Faculty of Decorative Art, Silapakrorn University in 2008Supported by King Mongkut's University of Technology North Bangkok. Since 2006 to present, he has been a lecturer of Department of Ceramics Design, Faculty of Architecture and Design, King Mongkut's University of Technology North Bangkok. In year 2009, he furthered the study for Doctoral Degree, supported by King Mongkut's University of Technology North Bangkok, In Ceramic Engineering at School of Ceramic Engineering, Institute of Engineering at Suranaree University of Technology from 2009 to 2015. During his Doctoral Degree study, he has one paper-published in international journal and one oral paper presentation.